Aus dem Fachbereich Medizin
der Johann Wolfgang Goethe-Universität
Frankfurt am Main

betreut am
Zentrum der Biochemie
Institut für Biochemie I (Pathobiochemie)
Direktor: Prof. Dr. Bernhard Brüne

Changes in RNA dynamics in the course of hypoxia in myeloid cells

Thesis
zur Erlangung des Grades Doctor of Philosophy (PhD)
des Fachbereichs Medizin
der Johann Wolfgang Goethe-Universität
Frankfurt am Main

vorgelegt von
Rebekka Bauer

aus Offenbach am Main

Frankfurt am Main, 2023

Dekan:	Prof. Dr. Stefan Zeuzem
Referent:	Prof. Dr. Bernhard Brüne
Korreferentin:	Prof. Dr. Sabine Grösch
2. Korreferent:	Prof. Dr. Reinier Abraham Boon
Tag der mündlichen Prüfung:	11.01.2024

Table of contents

List of abbreviations

4sU	4-thiouridine
ACE2	angiotensin-converting enzyme 2
AH	acute hypoxia
ATP	adenosine triphosphate
CCL2	C-C motif chemokine ligand 2
CH	chronic hypoxia
COVID-19	coronavirus disease-2019
CPT1A	carnitine palmitoyltransferase 1A
CXCL10	C-X-C motif chemokine ligand 10
DAMPs	danger-associated molecular patterns
DDNS	differential *de novo* synthesis
DGE	differential gene expression
DSR	differential stability regulation
ER	endoplasmic reticulum
FBS	fetal bovine serum
GRAND-SLAM	globally refined analysis of newly transcribed RNA and decay rates using SLAM-seq
HIF	hypoxia-inducible factor
HMGB1	high mobility group protein B1
IFN	interferon
IRF7	interferon regulatory factor 7
ISG	interferon-stimulated gene
KO	knockout
LDL	low-density lipoprotein
LSS	lanosterol synthase
MAVS	mitochondrial antiviral signaling protein
MDSCs	myeloid-derived suppressor cells
MRPL40	mitochondrial ribosomal protein L40
MSMO1	methylsterol monooxygenase 1
mt	mitochondrial
MyD88	myeloid differentiation primary response 88
N	normoxia

NF-κB	nuclear factor kappa B
NPC1	Niemann-Pick C1 protein
O_2	molecular oxygen
OAS1	2'-5'-oligoadenylate synthetase 1
OXPHOS	oxidative phosphorylation
PAMPs	pathogen-associated molecular patterns
Pol II	RNA polymerase II
PRR	pattern recognition receptor
ROS	reactive oxygen species
S100A8	S100 calcium-binding protein A8
SARS-CoV-2	severe acute respiratory syndrome coronavirus type 2
SLAM-Seq	thiol-linked alkylation for the metabolic sequencing of RNA
SREBP2	sterol regulatory element-binding protein 2
STING	stimulator of interferon response cGAMP interactor
TAMs	tumor-associated macrophages
TBK1	TANK-binding kinase 1
TIM	translocase of the inner mitochondrial membrane
TLR	toll-like receptor
TMPRSS2	transmembrane serine protease 2
TOM/TOMM	translocase of the outer mitochondrial membrane
TRIF	TIR-domain-containing adapter-inducing interferon-β

1. Zusammenfassung

Molekularer Sauerstoff (O_2) ist für zahlreiche Stoffwechselvorgänge unerlässlich. Dementsprechend ist ein Zusammenhang zwischen reduzierter Sauerstoffverfügbarkeit, d.h. Hypoxie, den resultierenden Anpassungen und pathophysiologischen Prozessen wie der Entstehung von Krebs oder entzündlichen Erkrankungen nicht verwunderlich. Zudem ist bekannt, dass myeloide Zellen in hypoxischen Regionen, wie schlecht durchbluteten Tumorbereichen, oder in entzündeten Gelenken, z.B. bei der rheumatoiden Arthritis, akkumulieren, wo sie zum Fortschreiten der Krankheit beitragen können. Während sich die meisten Studien bislang auf transkriptionelle Anpassung durch die Hypoxie-induzierbaren Faktoren (HIF) 1 und 2 unter akuter Hypoxie konzentrierten, sind anhaltender Sauerstoffmangel und alternative post-transkriptionelle Regulationsmechanismen bisher weniger gut verstanden. Ziel meiner Studie war es daher, die *de novo* Synthese und den Abbau von mRNAs und die resultierenden Konsequenzen auf die mRNA-Expressionslevel in Monozyten unter Hypoxie umfassend zu charakterisieren.

Um die RNA-Dynamik unter Hypoxie zu untersuchen, habe ich in monozytären THP-1-Zellen unter Normoxie (N), akuter Hypoxie (AH; 8 h 1% O_2) oder chronischer Hypoxie (CH; 72 h 1% O_2) mittels metabolischer RNA-Sequenzierung Transkriptom-weit *de novo* synthetisierte mRNAs identifiziert und deren Halbwertszeiten bestimmt. Expressionsanalysen der Gesamt-mRNA zeigten, dass die meisten Veränderungen erst unter CH auftraten. Da zudem bekannt ist, dass HIF-vermittelte Transkriptionsveränderungen unter CH abnehmen, habe ich zunächst den Einfluss von RNA-Stabilität auf die Genexpression analysiert. Dabei beobachtete ich eine globale Reduktion der RNA-Halbwertszeit unter Hypoxie, was möglicherweise eine generelle Verringerung Energie-verbrauchender Proteinbiosynthese zur Folge hat. Außerdem identifizierte ich eine Untergruppe hypoxisch-destabilisierter Transkripte, bestehend aus 59 Kern-kodierten mitochondrialen mRNAs, deren Gesamt-mRNA-Expression vermutlich infolgedessen unter CH ebenfalls abnahm. Dies könnte auf einen protektiven Mechanismus hindeuten, der eine reduzierte Produktion von Mitochondrien zur Folge hat, wenn diese sogar aktiv abgebaut werden, um die Generierung reaktiver Sauerstoffspezies zu limitieren.

Während durch ihre Halbwertszeit regulierte Transkripte unter Hypoxie hauptsächlich destabilisiert wurden, war die Mehrheit der differentiell *de novo* synthetisierten mRNAs hochreguliert. Dabei waren mit Hypoxie, Cholesterin-Homöostase und Entzündungsreaktionen assoziierte Transkripte am stärksten angereichert. Zunächst fokussierte ich mich auf den veränderten Cholesterin-Stoffwechsel und beobachtete eine Akkumulation von frühen und eine Abnahme von späten Cholesterin-Vorläufern, die durch mehrere Sauerstoff-abhängige Schritte verbunden sind. Außerdem weisen meine Daten auf lokal erniedrigte Cholesterin-Mengen am endoplasmatischen Retikulum (ER) unter Hypoxie hin, die für die Aktivierung des ER-Cholesterin-regulierten Transkriptionsfaktors Sterol-regulatorisches Element-bindendes Protein 2 (SREBP2) und die Induktion von Cholesterin-Biosynthese-Enzymen verantwortlich sind. Interessanterweise wurden unter Hypoxie zusätzlich zu den SREBP2-regulierten mRNAs mit ähnlicher Kinetik viele Interferon-stimulierte Gene (ISG) induziert, was auf eine immunmetabolische Wechselwirkung hindeutet. Während sich die Verfügbarkeit bestimmter Cholesterin-Vorstufen sowie die SREBP2-Aktivität als irrelevant für die hypoxische ISG-Induktion darstellten, schien eine modifizierte intrazelluläre Cholesterin-Verteilung entscheidend für die hypoxische Chemokin-ISG-Induktion zu sein. Meine Daten weisen darauf hin, dass Veränderungen in der Cholesterin-Dynamik zu einer verstärkten MyD88-abhängigen TLR4 (*toll-like receptor 4*)-Signaltransduktion führen, die für die hypoxische ISG-Induktion wichtig ist. Außerdem amplifizierte Hypoxie die Chemokin-ISG-Induktion in Monozyten nach Kontakt mit SARS-CoV-2 (*severe acute respiratory syndrome coronavirus type 2*) Spike-Protein über TLR4 ähnlich stark wie nach Zugabe von infektiösem Virus, was zu systemischer Entzündung in hypoxämischen Patienten mit schwerer COVID-19 (*corona virus disease 2019*)-Erkrankung beitragen könnte.

Zusammenfassend analysierte ich die RNA-Dynamik unter Sauerstoffmangel umfassend. Ich identifizierte RNA-Stabilität als einen modulierenden Faktor, der die Mitochondrien-Produktion unter Hypoxie limitiert. Außerdem charakterisierte ich die immunmetabolische Interaktion zwischen gestörter Cholesterin-Biosynthese und spontaner ISG-Induktion in hypoxischen Monozyten, die in schweren COVID-19-Verläufen zu systemischer Entzündung beitragen könnte.

2. Summary

Molecular oxygen (O_2) is essential for numerous metabolic processes. Not surprisingly, hypoxia and the resulting adaptations play a pivotal role in pathophysiology, e.g., in cancer or in inflammatory diseases. Of note, myeloid cells are known to accumulate in hypoxic regions such as tumor cores or rheumatoid arthritis joints and may contribute to disease progression. While most studies so far concentrated on transcriptional adaptation by the hypoxia-inducible factors (HIF) 1 and 2 under short term hypoxia, prolonged oxygen deprivation and alternative post-transcriptional regulation are rather poorly investigated. Consequently, the aim of the study was to generate a comprehensive overview of mRNA *de novo* synthesis and degradation and its contribution to total mRNA changes in monocytic cells in the course of hypoxia.

To this end, I used thiol-linked alkylation for the metabolic sequencing of RNA (SLAM-Seq) to characterize RNA dynamics under hypoxia. Specifically, I labeled monocytic THP-1 cells under normoxia (N), acute hypoxia (AH; 8 h 1% O_2), or chronic hypoxia (CH; 72 h 1% O_2) with 4-thiouridine (4sU), which allows for transcriptome-wide identification of *de novo* synthesized mRNAs and estimation of their half-lives. Total mRNA expression analyses revealed that most changes occurred under CH. Considering that HIF accumulation and resulting transcriptional regulation was shown to decline again under CH, I further analyzed the impact of RNA stability on gene expression. I observed a global reduction in RNA half-lives under hypoxia, indicative for the attenuation of energy-consuming protein synthesis upon oxygen deprivation. Moreover, I observed a subgroup of hypoxic destabilized transcripts with resulting decreased mRNA expression under CH, which consisted of 59 nuclear-encoded mitochondrial mRNAs. This might prevent futile production of new mitochondria under conditions, where mitochondria are even actively degraded to prevent production of detrimental reactive oxygen species.

While stability-regulated transcripts were mainly destabilized under hypoxia, the vast majority of differentially *de novo* synthesized transcripts were upregulated. Functional analyses revealed not only hypoxia, but also cholesterol homeostasis and inflammatory response as top enriched terms, corroborating findings on total mRNA level. Focusing on hypoxia-altered cholesterol metabolism, I observed an

accumulation of early and a decrease in late cholesterol precursors, which are separated by several oxygen-dependent enzymatic steps. Although total cholesterol levels were only slightly reduced, my data indicate locally lowered endoplasmic reticulum (ER) cholesterol levels under hypoxia, which cause feedback activation of the ER cholesterol-sensing transcription factor sterol regulatory element-binding protein 2 (SREBP2) and induction of cholesterol biosynthesis enzymes. Interestingly, a broad range of interferon-stimulated genes (ISGs), mainly known for their antiviral function, was also induced under hypoxia with similar kinetics as SREBP2 targets, suggesting an immunometabolic crosstalk. While the availability of certain cholesterol biosynthesis intermediates as well as a direct involvement of SREBP2 seemed rather unlikely to cause hypoxic ISG induction, changes in intracellular cholesterol distribution appeared crucial for the hypoxic induction of chemokine-ISGs. Mechanistically, I found that MyD88-dependent toll-like receptor 4 (TLR4) signaling contributes to enhanced hypoxic ISG induction, likely sensitized by changes in cholesterol dynamics. Importantly, hypoxia amplified induction of chemokine-ISGs in monocytes upon treatment with severe acute respiratory syndrome coronavirus type 2 (SARS-CoV-2) spike protein via TLR4 similarly as after addition of infectious virus, which might contribute to systemic inflammation in hypoxemic patients with severe coronavirus disease-2019 (COVID-19).

Taken together, I comprehensively analyzed RNA dynamics in hypoxic monocytes. Specifically, I identified RNA stability as a modulating mechanism to limit production of mitochondria under oxygen-restricted conditions. Moreover, I characterized the immunometabolic crosstalk between disturbed cholesterol homeostasis and spontaneous induction of interferon (IFN)-signaling in hypoxic monocytes, which might contribute to systemic inflammation in severe cases of COVID-19.

3. Comprehensive summary

3.1. Introduction

Molecular oxygen (O_2) is essential for numerous metabolic processes[1]. Thus, most eukaryotic cells experience massive metabolic remodeling to survive under low oxygen conditions. As O_2 serves as final electron acceptor in oxidative phosphorylation (OXPHOS), a switch to glycolysis-driven adenosine triphosphate (ATP) generation takes place under hypoxia[2]. To limit the production of detrimental reactive oxygen species (ROS), the complexes of the mitochondrial respiratory chain are not only remodeled, but mitochondria are even actively degraded by mitophagy[3]. Moreover, lipid metabolism is highly altered under hypoxia, since β-oxidation as well as fatty acid desaturation and many steps within the cholesterol biosynthesis require O_2[4–6].

Not surprisingly, hypoxia and the resulting adaptations play a pivotal role in pathophysiology. Hypoxia is often observed as consequence of high cancer cell proliferation combined with abnormalities in the vasculature in solid tumors [7], and is tightly linked to more aggressive tumor phenotypes[8]. Moreover, a bidirectional crosstalk between hypoxia and inflammation is well known. On the one hand, hypoxia can occur as a consequence of massive immune cell infiltration into inflamed tissues, which increases local oxygen consumption[9,10]. On the other hand, it is widely accepted that hypoxia can drive inflammatory processes, e.g., by activation of one of the major inflammatory transcription factors nuclear factor kappa B (NF-κB)[11]. Remarkably, myeloid cells, e.g., tumor-associated macrophages (TAMs) and myeloid-derived suppressor cells (MDSCs), accumulate in hypoxic tumor areas[12–14]. Similar observations were made in inflammatory diseases as exemplified by accumulation of monocyte-derived cells in rheumatoid arthritis joints[15]. Thus, it is of special interest how monocytic cells adapt to and influence the hypoxic environment.

Although chronic forms of hypoxia seem to reflect the actual situation in most diseases, most studies so far investigated adaptations to short-term hypoxia, resulting in the groundbreaking discovery of the oxygen-sensitive transcription factors hypoxia-inducible factor (HIF) 1 and 2. They consist of a constitutively expressed β-subunit and an oxygen-degradable α-subunit, which accumulates

upon oxygen deprivation and allows the induction of target genes important for adaptation to hypoxia[16]. Interestingly though, HIF-1α and HIF-2α decline again under prolonged hypoxia, and a new steady state of typical hypoxia-induced transcripts evolves, used to define chronic hypoxia (CH) in previous studies[17,18]. Of note, the transition from acute to chronic hypoxia is gradual and highly dependent on the cell type. The decrease in HIF activity under CH points towards a shift from mainly transcriptional regulation to alternative modulatory principles, such as post-transcriptional regulation, under extended hypoxia (Figure 1). In fact, in addition to alternative splicing and altered translation, changes in RNA stabilities under hypoxia were already described[19,20], although not extensively characterized.

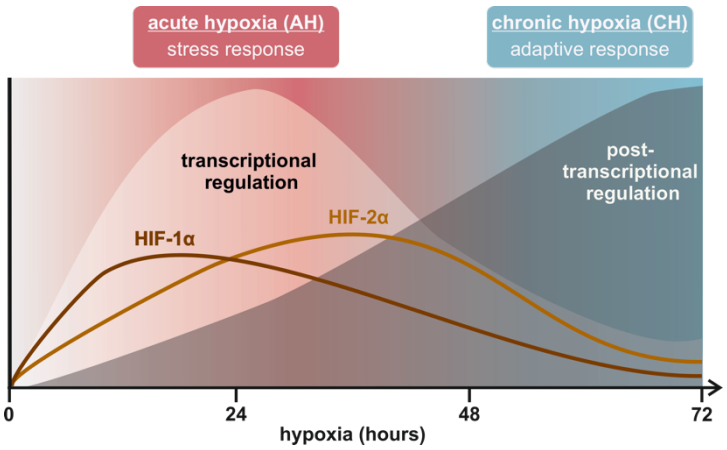

Figure 1: Proposed regulatory layers influencing gene expression during different phases of hypoxia. Accumulation of the oxygen-degradable α-subunits of HIF-1 and HIF-2 initiates fast transcriptional regulation of target genes to handle the stress factor hypoxia. The decline in HIF activity under chronic hypoxia suggests contribution of post-transcriptional regulation to the new steady state gene expression, which might be necessary for long-term adaptive responses. Abbreviation: HIF: hypoxia-inducible factor.

Consequently, the aim of the study was to generate a comprehensive overview of the RNA dynamics, i.e., the contribution of *de novo* synthesis and degradation to total mRNA changes, in monocytic cells in the course of hypoxia. Underlying regulatory principles contributing to total mRNA changes upon oxygen deprivation should be analyzed to finally elucidate functional implications of those adaptive processes.

3.2. Results and discussion

I used thiol-linked alkylation for the metabolic sequencing of RNA (SLAM-Seq)[21] to characterize RNA dynamics under hypoxia. For this, I incubated monocytic THP-1 cells under normoxia (21% O_2), acute hypoxia (AH; 8 h 1% O_2), or chronic hypoxia (CH; 72 h 1% O_2) and labeled them during the last hour (to determine *de novo* synthesis) or the last 8 hours (to determine RNA stability) with the thiol-containing nucleoside analog 4-thiouridine (4sU). Chemical conversion of 4sU by iodoacetamide treatment before mRNA sequencing resulted in T-to-C mutations in the final reads, and thus allowed to estimate total and *de novo* synthesized RNAs from the same sequencing sample. While the short labeling time, used for estimation of *de novo* synthesis, aimed at minimizing the biasing effects of RNA degradation, an equilibrium between synthesis and degradation of RNAs was intended in the long labeling approach.

Differential gene expression (DGE) analysis of the total (with or without T-to-C conversions) read counts revealed that most changes occurred under extended hypoxia. Despite marked differences in the magnitude of expression changes between N and either AH or CH, similar enriched functional terms were found for both conditions. While hypoxia appeared amongst the top positively enriched hallmarks, which validates the experimental setup, enrichment of the functional terms cholesterol homeostasis and glycolysis underlines the remodeling of metabolic processes under oxygen deprivation. Within the top negatively enriched hallmarks, Myc targets and E2F targets indicate reduced proliferation and cell cycle progression under hypoxia.

Considering the hypothesis that the ratio shifts from predominantly transcriptional to post-transcriptional regulation from AH to CH, and since I observed more prominent changes at total mRNA level under CH than under AH, I continued analyzing RNA stability changes under hypoxia. I estimated RNA half-lives using the GRAND-SLAM (globally refined analysis of newly transcribed RNA and decay rates using SLAM-seq) pipeline, which utilizes the new-to-old ratio of mRNAs[22]. Interestingly, the calculated median half-lives of 10,263 transcripts were significantly lower under hypoxia (AH: 3.30 h; CH: 3.13 h) compared to N (3.71 h). To validate the results obtained by GRAND-SLAM, I additionally performed a pulse-chase experiment. Therefore, normoxic or hypoxic monocytic

THP-1 cells were labeled with 4sU during the last 8 h of the incubation before a washout was performed and T-to-C conversions were measured over a time course of 6 h. While estimated half-lives in general appeared longer, the median RNA stability was again and in concordance with a previous report, reduced under hypoxia[23]. In line, almost all differentially stability-regulated (DSR) transcripts (99%) showed lower RNA stabilities under AH and CH compared to N. Functional analyses suggested negative enrichment of Myc targets, oxidative phosphorylation, and fatty acid metabolism under hypoxia, indicating a contribution of post-transcriptional regulation in the metabolic remodeling, especially of oxygen-dependent processes.

I continued analyzing which of the DSR changes might contribute to total mRNA changes under hypoxia, and identified a small subgroup of compensatory DSR transcripts, which appeared enriched for immune responses. Considering the connection between hypoxia and inflammation[24], compensatory mRNA stability reduction appears to contribute to resolution of inflammation[25]. Within downregulated DGE transcripts, a subgroup of transcripts (hereafter called functional DSR transcripts) was identified with reduced half-lives under hypoxia. Of note, reduced mRNA stabilities were observed already under AH and persisted during CH, whereas most changes at total mRNA level were only visible under CH, indicating that decreased RNA half-lives caused total mRNA reduction. Functional analyses revealed enrichment in oxidative metabolism and translation within functional DSR transcripts. In fact, an intimate link between RNA stability and translation is known[26]. On the one hand, reduced translation under hypoxia as stress response could cause destabilization of mRNAs[26,27]. On the other hand, instead of being just a consequence of reduced translation, lowered mRNA availability due to decreased global RNA stability could attenuate energy-consuming protein synthesis as also postulated by Tiana and colleagues[23], while it might increase the translation efficiency of selective hypoxia-induced transcripts. In line, my data indicate that translational processes are subject to mRNA stability changes under hypoxia. Additionally, a strong enrichment in mitochondrial functions was observed within the functional DSR transcripts. As mitochondria are known to be massively remodeled upon oxygen deprivation, and even actively degraded by mitophagy[3], I decided to analyze the

transcripts contributing to the functional term mitochondria in more detail. 59 nuclear-encoded transcripts associated with diverse mitochondrial functions were destabilized under hypoxia, with reduction in the median half-lives from 16.02 h under N to 8.31 h under both AH and CH, corroborating our observations of reduced mitochondrial mass and oxygen consumption rates in chronic hypoxic THP-1 cells. Of note, regulation at a post-transcriptional level might enable faster adaptation after reoxygenation. The shortened half-lives and consequently reduced total mRNA levels under hypoxia of selected candidates, namely *mitochondrial ribosomal protein L40* (*MRPL40*), *carnitine palmitoyltransferase 1A* (*CPT1A*), and *translocase of the outer mitochondrial membrane 34* (*TOMM34*), were further validated by the wash-out data and an experiment with the transcription inhibitor actinomycin D. Conclusively, my data indicate a global reduction of RNA stability under hypoxia with functional implications as compensation of immune responses, or prevention of production of new mitochondria under conditions, in which they are actively degraded (Figure 2).

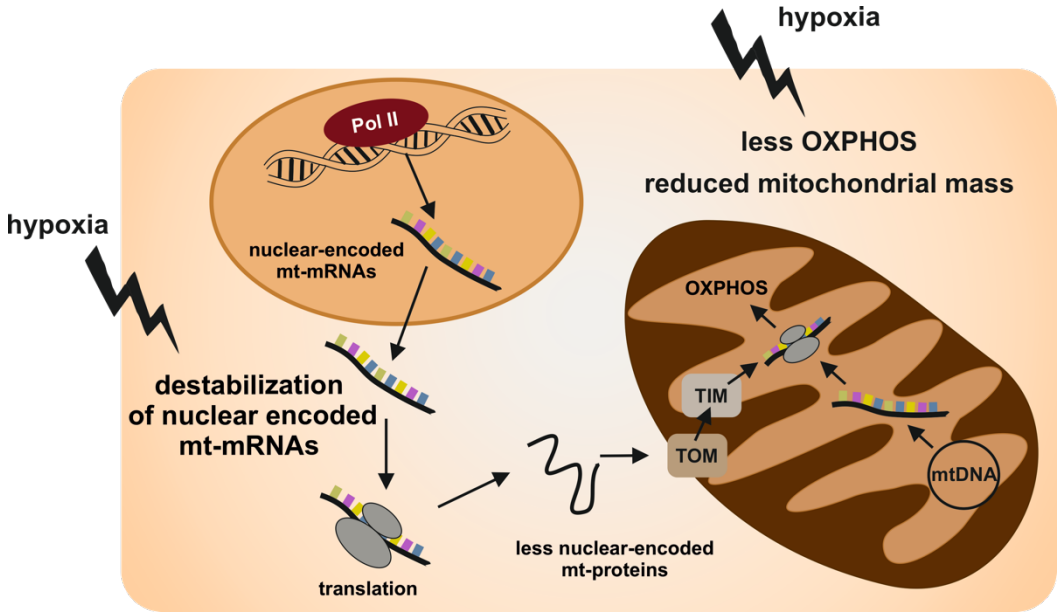

Figure 2: Functional implications of reduced RNA stability under hypoxia. Nuclear-encoded mt-mRNAs have reduced half-lives under hypoxia, causing lowered mRNA levels under chronic hypoxia, and thus probably less import of nuclear-encoded mt-proteins into mitochondria. This might prevent futile production of new mitochondria under conditions, in which mitochondrial mass and OXPHOS are reduced to prevent massive production of reactive oxygen species. Abbreviations: mt: mitochondrial; OXPHOS: oxidative phosphorylation; Pol II: RNA polymerase II; TIM/TOM: translocase of the inner/outer mitochondrial membrane.

To get further insights into the RNA dynamics under hypoxia, I performed differential gene expression analysis based on T-to-C counts, defined as differential *de novo* synthesis (DDNS). While DSR transcripts were mainly

destabilized, the vast majority of DDNS transcripts were upregulated under AH or CH compared to N. Functional analyses based on T-to-C counts revealed again hypoxia and cholesterol homeostasis as top positively enriched terms as previously observed for the DGE changes. Transcripts constituting the functional term hypoxia are mainly well-characterized HIF target genes. However, since regulation of cholesterol homeostasis under hypoxia, and especially its functional implications, are only partly understood, I decided to focus on those aspects in the second part of my PhD project. Indeed, most enzymes involved in cholesterol biosynthesis were upregulated already under AH, while maximal expression was reached after 24 – 48 h, before mRNA levels declined again. This was shown for the exemplary cholesterol biosynthesis transcripts *methylsterol monooxygenase 1* (*MSMO1*) and *lanosterol synthase* (*LSS*) in a time course experiment. In line with several oxygen-dependent steps during cholesterol biosynthesis and corroborating previous reports[5,6], I observed massive accumulation of lanosterol and 24,25-dihydrolanosterol, two early intermediates upstream of most oxygen-demanding steps, while the late cholesterol precursors desmosterol and lathosterol were reduced. Total cholesterol levels were only slightly reduced after oxygen deprivation. As transcriptional regulation can be assumed based on the DDNS analysis, I investigated involvement of the master transcription factor sterol regulatory element-binding protein 2 (SREBP2) known to induce cholesterol biosynthesis enzymes after sensing of local cholesterol depletion at the endoplasmic reticulum (ER). Inhibiting SREBP2 activity with PF-429242 and fatostatin indeed reduced hypoxic *MSMO1* induction, indicating that attenuated cholesterol biosynthetic flux under hypoxia causes SREBP2 feedback activation and consequently induction of cholesterol biosynthesis genes.

Of note, functional analyses of the upregulated DGE transcripts and the DDNS data set additionally revealed inflammation-associated terms to be enriched under hypoxia. Considering the continuously expanding field of immunometabolism[28], I wondered whether altered cholesterol metabolism might cause immune cell activation under hypoxia. Using the database Interferome v2.01[29], I found that approximately 75% of the transcripts were potential interferon-stimulated genes (ISGs), mainly known for their anti-viral function[30]. Interestingly, exemplary ISGs such as *2'-5'-oligoadenylate synthetase 1* (*OAS1*)

and *interferon regulatory factor 7* (*IRF7*) showed similar kinetics under hypoxia as SREBP2 targets, pointing towards a potential interplay.

In fact, reduced cholesterol biosynthesis flux was shown to enhance interferon (IFN) responses[31,32], whereas viral infection or IFNs can reduce SREBP2 target expression[33,34]. Although changes in specific cholesterol precursors, e.g., a reduction of desmosterol or an accumulation of 7-dehydrocholesterol, were postulated to cause enhanced ISG induction[31,35], inhibitors either mimicking hypoxic sterol alterations under normoxia or preventing accumulation of lanosterol/24,25-dihydrolanosterol under hypoxia did not change IFN responses in my experiments. Moreover, supplementation of early (mevalonate, geranylgeraniol) or late cholesterol precursors (lathosterol, 7-dehydrocholesterol, desmosterol), or cholesterol itself did not prevent hypoxic induction of *OAS1* and *IRF7*, indicating that changes of intermediates are not responsible for spontaneous ISG induction under hypoxia. Interestingly though, addition of late cholesterol precursors or cholesterol itself markedly reduced hypoxic *MSMO1* induction, whereas supplementation of early intermediates did not. Those data support the concept of SREBP2 activation as a consequence of locally lowered ER cholesterol levels due to reduced cholesterol biosynthesis flux (Figure 3).

In contrast to a previous study, which described SREBP2 to directly induce ISGs[36], my data indicate a SREPB2-independent mechanism under hypoxia. To further validate this assumption, I analyzed hypoxic ISG induction after treatment with the SREBP2 inhibitors PF-429242 and fatostatin. While inhibition of the activating SREBP2 cleavage at the golgi with PF-429242 had no influence, treatment of monocytic THP-1 with fatostatin markedly reduced hypoxic ISG induction. Of note, beside preventing SREBP2 translocation from ER to golgi, fatostatin was described to cause general reduction of ER-to-golgi trafficking and tubulin polymerization[37,38], suggesting that intact intracellular trafficking might be important for hypoxic ISG induction.

Since cholesterol homeostasis is regulated by a coordinated interplay between cholesterol uptake, *de novo* synthesis, intracellular redistribution, and export, I further aimed to characterize hypoxic monocytes under conditions, in which they rely on endogenous cholesterol synthesis. Interestingly, reducing the amount of fetal bovine serum (FBS), and thus the level of available low-density-lipoprotein

(LDL) cholesterol, not only increased *MSMO1*, but also *IRF7* and *OAS1* levels. Furthermore, I observed hypoxic induction of *CC motif chemokine ligand 2 (CCL2)* and *CXC motif chemokine ligand 10* (*CXCL10*), chemokine-ISGs, which were previously reported to be increased upon cholesterol disturbances[32], mainly under low FBS conditions. Inhibiting the Niemann-Pick C1 protein (NPC1), which prevents distribution of LDL-derived cholesterol from lysosomes to plasma membrane or ER, as well as re-supplementation of cholesterol confirmed a complex cholesterol-dependent regulatory network for different subgroups of ISGs. Future studies analyzing the intracellular cholesterol distribution under oxygen deprivation are necessary to fully understand the interplay between cholesterol homeostasis and ISG induction in hypoxic monocytes.

To further characterize the underlying regulatory principles, I analyzed hypoxic ISG induction in mitochondrial antiviral signaling protein (MAVS) or stimulator of interferon response cGAMP interactor (STING) knockout (KO) THP-1 cells. Both adaptor molecules get activated, when cytoplasmic pattern recognition receptors (PRRs) sense foreign nucleic acids[39,40]. Although MAVS deficiency reduced hypoxic induction of some ISGs, neither STING nor MAVS appeared as major signaling hubs, especially for the induction of *CCL2*. Interestingly, TLR4 inhibition markedly attenuated hypoxic induction of *OAS1* and *IRF7*, and generally reduced expression of *CCL2* and *CXCL10*. While the adaptor molecule myeloid differentiation primary response 88 (MyD88) appeared crucial for hypoxic induction of chemokine-ISGs, TIR-domain-containing adapter-inducing interferon-β (TRIF)-signaling seemed involved in hypoxic induction of *OAS1* and *IRF7* as indicated by inhibition of the downstream TANK-binding kinase 1 (TBK1). Of note, localization of TLR4 decides, if only MyD88- or additionally TRIF-dependent signaling takes place[41]. Taking into account that changes in cholesterol distribution can regulate motor proteins[42,43], I postulate a model, where altered cholesterol dynamics under hypoxia influence intracellular trafficking processes, endocytosis, or recycling processes, which again sensitizes TLR4-dependent signaling and causes ISG induction (Figure 3).

IFN responses are of special interest in the context of viral infections. Considering that coronavirus disease-2019 (COVID-19) is a viral disease, which in severe cases leads to hypoxemia, i.e., low blood oxygen levels, I wondered how hypoxic

priming influences the response of monocytes to severe acute respiratory syndrome coronavirus type 2 (SARS-CoV-2). Despite the lack of the major SARS-CoV-2 receptor angiotensin-converting enzyme 2 (ACE2) and its associated transmembrane serine protease 2 (TMPRSS2)[44], monocytic THP-1 were infected, although no active replication took place, corroborating earlier reports about monocytes[45]. I further observed that the viral load was unaffected by hypoxic priming, and the moderately raised *OAS1* and *IRF7* levels upon SARS-CoV-2 infection were only slightly increased in hypoxic monocytes. In contrast, the chemokine-ISGs *CCL2* and *CXCL10* were markedly increased in infected hypoxic THP-1. This observation was confirmed at protein level in supernatants. Considering that expression of both chemokines in macrophages from bronchoalveolar lavages of COVID-19 patients correlated positively with disease severity[46,47], hypoxemia might reprogram monocytes to promote the progression from a local inflammatory disease to a systemic inflammatory response syndrome[48–50]. In line with a previous report that SARS-CoV-2 spike protein directly activates TLR4[51], I observed similar *CCL2* and *CXCL10* induction in hypoxic THP-1 after spike protein incubation as after SARS-CoV-2 infection, whereas *OAS1* and *IRF7* levels only weakly increased by spike protein. Moreover, TLR4 inhibition mitigated both SARS-CoV-2 and spike protein-mediated *CCL2* and *CXCL10* induction strongly, while it reduced SARS-CoV-2-mediated *OAS1* and *IRF7* induction only marginally. This indicates that *OAS1* and *IRF7* are, in addition to TLR4, induced by single stranded SARS-CoV-2 RNA via TLR7/8[52]. In contrast, inhibition of SREBP2-associated trafficking by fatostatin reduced hypoxic induction of all ISGs upon spike protein or full SARS-CoV-2 treatment. Conclusively, these results support a concept of altered intracellular trafficking under hypoxia with enhanced TLR sensitivity, while ISG-specificity depends also on the availability of danger- or pathogen-associated molecular patterns (DAMPs/PAMPs). In concordance with the spontaneous hypoxic ISG induction, several DAMPs, e.g., high mobility group protein B1 (HMGB1) or S100 calcium-binding protein A8 (S100A8), were reported to be released under hypoxia and are able to activate TLR4[53,54]. However, further studies are necessary to identify the relevant DAMPs in this context, and to characterize the involvement of other TLRs in the hypoxic response to PAMPs like SARS-CoV-2.

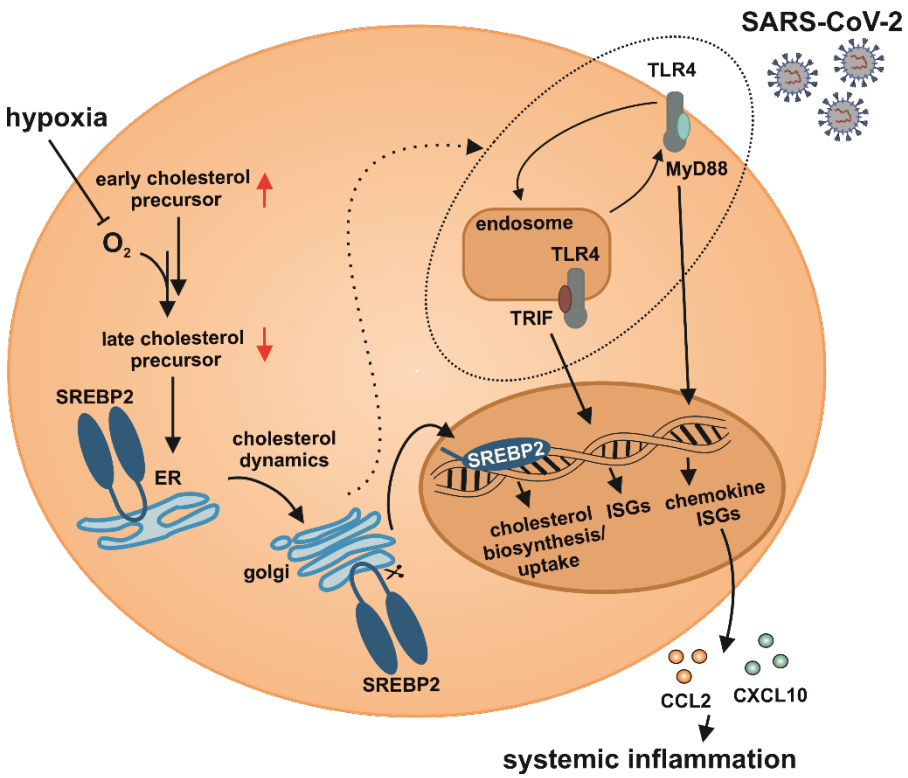

Figure 3: Model of functional implications of disturbed cholesterol metabolism under hypoxia. Cholesterol biosynthesis flux is reduced under hypoxia, lowering ER cholesterol levels and promoting SREBP2 feedback activation. Changed intracellular cholesterol distribution influences intracellular trafficking processes, thereby sensitizing TLR4-signaling, which causes ISG induction. Upon SARS-CoV-2 infection, hypoxic monocytes produce high levels of chemokine-ISGs, potentially contributing to systemic inflammation in severe cases of COVID-19. Abbreviations: CCL2: C-C motif chemokine ligand 2; CXCL10: C-X-C motif chemokine ligand 10; ER: endoplasmic reticulum; ISG: interferon-stimulated gene; MyD88: myeloid differentiation primary response 88; SARS-CoV-2: severe acute respiratory syndrome coronavirus type 2; SREBP2: sterol regulatory element-binding protein 2; TLR4: toll-like receptor 4; TRIF: TIR-domain-containing adapter-inducing interferon-β.

Taken together, I comprehensively analyzed RNA dynamics in monocytic cells in the course of hypoxia. While enhanced transcription correlated well with total mRNA changes under AH, mRNA destabilization became effective mainly under prolonged hypoxia. Beside a global reduction of mRNA half-lives under hypoxia, RNA destabilization added most notably to a massive decrease in nuclear-encoded mitochondrial transcripts, which might prevent the futile production of mitochondria under oxygen-restricted conditions (Figure 2). Furthermore, transcriptional induction of cholesterol biosynthesis genes revealed an immunometabolic crosstalk between disturbed cholesterol homeostasis and spontaneous induction of IFN-signaling in hypoxic monocytes. Thereby, hypoxia causes chemokine-ISG production upon SARS-CoV-2 infection, likely via the spike protein/TLR4/MyD88 axis, potentially contributing to systemic inflammation in severe cases of COVID-19 (Figure 3).

4. List of publications

1. **Bauer R**, Meyer SP, Raue R, Palmer MA, Guerrero Ruiz VM, Cardamone G, Rösser S, Heffels M, Roesmann F, Wilhelm A, Lütjohann D, Zarnack K, Fuhrmann DC, Widera M, Schmid T, Brüne B. Hypoxia-altered cholesterol homeostasis enhances the expression of interferon-stimulated genes upon SARS-CoV-2 infections in monocytes. *Front Immunol.* 2023;14:1121864. doi: 10.3389/fimmu.2023.1121864

2. **Bauer R**, Brüne B., Schmid T. Cholesterol metabolism in the regulation of inflammatory responses. *Front Pharmacol.* 2023;14:1121819. doi: 10.3389/fphar.2023.1121819

3. **Bauer R**, Meyer SP, Kloss KA, Guerrero Ruiz VM, Reuscher S, Zhou Y, Fuhrmann DC, Zarnack K, Schmid T, Brüne B. Functional RNA Dynamics Are Progressively Governed by RNA Destabilization during the Adaptation to Chronic Hypoxia. *Int J Mol Sci*. 2022;23(10):5824. doi: 10.3390/ijms23105824

4. Raue R, Frank AC, Fuhrmann DC, de la Cruz-Ojeda P, Rösser S, **Bauer R**, Cardamone G, Weigert A, Syed SN, Schmid T, Brüne B. MicroRNA-200c Attenuates the Tumor-Infiltrating Capacity of Macrophages. *Biology (Basel)*. 2022;11(3):349. doi: 10.3390/biology11030349

5. Knuth AK, Huard A, Naeem Z, Rappl P, **Bauer R**, Mota AC, Schmid T, Fleming I, Brüne B, Fulda S, Weigert A. Apoptotic Cells induce Proliferation of Peritoneal Macrophages. *Int J Mol Sci*. 2021;22(5):2230. doi: 10.3390/ijms22052230

6. Rappl P, Rösser S, Maul P, **Bauer R**, Huard A, Schreiber Y, Thomas D, Geisslinger G, Jakobsson PJ, Weigert A, Brüne B, Schmid T. Inhibition of mPGES-1 attenuates efficient resolution of acute inflammation by enhancing CX3CL1 expression. *Cell Death Dis*. 2021;12(2):135. doi: 10.1038/s41419-021-03423-2

7. Rehwald C, Schnetz M, Urbschat A, Mertens C, Meier JK, **Bauer R**, Baer P, Winslow S, Roos FC, Zwicker K, Huard A, Weigert A, Brüne B, Jung M. The iron load of lipocalin-2 (LCN-2) defines its pro-tumour function in clear-

cell renal cell carcinoma. *Br J Cancer*. 2020;122(3):421-433. doi: 10.1038/s41416-019-0655-7

8. Susen RM, **Bauer R**, Olesch C, Fuhrmann DC, Fink AF, Dehne N, Jain A, Ebersberger I, Schmid T, Brüne B. Macrophage HIF-2α regulates tumor-suppressive Spint1 in the tumor microenvironment. *Mol Carcinog*. 2019;58(11):2127-2138. doi: 10.1002/mc.23103

9. Fettel J, Kühn B, Guillen NA, Sürün D, Peters M, **Bauer R**, Angioni C, Geisslinger G, Schnütgen F, Meyer Zu Heringdorf D, Werz O, Meybohm P, Zacharowski K, Steinhilber D, Roos J, Maier TJ. Sphingosine-1-phosphate (S1P) induces potent anti-inflammatory effects in vitro and in vivo by S1P receptor 4-mediated suppression of 5-lipoxygenase activity. *FASEB J*. 2019;33(2):1711-1726. doi: 10.1096/fj.201800221R

10. Jung M, Mertens C, **Bauer R**, Rehwald C, Brüne B. Lipocalin-2 and iron trafficking in the tumor microenvironment. *Pharmacol Res*. 2017;120:146-156. doi: 10.1016/j.phrs.2017.03.018

5. Contribution statement on publications

1. I contributed to the conceptualization of the study, performed and analyzed the experiments, was responsible for the bioinformatics analysis, and wrote the original draft of the manuscript.

2. I wrote major parts of the review article.

3. I conceived the study and experimental design, performed and analyzed the experiments, conducted the bioinformatics analysis, and contributed to writing the manuscript draft.

4. As a co-author, I supported molecular biology analyses.

5. As a co-author, I supported the next-generation sequencing experiments.

6. As a co-author, I supported the next-generation sequencing experiments.

7. As a co-author, I was responsible for site-directed plasmid mutagenesis.

8. As a co-author, I supported molecular biology analyses and cell culture experiments.

9. As a co-author, I supported isolation of primary cells, protein activity assays and molecular biology analyses.

10. As a co-author, I contributed to writing the manuscript.

6. Publications

frontiers | Frontiers in Immunology

TYPE Original Research
PUBLISHED 12 June 2023
DOI 10.3389/fimmu.2023.1121864

OPEN ACCESS

EDITED BY
Miguel Angel Alejandre Alcazar,
University Hospital of Cologne, Germany

REVIEWED BY
Michael B. Fessler,
National Institute of Environmental Health Sciences (NIH), United States
Marten A. Hoeksema,
Amsterdam UMC, Netherlands

*CORRESPONDENCE
Tobias Schmid
t.schmid@biochem.uni-frankfurt.de

RECEIVED 12 December 2022
ACCEPTED 30 May 2023
PUBLISHED 12 June 2023

CITATION
Bauer R, Meyer SP, Raue R, Palmer MA, Guerrero Ruiz VM, Cardamone G, Rösser S, Heffels M, Roesmann F, Wilhelm A, Lütjohann D, Zarnack K, Fuhrmann DC, Widera M, Schmid T and Brüne B (2023) Hypoxia-altered cholesterol homeostasis enhances the expression of interferon-stimulated genes upon SARS-CoV-2 infections in monocytes.
Front. Immunol. 14:1121864.
doi: 10.3389/fimmu.2023.1121864

Hypoxia-altered cholesterol homeostasis enhances the expression of interferon-stimulated genes upon SARS-CoV-2 infections in monocytes

Rebekka Bauer[1], Sofie Patrizia Meyer[1], Rebecca Raue[1], Megan A. Palmer[1], Vanesa Maria Guerrero Ruiz[1], Giulia Cardamone[1], Silvia Rösser[1], Milou Heffels[1], Fabian Roesmann[2], Alexander Wilhelm[2], Dieter Lütjohann[3], Kathi Zarnack[4], Dominik Christian Fuhrmann[1,5], Marek Widera[2], Tobias Schmid[1,5]* and Bernhard Brüne[1,5,6,7]

[1]Institute of Biochemistry I, Faculty of Medicine, Goethe University Frankfurt, Frankfurt, Germany, [2]Institute of Medical Virology, University Hospital Frankfurt, Goethe University Frankfurt, Frankfurt, Germany, [3]Institute of Clinical Chemistry and Clinical Pharmacology, University of Bonn, Bonn, Germany, [4]Buchmann Institute for Molecular Life Sciences (BMLS), Faculty of Biological Sciences, Goethe University Frankfurt, Frankfurt, Germany, [5]German Cancer Consortium (DKTK), Partner Site Frankfurt, Frankfurt, Germany, [6]Frankfurt Cancer Institute, Goethe University Frankfurt, Frankfurt, Germany, [7]Fraunhofer Institute for Translational Medicine and Pharmacology ITMP, Frankfurt, Germany

Hypoxia contributes to numerous pathophysiological conditions including inflammation-associated diseases. We characterized the impact of hypoxia on the immunometabolic cross-talk between cholesterol and interferon (IFN) responses. Specifically, hypoxia reduced cholesterol biosynthesis flux and provoked a compensatory activation of sterol regulatory element-binding protein 2 (SREBP2) in monocytes. Concomitantly, a broad range of interferon-stimulated genes (ISGs) increased under hypoxia in the absence of an inflammatory stimulus. While changes in cholesterol biosynthesis intermediates and SREBP2 activity did not contribute to hypoxic ISG induction, intracellular cholesterol distribution appeared critical to enhance hypoxic expression of chemokine ISGs. Importantly, hypoxia further boosted chemokine ISG expression in monocytes upon infection with severe acute respiratory syndrome coronavirus type 2 (SARS-CoV-2). Mechanistically, hypoxia sensitized toll-like receptor 4 (TLR4) signaling to activation by SARS-CoV-2 spike protein, which emerged as a major signaling hub to enhance chemokine ISG induction following SARS-CoV-2 infection of hypoxic monocytes. These data depict a hypoxia-regulated immunometabolic mechanism with implications for the development of systemic inflammatory responses in severe cases of coronavirus disease-2019 (COVID-19).

KEYWORDS

hypoxia, immunometabolism, cholesterol, SREBP2, COVID-19, systemic inflammation

1 Introduction

The availability of molecular oxygen (O_2) is critical for many cellular functions, most notably cellular energy production via oxidative phosphorylation. Thus, various mechanisms evolved to cope with hypoxia, especially with respect to metabolic rewiring in order to protect cells from detrimental effects due to the lack of oxygen (1, 2). Not surprisingly, hypoxia and the resulting adaptive processes are tightly linked to numerous diseases including cancer, as well as metabolic and inflammatory disorders (3). The multilayered crosstalk between metabolic changes and immune responses also forms the basis for the emerging field of immunometabolism (4). While the concept of immunometabolism was termed merely 10 years ago, initial evidence dates back to the early 1990s, when increased expression of the pro-inflammatory cytokine tumor necrosis factor α (TNFα) was observed in rodent models of obesity and was shown to contribute to the development of insulin resistance (5). Along similar lines, altered cholesterol dynamics affect immune functions, as exemplified by observations that upon excessive uptake of low density lipoprotein (LDL)-cholesterol macrophages acquire a pro-inflammatory, foam cell phenotype within atherosclerotic lesions (6). Moreover, using statins to lower plasma LDL-cholesterol concentrations elicited potent anti-inflammatory effects in patients with inflammatory diseases like rheumatoid arthritis or metabolic syndrome (7, 8). Furthermore, intracellular cholesterol trafficking and biosynthetic signaling were shown to activate the inflammasome (9, 10), whereas accumulation of the cholesterol precursor mevalonate induced a trained immunity phenotype in monocyte-derived cells (11). Of note, changes in cholesterol biosynthesis flux also altered anti-viral responses by enhancing interferon (IFN) signaling (12, 13). The connection between IFN signaling and cholesterol metabolism appears to be bidirectional though, as cholesterol biosynthesis enzymes were downregulated in response to viral infection or IFN treatment (14, 15).

In this study, we observed a coinciding transcriptional upregulation of cholesterol biosynthesis enzymes and IFN-stimulated genes (ISGs) in hypoxic monocytes. Mechanistically, hypoxia-evoked changes in cholesterol dynamics enhanced toll-like receptor (TLR) signaling and consequently IFN responses. Hypoxia further increased chemokine ISG production in monocytes upon infection with severe acute respiratory syndrome coronavirus type 2 (SARS-CoV-2), thereby providing a novel concept how hypoxemia, i.e., low blood oxygen levels, might favor systemic inflammation in severe cases of coronavirus disease-2019 (COVID-19).

2 Materials and methods

2.1 Chemicals

All chemicals were purchased from Thermo Fisher Scientific GmbH (Dreieich, Germany), if not indicated otherwise. Fatostatin hydrobromide, TAK-242, IKK-16 hydrochloride, lathosterol, 7-dehydrocholesterol, and desmosterol were purchased from Cayman Chemical (Ann Harbor, MI, USA), PF-429242 dihydrochloride, ketoconazole, methyl-β-cyclodextrin-complexed (water-soluble) cholesterol, mevalonolactone, and geranylgeraniol from Sigma-Aldrich (Taufkirchen, Germany), U18666A from Enzo Life Sciences (Lausen, Switzerland), simvastatin from Selleck Chemicals (Planegg, Germany), NB-598 maleate from Adooq Bioscience (Irvine, CA, USA), enpatoran from TargetMol (Wellesley Hills, MA, USA), T0901317 from Tocris (Wiesbaden-Nordenstadt, Germany), TJ-M2010-5 from Hycultec GmbH (Beutelsbach, Germany), and BX-795 from MedChemExpress (Monmouth Junction, NJ, USA).

2.2 Cell culture

THP-1 cells were obtained from ATCC, and THP-1 STING- and MAVS-KO cells as well as the corresponding original WT THP-1 cells were kindly provided by Prof. Veit Hornung (LMU Munich, Germany) (16). THP-1 cells were cultured in Roswell Park Memorial Institute (RPMI) 1640 medium, supplemented with 100 U/mL penicillin, 100 µg/mL streptomycin, and 10% or 5% FBS (Capricorn Scientific GmbH, Ebsdorfergrund, Germany or Sigma-Aldrich), dependent on the cholesterol concentration of the respective FBS batch. For experiments performed under low FBS levels, the percentage of FBS was reduced to $1/10^{th}$ of the FBS amount used for maintaining the cells. Cells were kept at 37°C in a humidified atmosphere with 5% CO_2. For hypoxic incubations, cells were transferred to a hypoxia workstation (SCI-tive, Baker Ruskinn, Bridgend, South Wales, UK) at 37°C with 5% CO_2 and 1% O_2.

2.3 IFNAR neutralization

THP-1 cells were treated with 5 µg/mL α-IFNAR2 antibody (Clone MMHAR-2 Mab, PBL assay science, Piscataway, NJ, USA; cat. no. 21385) or IgG2a isotype control antibody (Clone C1.18.4, Bio X Cell, Lebanon, NH, USA; cat. no. BE0085) prior to normoxic or hypoxic incubation for 24 h.

2.4 SARS-CoV-2 infection

Lung-derived A549-AT cells, constitutively expressing ACE2 and TMPRSS2 (17), were infected with SARS-CoV-2 strain FFM1 (accession number MT358638.1) (18) using a multiplicity of infection (MOI) of 0.1 in Minimum Essential Medium (MEM) containing 1% FBS, 100 U/mL penicillin, 100 µg/mL streptomycin, and 4 mM L-glutamine (all Sigma-Aldrich). After 1 h inoculation at 37°C and 5% CO_2, cells were washed once with PBS and fresh medium was added. 48 h post infection (hpi), virus-containing supernatants were centrifuged and stored at -80°C until further usage.

Monocytic THP-1 cells were cultured for 24 h in RPMI 1640 with 1% FBS, 100 U/mL penicillin, and 100 µg/mL streptomycin

(all Sigma-Aldrich) at 37°C with 5% CO_2 and either 21% or 1% O_2. Optionally, 10 µM fatostatin, 10 µM TAK-242, or 0.1% DMSO (Carl Roth, Karlsruhe, Germany) were added 1 h before starting hypoxic cultures. Experiments involving SARS-CoV-2 were carried out in an oxygen-adjustable incubator in a biosafety level 3 (BSL3) facility. After 24 h normoxic or hypoxic incubations, THP-1 cells were infected with the SARS-CoV-2 containing virus supernatants. Supernatants of non-infected A549-AT were used as controls. Cells were washed 1 hpi with PBS, and either directly lysed for RNA isolation, or incubated for additional 5 h, before freezing debris-free supernatants at -80°C for subsequent ELISAs and lysing cells for RNA isolation. Sample inactivation for further processing was performed with previously evaluated methods (19).

2.5 Stimulation with SARS-CoV-2 spike protein

THP-1 cells were pre-incubated for 24 h under normoxia or hypoxia before 5 µg/mL recombinant SARS-CoV-2 spike trimer (S1 +S2) (BPS Bioscience, San Diego, CA, USA; cat. no. 100728) or 0.04% glycerol (Sigma-Aldrich) as vehicle control were added for additional 8 h normoxic or hypoxic incubations.

2.6 RNA isolation, reverse transcription, and quantitative polymerase chain reaction

Total RNA from THP-1 cells was extracted using either TRIzol or the RNeasy mini kit (for SARS-CoV-2 experiments; Qiagen, Hilden, Germany) according to the manufacturer's instructions. The Maxima First Strand cDNA synthesis kit was used for reverse transcription and qPCR analyses were performed using PowerUp SYBR Green Master Mix on QuantStudio 3 and 5 PCR Real-Time Systems (Thermo Fisher Scientific). Primers were ordered from Biomers (Ulm, Germany) and are listed in Supplementary Table S1, except the primer for *IRF7* (Hs_IRF7_1_SG QuantiTect Primer Assay), which was purchased from Qiagen.

2.7 Differential gene expression analysis

Previously, we characterized transcriptome-wide changes in *de novo* synthesis and RNA stability under hypoxia in monocytes by a metabolic labeling approach. Here, we focused on total mRNA changes within the previously published comprehensive metabolic RNA sequencing data of THP-1 cells incubated for 8 h and for 72 h under hypoxia (acute hypoxia (= AH) and chronic hypoxia (= CH), respectively), or under normoxia (N) (GSM5994456 to GSM5994464) (20). For differential gene expression analyses, raw reads were quality-, adapter-, and polyA-trimmed using Cutadapt (21) and unique molecular identifier and linker sequences were removed before the processed reads were aligned to the human genome (GRCh38) with Ensembl gene annotation (release 80) using STAR (version 2.7.6a) (22). Transcript counts were determined using htseq-count with default parameters (23) and Ensembl gene annotation (release 80). Differentially expressed genes were determined using DESeq2 in R (24). Log_2-transformed fold changes in genes were shrunken using the estimator "ashr". Adjusted *p*-values (*padj*) were determined using Benjamini-Hochberg correction, and differentially regulated transcripts between N, AH, and CH were visualized with ComplexHeatmaps (25). Hereto, read counts were corrected for library size using DESeq2 size factors and subjected to a row-wise *z*-score normalization. Transcripts were grouped into three groups by *k*-means clustering. For the identification of enriched functional annotation clusters, transcripts downregulated (first cluster) or upregulated (second and third clusters) by hypoxia were analyzed separately using the Database for Annotation, Visualization and Integrated Discovery (DAVID) against the gene sets "GOTERM_BP_DIRECT" and "UP_KW_BIOLOGICAL_PROCESS" (26, 27). A list of all detected transcripts (basemean > 0, for all conditions) served as background data set.

2.8 Interferome analysis

Transcripts constituting the functional annotation cluster "immune cell activation" within the hypoxic upregulated transcripts were used as input for Interferome v2.01 (28). Interferome v2.01 compared the input transcripts with a comprehensive database of collected gene expression data from different cell types after treatment with type I, II, or III IFNs. For further analyses, we used only the interferon-stimulated genes (ISGs) from all identified interferon-regulated genes (IRGs) within the "immune cell activation" cluster. The distribution of the putative type I, II, and/or III IFN targets was visualized using VennDiagram (29), and the library-size and row-wise *z*-score normalized read counts of the so-identified ISGs under N, AH, and CH were visualized with ComplexHeatmaps (25).

2.9 Immunoblots

All reagents used for immunoblotting were purchased from Sigma-Aldrich, if not indicated otherwise. THP-1 cells were resuspended in lysis buffer (10 mM Tris-HCl, 6.65 M Urea, 10% glycerol, 1% SDS (Carl Roth), pH 7.4; freshly supplemented with 1 mM DTT (Carl Roth), protease inhibitor and phosphatase inhibitor mixes (cOmplete and phosSTOP, respectively (Roche, Grenzach-Wyhlen, Germany)), and sonicated. 70 µg total protein were separated by sodium dodecylsulfate polyacrylamide gel electrophoresis and transferred onto nitrocellulose membranes (GE Healthcare, Chalfont St Giles, UK). Proteins were detected using specific antibodies for LSS (Proteintech, Planegg-Martinsried, Germany; cat. no. 13715-1-AP), β-tubulin (Abcam, Cambridge, UK; cat. no. ab7780), pSTAT1 (Tyr701; Cell Signaling, Leiden, Netherlands; cat. no. 7649S), or STAT1 (Cell Signaling; cat. no. 9172S) and appropriate IRDye secondary antibodies (LI-COR Biosciences, Bad Homburg, Germany), and visualized using the Odyssey infrared imaging system (LI-COR Biosciences).

2.10 Immunofluorescent staining

THP-1 cells were incubated for 8 h under normoxia or hypoxia and subsequently fixed with ROTI®Histofix (Carl Roth) for 10 min at 4°C. After transferring to object slides using a cytospin centrifuge, cells were permeabilized with 0.1% triton X in PBS for 10 min, followed by blocking with 10% normal goat serum (Sigma-Aldrich) with 100 mM glycine. Primary rabbit anti-SREBP2 antibody (Cayman Chemical; cat. no. 10007663) was incubated at 1:500 in 2% normal goat serum overnight at 4°C. F(ab')2 goat anti-rabbit IgG Alexa fluor™ plus 488 secondary antibody (Thermo Fisher Scientific; cat. no. A48282) was incubated at 1:500 in 2% normal goat serum for 45 min at room temperature. Cells were counterstained with 1 µg/mL 4',6-diamidino-2-phenylindole (DAPI) for 1 min. Whole slide scans were performed using Vectra Polaris (Akoya Biosciences, Marlborough, MA, USA) at 20x magnification. Image analysis was performed in QuPath v0.4.2 (30), cell detection with a 5 µm expansion was performed on annotations of the whole cytospin area. Mean nuclear intensity values per cell were generated for analysis.

2.11 ELISAs

CCL2 and CXCL10 protein levels in the supernatants of SARS-CoV-2 infected THP-1 cells were quantified using SimpleStep ELISA kits from Abcam according to the manufacturer's instructions.

2.12 Sterol measurements

THP-1 cells were incubated for up to 24 h under normoxia or hypoxia. Optionally, cells were pre-incubated with 1 µM simvastatin, 10 µM NB-598, 10 µM ketoconazole, or 0.1% DMSO for 1 h. Sterol content was determined by gas chromatography-mass spectrometry-selected ion monitoring (GC-MS-SIM) as previously described (31–33). Briefly, cell pellets were dried in a speedvac concentrator (12 mbar; Savant AES 1000) and weighed. Cholesterol and cholesterol precursors were extracted using chloroform. After alkaline hydrolysis, the concentrations of the cholesterol precursors lanosterol, 24,25-dihydrolanosterol, lathosterol, and desmosterol were measured with GC-MS-SIM in selected ion monitoring mode. The trimethylsilyl-ethers of the sterols were separated on a DB-XLB (30 m length x 0.25 mm internal diameter, 0.25 µm film) column (Agilent Technologies, Waldbronn, Germany) using the 6890N Network GC system (Agilent Technologies). Epicoprostanol (Steraloids, Newport, RI, USA) was used as an internal standard, to quantify the non-cholesterol sterols (Medical Isotopes, Pelham, NH, USA) on a 5973 Network MSD (Agilent Technologies). Total cholesterol was measured by GC-flame ionization detection on an HP 6890 GC system (Hewlett Packard, Waldbronn, Germany), equipped with a DB-XLB (30 m length x 0.25 mm internal diameter, 0.25 µm film) column (Agilent Technologies) using 5α-cholestane (Steraloids) as internal standard.

2.13 Statistical analysis

Data are reported as means ± SEM of at least three independent experiments. Statistical analyses were carried out using GraphPad Prism v9.3.1 (GraphPad Software, San Diego, CA, USA) or R v4.0.5 (34). Statistical significance was estimated either using two-tailed paired t-test, one-way or two-way repeated measures ANOVA with Holm-Šídák's multiple comparisons test as applicable. If residuals were assumed to be not normally distributed (based on quantile-quantile (Q-Q) plots), data were log-transformed before statistical testing.

3 Results

3.1 Hypoxia enhances expression of cholesterol biosynthesis enzymes and increases IFN signaling

Since hypoxia is a major contributing factor to various immune system-associated diseases, we determined RNA dynamics in human monocytic THP-1 cells in response to acute (8 h 1% O_2 = AH) and chronic (72 h 1% O_2 = CH) hypoxia (20). In line with the major regulatory impact of hypoxia, 2632 transcripts appeared differentially expressed (*padj* < 0.05, |log2FC| > 0.3) between normoxia (21% O_2 = N) and hypoxia (AH and/or CH), however, following different regulatory dynamics (Figure 1A). While 1268 targets decreased under acute and/or chronic hypoxia (first cluster), 1364 targets increased either cumulatively during hypoxic incubations (second cluster) or only in response to CH (third cluster) (Supplementary Table S2). Functionally, cell cycle and respiration emerged as top enriched annotations amongst the downregulated transcripts, whereas cholesterol metabolism and immune cell activation were enriched within the upregulated candidates (Figure 1B; Supplementary Table S2). In fact, the majority of enzymes involved in the cholesterol biosynthesis cascade were upregulated, mostly already under AH (Figures 1A, C). To obtain further insights into the dynamics of cholesterol biosynthesis gene expression under hypoxia, we determined expression of representative genes in THP-1 cells over a time course of up to 72 h of hypoxia. mRNA expression of the selected candidates *lanosterol synthase* (*LSS*) and *methylsterol monooxygenase 1* (*MSMO1*) increased after 8 h of hypoxia, reaching maximal levels at 24 - 48 h, thereafter decreasing (Figure 1D). In line, LSS protein expression increased after 24 h and remained elevated up to 72 h of hypoxia (Figure 1E).

Of note, changes in cholesterol metabolism were previously linked to altered immune responses (35), especially to interferon (IFN) signaling (12, 13). Since "immune cell activation" emerged as the second most enriched function within the differentially induced genes in hypoxic THP-1 monocytes (Figure 1B), we determined the contribution of interferon-stimulated genes (ISGs) to the hypoxia-induced immune response using the Interferome v2.01 database (28). Of note, 75% (60 of 80) of the immune activation-associated transcripts regulated under hypoxia in THP-1 cells were potential ISGs. Of these the vast majority, i.e., 60% (= 36), were proposed

10.3389/fimmu.2023.1121864

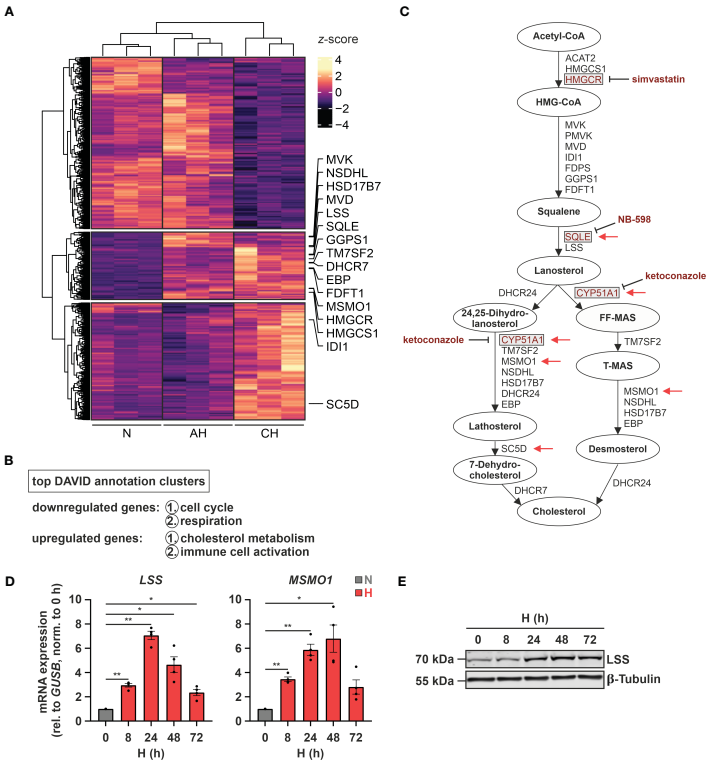

FIGURE 1
Hypoxia induces cholesterol biosynthesis enzymes. **(A)** RNA expression in THP-1 cells exposed to hypoxia (H; 1% O_2) for 8 h (acute hypoxia = AH) or 72 h (chronic hypoxia = CH) was determined relative to normoxic THP-1 cells (N; 21% O_2) by RNA-Seq (n = 3). Differentially expressed genes (*padj* < 0.05, |log2FC| > 0.3) were visualized in a heatmap (*z*-score normalized counts) and categorized by *k*-means clustering. Cholesterol biosynthesis genes are highlighted. **(B)** Top two functional annotation clusters of down- or upregulated transcripts identified by DAVID (26, 27). **(C)** Schematic representation of the cholesterol biosynthesis cascade. Oxygen-demanding steps are highlighted by red arrows and selected inhibitors as well as their target enzymes are marked in red. **(D, E)** THP-1 cells were incubated under N (grey) or H (red) for the indicated times (n = 4). **(D)** *LSS* and *MSMO1* mRNA expression was analyzed by RT-qPCR and normalized to *GUSB* expression. **(E)** LSS protein expression was determined by Western blot analysis. β-tubulin served as loading control. The blot is representative of four independent experiments. All data are means ± SEM and were statistically analyzed using one-way repeated measures ANOVA with Holm-Šídák's multiple comparisons test (*p < 0.05, **p < 0.01).

targets of both type I and II IFNs, 28% (= 17) were exclusive type II IFN targets, two exclusive type I IFN targets, and five associated with type I, II, as well as III IFNs (Figure 2A; Supplementary Table S3). Interestingly, in contrast to cholesterol biosynthesis-associated targets most ISGs (49 of 60) were predominantly induced under CH (Figure 2B; Supplementary Table S3). Refined hypoxia time course experiments validated maximal induction of *2'-5'-oligoadenylate synthetase 1* (*OAS1*), *interferon regulatory factor 7* (*IRF7*), and *interferon α-inducible protein 6* (*IFI6*) at 48 h of hypoxia, whereas *interferon β1* (*IFNB1*) was maximal after 24 h (Figure 2C). To determine whether early IFN-β induction in hypoxia might contribute to the expression of some of the ISGs increasing later on, we blocked IFN-β-receptor-dependent signaling in hypoxic THP-1 cells (24 h) using an α-interferon-α/β-receptor subunit 2 (IFNAR2) antibody (5 µg/mL). While *IFNB1* and *IRF7* expression was not influenced by IFNAR2 neutralization compared to the respective IgG2a-isotype control, *OAS1* and *IFI6* induction were markedly reduced upon IFNAR2 blockage (Figure 2D). In line with activation of type I IFN receptor signaling, the downstream effector signal transducer and activator of transcription 1 (STAT1) was phosphorylated (Tyr701) after 8 - 24h of hypoxia (Supplementary Figure 1).

Taken together, hypoxia enhances the expression of nearly all enzymes of the cholesterol biosynthesis cascade and at the same time induces a broad range of ISGs in monocytic THP-1 cells, in part by a secondary IFNAR-dependent amplification loop.

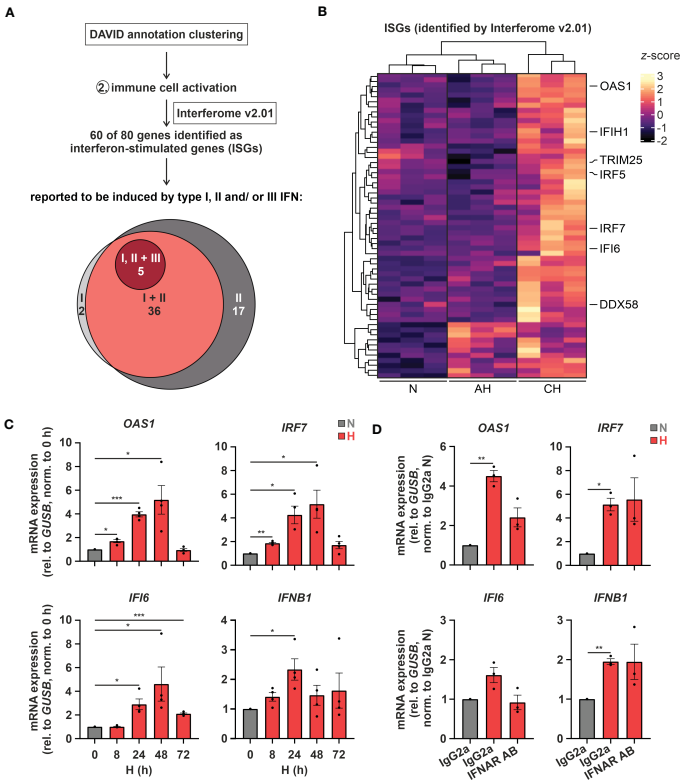

FIGURE 2
Hypoxia increases interferon (IFN) signaling. **(A)** IFN-stimulated genes (ISGs) within the transcripts constituting the functional annotation cluster "immune cell activation" were identified using Interferome v2.01 (28). Venn diagram depicts proposed ISGs regulated by type I, II, and/or III IFNs according to Interferome v2.01. **(B)** Heatmap representing differentially expressed, hypoxia-induced ISGs (*z*-score normalized count data) under normoxia (N), acute hypoxia (AH; 8 h), and chronic hypoxia (CH; 72h) (n = 3; *padj* < 0.05, |log2FC| > 0.3). Selected ISGs are highlighted. **(C)** THP-1 cells were incubated under N (grey) or H (red) for the indicated times (n = 4) or **(D)** treated with 5 µg/mL α-IFNAR2 antibody or an IgG2a-isotype control and incubated under N (grey) or H (red) for 24 h (n = 3). *OAS1*, *IRF7*, *IFI6*, and *IFNB1* mRNA expression was analyzed by RT-qPCR and normalized to *GUSB* expression. All data are means ± SEM and were statistically analyzed by one-way repeated measures ANOVA with Holm-Šídák's multiple comparisons test (*$p < 0.05$, **$p < 0.01$, ***$p < 0.001$).

3.2 Hypoxic ISG induction is not directly affected by cholesterol biosynthesis intermediates

Considering previous reports showing that a disturbance in cholesterol metabolism may increase IFN signaling (12, 13), we asked whether changes in cholesterol metabolism might also contribute to ISG induction under hypoxia. To this end, we initially measured sterol levels in THP-1 cells in the course of hypoxia. In accordance with several oxygen-demanding steps within the cholesterol biosynthesis cascade (Figure 1C, red arrows), lathosterol and desmosterol, i.e., sterol intermediates downstream of the major oxygen-demanding reactions, were reduced, while the early cholesterol precursors lanosterol and 24,25-dihydrolanosterol markedly accumulated under hypoxia (Figure 3A; Supplementary Figure 2). Levels of total cholesterol appeared to be only minimally attenuated by reduced oxygen, though at much higher total amounts than the other sterols. Noteworthy, while changes in lanosterol and lathosterol were almost maximal already at 4 h of hypoxia (Figure 3A), expression of cholesterol biosynthesis enzymes as well as of ISGs remained unaltered at this early time point (Supplementary Figure 3), suggesting that changes in cholesterol metabolites might contribute to the observed gene expression changes. To prevent or mimic hypoxic accumulation of lanosterol and 24,25-dihydrolanosterol, we next pre-treated THP-1 cells with either the

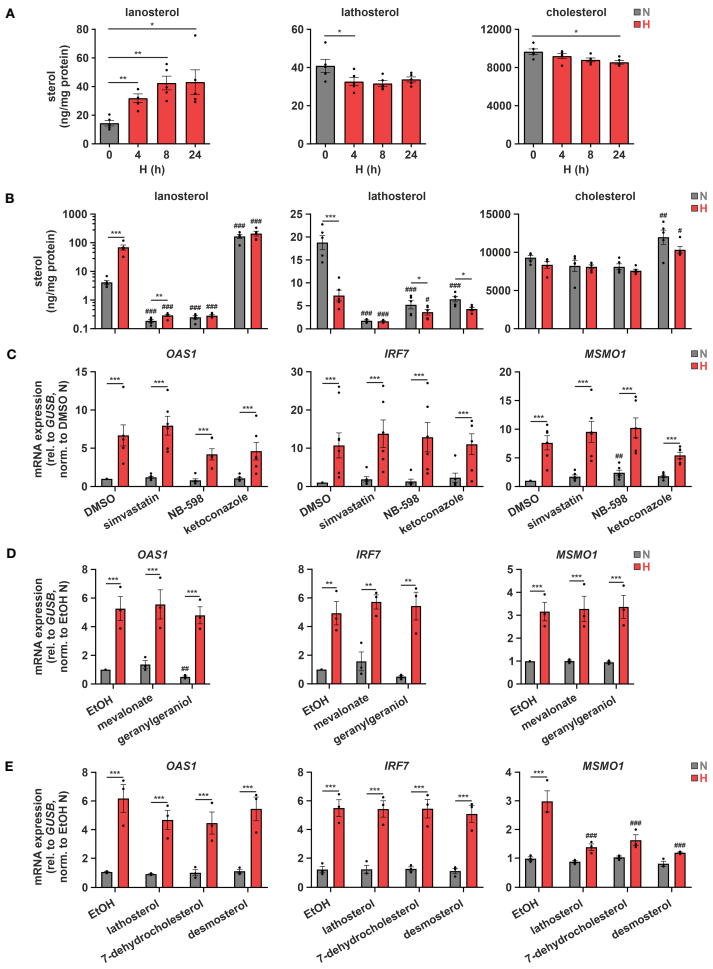

FIGURE 3
Hypoxic ISG induction is not directly affected by cholesterol biosynthesis intermediates. **(A)** THP-1 cells were incubated under N (grey) or H (red) for the indicated times (n = 5). Sterol levels were measured by GC-MS. **(B, C)** THP-1 cells were pre-incubated for 1 h with 1 µM simvastatin, 10 µM NB-598, 10 µM ketoconazole, or DMSO, prior to incubation under N (grey) or H (red) for 24 h (n = 5). **(B)** Cellular sterol levels were measured by GC-MS. **(C)** *OAS1*, *IRF7*, and *MSMO1* mRNA expression was analyzed by RT-qPCR and normalized to *GUSB* expression. **(D, E)** THP-1 cells were pre-incubated for 1 h with **(D)** the early cholesterol precursors mevalonate (300 µM) or geranylgeraniol (15 µM) (n = 3), **(E)** the late cholesterol precursors lathosterol, 7-dehydrocholesterol, or desmosterol (each 5 µM) (n = 3), or appropriate solvent controls, prior to incubation under N (grey) or H (red) for 24 h. *OAS1*, *IRF7*, and *MSMO1* mRNA expression was analyzed by RT-qPCR and normalized to *GUSB* expression. All data are means ± SEM and were statistically analyzed using one-way repeated measures ANOVA with Holm-Šidák's multiple comparisons test **(A)**, or two-way repeated measures ANOVA with Holm-Šidák's multiple comparisons test **(B–E)** (*$p < 0.05$, **$p < 0.01$, ***$p < 0.001$; #$p < 0.05$, ##$p < 0.01$, ###$p < 0.001$ (compared to respective solvent controls)).

3-hydroxy-3-methylglutaryl-CoA reductase (HMGCR) inhibitor simvastatin (1 µM), the squalene epoxidase (SQLE) inhibitor NB-598 (10 µM), or the cytochrome P450 51A1 (CYP51A1, lanosterol 14α-demethylase) inhibitor ketoconazole (10 µM) for 1 h before incubating them for 24 h under normoxia or hypoxia (see Figure 1C for interventions). Inhibition of HMGCR and SQLE significantly reduced lanosterol and lathosterol levels already under normoxia and prevented hypoxia-mediated accumulation of lanosterol (Figure 3B). As expected, inhibition of the lanosterol/24,25-dihydrolanosterol-metabolizing enzyme CYP51A1 reduced the

late intermediate lathosterol, while it massively increased lanosterol under normoxia, even overruling the hypoxia-induced increase. As observed under hypoxia, cholesterol levels displayed only slight changes in response HMGCR and SQLE inhibition, but surprisingly increase markedly upon ketoconazole treatment. Despite pronounced changes in sterol *de novo* synthesis, all three inhibitors only minimally affected *MSMO1* levels under normoxia and did not alter its hypoxic induction (Figure 3C). These findings suggest that total cholesterol levels are an imprecise measure to predict changes in intracellular cholesterol dynamics. Similarly, *OAS1* and *IRF7*, i.e., IFNAR-dependent and -independent ISGs, respectively, remained unaffected by the three inhibitors under normoxia and hypoxia, indicating that accumulation of early cholesterol precursors did not contribute to hypoxic ISG induction. To determine if cholesterol biosynthesis intermediates might still be involved in hypoxic ISG induction, we supplemented THP-1 cells with early (mevalonate (300 μM), geranylgeraniol (15 μM)) or late cholesterol precursors (lathosterol, 7-dehydrocholesterol, desmosterol (5 μM each)) prior to 24 h of hypoxia. Corroborating the observation that cholesterol biosynthesis inhibitors did not alter hypoxic ISG induction, supplementation of neither early nor late cholesterol precursors substantially attenuated the hypoxia-mediated increase in *OAS1* and *IRF7* expression (Figures 3D, E). In line with the oxygen requirements for cholesterol biosynthesis, early cholesterol intermediates did not affect hypoxic *MSMO1* induction (Figure 3D), while late intermediates almost completely prevented the hypoxic increase in *MSMO1* expression (Figure 3E).

Subcellular changes in cholesterol concentrations provide a rheostat to control the activities of the transcription factors sterol regulatory element-binding protein 2 (SREBP2), which is activated after sterol depletion at the endoplasmic reticulum (ER) to enhance cholesterol biosynthesis and uptake (36), and liver X receptor (LXR), which is activated by desmosterol or oxysterols to reduce cholesterol uptake and enhance cholesterol export (Figure 4A) (37). First, we addressed the involvement of SREBP2, the master regulator of the enzymes involved in cholesterol biosynthesis, in the hypoxic induction of the cholesterol biosynthesis enzymes. Indeed, after 8 h of hypoxia nuclear SREBP2 levels, reflecting active SREBP2, were increased (Figure 4B). Furthermore, pre-incubation of THP-1 cells with the established SREBP2 inhibitors PF-429242 (1 μM) or fatostatin (10 μM) effectively blocked hypoxic *MSMO1* induction (Figures 4C, D). While SREBP2 was previously described to directly bind and activate IFN response genes (38), and inhibition of SREBP2 cleavage and release from the Golgi with the S1P (site 1 protease) inhibitor PF-429242 completely blocked SREBP2 target expression even under normoxia, it did not affect hypoxic *OAS1* and *IRF7* induction (Figure 4C). In contrast, inhibition of SREBP2 activation with fatostatin (10 μM), which selectively blocked the hypoxic increase in *MSMO1* expression, also attenuated the hypoxic ISG expression (Figure 4D). To further test if cholesterol homeostasis changes might affect ISG expression, we incubated THP-1 cells with the LXR agonist T0901317 (1 μM). In line with reduced cholesterol biosynthesis and desmosterol levels, expression of the cholesterol exporter *ATP binding cassette subfamily A member 1* (*ABCA1*), a proto-typical LXR target, was reduced under hypoxia (Supplementary Figure 4). Interestingly, small molecule-based activation of LXR significantly increased the hypoxic ISG induction (Figure 4E).

Conclusively, our data indicate that while the hypoxic ISG induction in monocytes is not directly affected by changes in cholesterol biosynthetic flux, modulation of subcellular cholesterol dynamics might contribute to the enhanced ISG expression under hypoxia.

3.3 Intracellular cholesterol distribution determines hypoxic chemokine ISG induction

As altering ER-to-Golgi dynamics with fatostatin or cholesterol import/export processes via LXR activation both impacted hypoxic ISG induction, we aimed to gain further insights into the potential relevance of subcellular cholesterol dynamics. Since cellular cholesterol homeostasis relies on a tightly regulated interplay between cholesterol uptake, *de novo* synthesis, transport between different compartments, and eventually export (Figure 5A), we next addressed ISG induction under conditions when extracellular cholesterol resources are limited. Therefore, we reduced the availability of exogenous cholesterol by lowering the amount of fetal bovine serum (FBS) in the medium. Reduced exogenous cholesterol availability enhanced *OAS1* and *IRF7* expression under normoxia and hypoxia to a similar extend (Figure 5B). In contrast, low FBS exclusively enhanced the hypoxic expression of the well-characterized chemokine ISGs *CC motif chemokine ligand 2* (*CCL2*) and *CXC motif chemokine ligand 10* (*CXCL10*), which were previously shown to be induced upon cholesterol disturbances (12). To assess if the ISG-inducing effects of low FBS might indeed be due to decreased uptake of cholesterol, we used the Niemann-Pick C1 protein (NPC1) inhibitor U18666A, which prevents redistribution of LDL-derived cholesterol from lysosomes to cellular organelles such as ER and mitochondria, but also to the plasma membrane (Figure 5A). Strikingly, while hypoxic *OAS1* and *IRF7* induction remained unaltered by NPC1 inhibition at high FBS, their serum depletion-dependent increase under hypoxia was prevented (Figure 5B). In contrast, *CXCL10* induction by both FBS reduction and/or hypoxia remained largely unaffected, and *CCL2* even increased upon NPC1 inhibition under both normoxia and hypoxia, which was further enhanced when combined with FBS depletion. The differential responses of the ISGs to low serum and/or NPC1 inhibition point towards a complex, cholesterol-associated regulatory network, specific for each ISG. Therefore, we next tested if supplementation of THP-1 cells with methyl-β-cyclodextrin (MβCD)-complexed cholesterol under low serum conditions might affect hypoxic ISG expression patterns. While cholesterol supplementation did not affect *OAS1* and *IRF7* expression at all, it enhanced *CCL2* and *CXCL10* expression predominantly under normoxia (Figure 5C). Consequently, the hypoxic induction of chemokine ISGs in serum reduced conditions appeared to be attenuated by cholesterol addition. Not surprisingly, cholesterol supplementation massively reduced both normoxic and hypoxic *MSMO1* expression. Moreover, forced cholesterol loading of THP-1 cells with MβCD-cholesterol under low serum conditions overruled

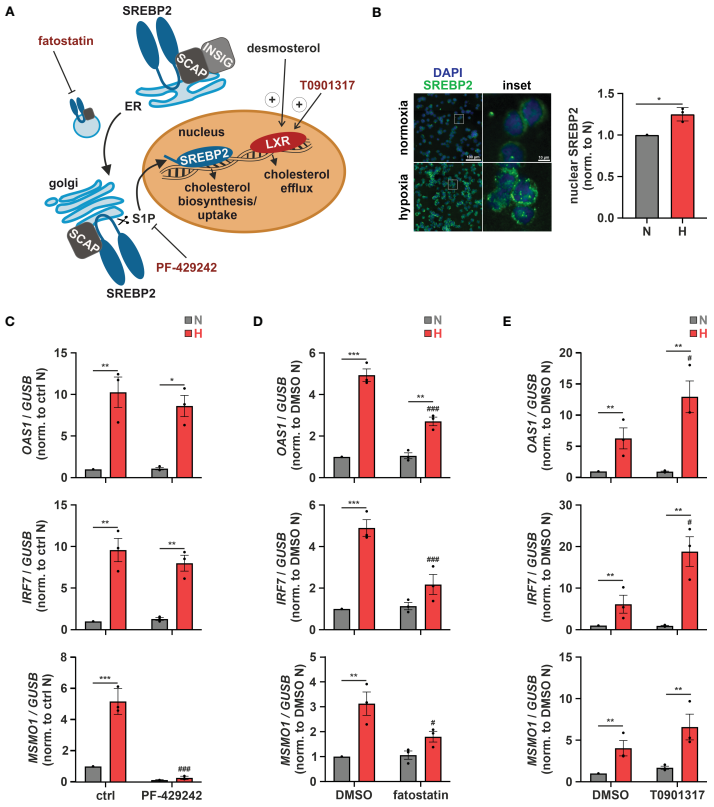

FIGURE 4
Altered cholesterol homeostasis affects hypoxic ISG induction. **(A)** Overview of the mechanisms of activation of the cholesterol-associated transcription factors LXR and SREBP2. The LXR agonist T0901317 as well as the SREBP2 inhibitors PF-429242 and fatostatin are highlighted in red. **(B)** THP-1 cells were incubated under N (grey) or H (red) for 8 h (n = 3). Immunofluorescence staining for SREBP2 (green) was performed. Nuclei were counterstained with DAPI (blue). Mean fluorescence intensity was quantified for nuclear SREBP2. Images are representative of three independent experiments. **(C–E)** THP-1 cells were pre-incubated for 1 h with **(C)** 1 μM PF-429242, **(D)** 10 μM fatostatin, **(E)** 1 μM T0901317, or appropriate solvent controls, prior to incubation under N (grey) or H (red) for 24 h (n = 3). *OAS1*, *IRF7*, and *MSMO1* mRNA expression was analyzed by RT-qPCR and normalized to *GUSB* expression. Data are means ± SEM and were statistically analyzed using two-tailed paired t-test **(B)**, or two-way repeated measures ANOVA with Holm-Šídák's multiple comparisons test **(C–E)** (*$p < 0.05$, **$p < 0.01$, ***$p < 0.001$; #$p < 0.05$, ###$p < 0.001$ (compared to ctrl or DMSO, respectively)).

the changes elicited by the NPC1 inhibitor for all ISGs as well as for *MSMO1* (Figure 5C). These findings underscore the notion that the impact of intracellular cholesterol dynamics on the expression of ISGs in the context of hypoxia is extremely versatile.

Functionally, interferon-associated immune responses are of special interest when considering virus infections. The β-coronavirus SARS-CoV-2 was first detected in 2019 and described to be the causative agent of a novel lung disease named COVID-19, in which severe clinical manifestations are caused by dysregulated host immune responses (39–41). As COVID-19 is a respiratory disease, which, in severe cases leads to hypoxemia, i.e., low blood oxygen levels, we wondered if hypoxia might influence SARS-CoV-2 infections. Therefore, we incubated THP-1 cells for 24 h under normoxia or hypoxia before adding infectious SARS-CoV-2 (strain FFM1) (18) for 1 h under low serum conditions. Due to technical considerations, all infections had to be carried out under normoxia. Of note, primary monocytes were previously shown to express only low levels of the main SARS-CoV-2 receptor angiotensin-converting enzyme 2 (ACE2) and its associated transmembrane serine protease 2 (TMPRSS2) (42). Despite the fact that THP-1 monocytes only minimally express ACE2, they were substantially infected with SARS-CoV-2 as indicated by the expression of viral *M*

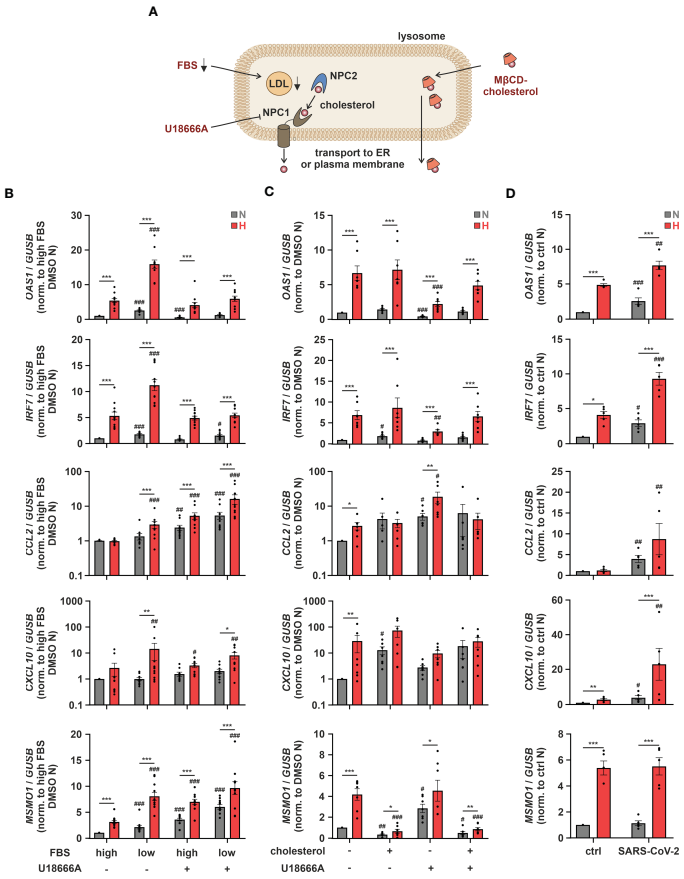

FIGURE 5
Intracellular cholesterol distribution determines hypoxic chemokine ISG induction. **(A)** Overview of the lysosomal cholesterol distribution machinery. Relevant interventions are indicated in red. **(B)** THP-1 cells were pre-incubated for 1 h with 5 μM U18666A or DMSO in medium containing high or low levels of FBS prior to incubation under N (grey) or H (red) for 24 h (n = 11). **(C)** THP-1 cells were pre-incubated for 1 h with 5 μM U18666A or DMSO in medium containing low levels of FBS ± 0.25 mg/mL methyl-β-cyclodextrin-complexed cholesterol prior to incubation under N (grey) or H (red) for 24 h (n = 7). **(D)** THP-1 cells were incubated under N (grey) or H (red) for 24 h in medium containing low levels of FBS prior to infection with SARS-CoV-2 (strain FFM1) under N. RNA was isolated 1 hour post infection (n = 5). *OAS1*, *IRF7*, *CCL2*, *CXCL10*, and *MSMO1* mRNA expression was analyzed by RT-qPCR and normalized to *GUSB* expression. All data are means ± SEM and were statistically analyzed using two-way repeated measures ANOVA with Holm-Šídák's multiple comparisons test (*$p < 0.05$, **$p < 0.01$, ***$p < 0.001$; #$p < 0.05$, ##$p < 0.01$, ###$p < 0.001$ (compared to to FBS high/DMSO **(B)**, FBS low/DMSO **(C)**, or FBS low/ctrl **(D)**, respectively)).

gene (C_t = 24.10 ± 0.96), yet hypoxic priming only slightly increased virus abundance (Supplementary Figure 5). The infection of THP-1 cells was not productive, though, as no active replication of the virus (subgenomic RNA4 encoding E gene) was observed. In line with previous reports suggesting mild interferon responses to SARS-CoV-2 infections (43), *OAS1* and *IRF7* were only slightly elevated in THP-1 cells after infection with SARS-CoV-2 under normoxia and hypoxia. Remarkably, *CCL2* and *CXCL10*, both of which are increased in patients developing a systemic inflammatory response syndrome following SARS-CoV-2 infections (44), showed a strong hypoxic induction upon subsequent infection with SARS-CoV-2 (Figure 5D).

Taken together, our data show that cholesterol homeostasis impinges on diverse mechanisms regulating various sub-groups of ISGs under conditions of low oxygen tensions. Of note, hypoxic elevation of chemokine ISGs, which were massively enhanced upon

concomitant SARS-CoV-2 infection, appeared to be extremely sensitive to extracellular cholesterol availability and the distribution thereof.

3.4 TLR4 signaling contributes to hypoxic ISG induction

As hypoxia-enhanced chemokine production in response to SARS-CoV-2 infection might be of major relevance with respect to COVID-19-related systemic inflammation, we further characterized the underlying regulatory principles. We next aimed to determine potentially involved pattern recognition receptors (PRRs). To this end, we first used THP-1 cells deficient for mitochondrial antiviral signaling protein (MAVS) (16), which integrates activity of retinoic acid-inducible gene I (RIG-1) and melanoma differentiation-associated protein 5 (MDA5) (45), or for stimulator of interferon response cGAMP interactor (STING) (16), which is activated by cyclic GMP-AMP synthase (cGAS) (46). In line with the complex, ISG-specific regulation, hypoxic *OAS1*, *IRF7*, and *CXCL10* induction under low serum conditions was lower in MAVS-deficient cells than in STING-knockout (KO) or the corresponding wildtype (WT) THP-1 cells, while hypoxic *CCL2* induction remained unaltered (Supplementary Figure 6). Since neither the cGAS/STING nor the RIG-1/MDA5/MAVS axis appeared sufficient for the hypoxic chemokine ISG induction, we asked if toll-like receptors (TLRs) might be involved as well, since they have been shown to not only regulate classical pro-inflammatory cytokines, but also ISGs (Figure 6A) (47). Of the 10 known TLRs, *TLR1*, *TLR2*, *TLR4*, and *TLR9* were most abundant, *TLR5*, *TLR6*, and *TLR7* were expressed at intermediate levels, whereas *TLR3*, *TLR8*, and *TLR10* appeared not to be expressed at all in THP-1 cells (Supplementary Figure 7A). While *TLR2* and *TLR5* expression did not change in response to hypoxia and/or serum deprivation, expression of *TLR1*, *TLR6*, *TLR7*, and *TLR9* was enhanced by hypoxia and further increased upon serum depletion (Figure 6B; Supplementary Figure 7B), as observed for *OAS1*, *IRF7*, and *CXCL10* (Figure 5B). Interestingly, similar to *CCL2* (Figure 5B), *TLR4* was only elevated under hypoxia at low FBS concentrations (Figure 6B). To test a general involvement of TLRs in the hypoxic ISG induction, we inhibited myeloid differentiation primary response 88 (MyD88), the intracellular signal transduction adapter for most TLRs, using TJ-M2010-5 (10 μM) (Figure 6A). MyD88 inhibition reduced hypoxic induction of *OAS1* and *IRF7* more efficiently under low serum conditions and completely abrogated hypoxia-induced chemokine ISG expression (Figure 6C). While TLR-mediated activation of MyD88/inhibitors of nuclear factor kappa B (NF-κB) kinase α/β (IKKα/β)/NF-κB signaling is well established to drive pro-inflammatory cytokine expression, TLR-dependent ISG induction commonly relies on the TIR-domain containing adaptor-inducing interferon-β (TRIF)/TANK-binding kinase 1 (TBK1)/IKKε/IRF axis (48). To shed further light on the involved signaling cascade, we inhibited TBK1 using BX-795 (0.5 μM) or canonical IKKs using IKK-16 (0.1 μM), both of which known to be critical for TLR-dependent activation of ISGs (49). While both TBK1 and IKK inhibition significantly reduced hypoxic induction of *OAS1* and *IRF7*, *MSMO1* expression was not altered (Figure 6D). Moreover, the prominent hypoxic induction of the chemokine ISGs *CCL2* and *CXCL10* under low serum conditions remained largely unaffected by TBK1 inhibition, whereas IKK inhibition appeared to efficiently reduce *CXCL10* induction, yet leaving *CCL2* unaltered. These findings not only suggest that MyD88- rather than TRIF-dependent signaling underlies the hypoxic chemokine ISG induction, but again underscore the complexity of mechanisms contributing to the hypoxic elevation of the different ISGs.

Since TLR7 and 8 are activated by single stranded RNA viruses such as SARS-CoV-2, and TLR4 has recently been proposed to be activated by SARS-CoV-2 as well (50), we next asked, if they might be also involved in the hypoxic ISG induction. To this end, we used the selective TLR4 inhibitor TAK-242 (10 μM) or the TLR7/8 inhibitor enpatoran (0.1 μM). While enpatoran efficiently blocked ISG expression induced by the specific TLR7/8 agonist resiquimod (R848) (Supplementary Figure 8), it did not affect hypoxic induction of any of the tested ISGs irrespective of the serum conditions (Figure 6E). In contrast, TLR4 inhibition not only prevented the low serum-dependent increase of the hypoxic *OAS1* and *IRF7* induction, it further blocked chemokine ISG expression altogether. As a side note, reduced hypoxic *MSMO1* induction after TLR4 or MyD88 inhibition corroborated the bidirectionality between IFN signaling and cholesterol metabolism (14).

In summary, TLR4-dependent signaling appears of major importance for the cholesterol dynamic-associated, hypoxic induction of ISGs in monocytes. Herein, chemokine ISGs, such as *CCL2* and *CXCL10*, displayed the strongest addiction to intact TLR4/MyD88 signaling. Moreover, owing to the hypoxic upregulation of various TLRs, a general sensitization of TLR signaling under hypoxia might be predicted.

3.5 Hypoxic priming increases the production of chemokine ISGs after SARS-CoV-2 infection via TLR4 activation

Since TLR4 contributed to hypoxic ISG induction and relevant ISGs increased after SARS-CoV-2 infection in monocytic THP-1 cells, and further taking into account that a direct binding and activation of TLR4 by SARS-CoV-2 spike protein was recently proposed (50), we wondered if SARS-CoV-2 spike protein alone might induce the hypoxic phenotype. Therefore, we pre-incubated THP-1 cells in serum-reduced conditions under either normoxia or hypoxia for 24 h, and continued incubations for additional 8 h in the presence or absence of SARS-CoV-2 spike protein (5 μg/mL). While expression of *OAS1* and *IRF7* only minimally increased in the presence of SARS-CoV-2 spike protein, *CCL2* and *CXCL10*, i.e., chemokine ISGs associated with severe cases of SARS-CoV-2 infections, robustly increased (Figure 7A). This became evident already under normoxia and was further enhanced under hypoxia. Inhibition of TLR4 with TAK-242 (10 μM) drastically diminished hypoxia- and SARS-CoV-2 spike protein-induced *CCL2* and *CXCL10* expression and also attenuated hypoxic induction of *OAS1* and *IRF7*. Of note, fatostatin (10 μM) diminished hypoxia-

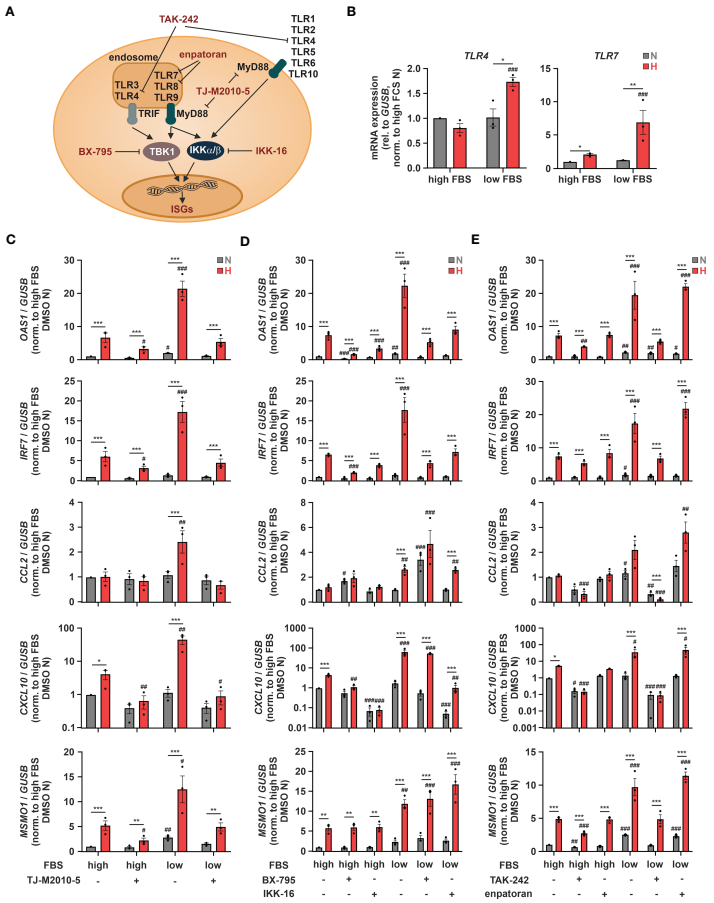

FIGURE 6
TLR4 signaling contributes to hypoxic ISG induction. **(A)** Overview of toll-like receptors (TLRs), adaptor proteins, and kinases regulating ISG induction. Relevant inhibitors are highlighted in red. **(B)** THP-1 cells were incubated under N (grey) or H (red) for 24 h in medium containing high or low levels of FBS (n = 3). *TLR4* and *TLR7* mRNA expression was analyzed by RT-qPCR and normalized to *GUSB* expression. **(C–E)** THP-1 cells were pre-incubated for 1 h with **(C)** 10 μM TJ-M2010-5 (MyD88 inhibitor), **(D)** 0.5 μM BX-795 (TBK1/IKKε inhibitor), 0.1 μM IKK-16 (IKKα/β inhibitor), **(E)** 10 μM TAK-242 (TLR4 inhibitor), 0.1 μM enpatoran (TLR7/8 inhibitor), or DMSO in medium containing high or low levels of FBS prior to incubation under N (grey) or H (red) for 24 h (n = 3). *OAS1*, *IRF7*, *CCL2*, *CXCL10*, and *MSMO1* mRNA expression was analyzed by RT-qPCR and normalized to *GUSB* expression. All data are means ± SEM and were statistically analyzed using two-way repeated measures ANOVA with Holm-Šídák's multiple comparisons test (*$p < 0.05$, **$p < 0.01$, ***$p < 0.001$; #$p < 0.05$, ##$p < 0.01$, ###$p < 0.001$ (compared to to FBS high **(B)** or FBS high/DMSO **(C–E)**, respectively)).

enhanced expression of ISGs and *MSMO1* also in the context of stimulation with SARS-CoV-2 spike protein. Having established that SARS-CoV-2 spike protein induces comparable ISG responses in THP-1 monocytes as the infectious virus and enhances chemokine ISG expression in response to hypoxia, we reached out to determine if TLR4 and cholesterol dynamics are also involved in interferon-associated immune responses in monocytic THP-1 cells upon infection with SARS-CoV-2 in a hypoxic environment. To this end, we primed THP-1 cells for 24 h under hypoxia prior to infecting them with SARS-CoV-2 (FFM1 strain) for 6 h under normoxia. Owing to the reoxygenation, expression of the SREBP2 target *MSMO1* was not elevated in hypoxia-primed THP-1 cells after infection (Figure 7B). In contrast to the spike protein, SARS-CoV-2 infection induced *OAS1* and *IRF7* expression already under normoxic conditions, still showing a slight enhancement by hypoxic priming. *CCL2* and *CXCL10* mRNA levels on the other hand were

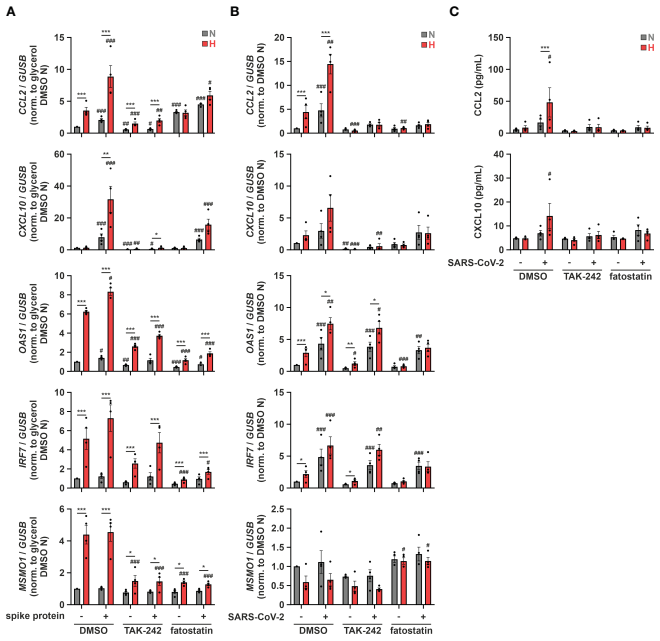

FIGURE 7
Hypoxic priming increases production of chemokine ISGs after SARS-CoV-2 infection via TLR4 activation. **(A)** THP-1 cells were pre-incubated for 1 h with 10 µM TAK-242, 10 µM fatostatin, or DMSO in medium containing low levels of FBS prior to incubation under N (grey) or H (red) for 32 h 5 µg/mL SARS-CoV-2 spike protein or glycerol were added for the last 8 h (n = 4). *CCL2*, *CXCL10*, *OAS1*, *IRF7*, and *MSMO1* mRNA expression was analyzed by RT-qPCR and normalized to *GUSB* expression. **(B, C)** THP-1 cells were pre-incubated for 1 h with 10 µM TAK-242, 10 µM fatostatin, or DMSO in medium containing low levels of FBS prior to incubation under N (grey) or H (red) for 24 h Subsequently, cells were infected with SARS-CoV-2 (strain FFM1) under N (n = 4). **(B)** RNA was isolated 6 hours post infection. *CCL2*, *CXCL10*, *OAS1*, *IRF7*, and *MSMO1* mRNA expression was analyzed by RT-qPCR and normalized to *GUSB* expression. **(C)** Secreted CCL2 and CXCL10 protein levels were determined by ELISA in supernatants 6 hours post infection. All data are means ± SEM and were statistically analyzed using two-way repeated measures ANOVA with Holm-Šídák's multiple comparisons test (*$p < 0.05$, **$p < 0.01$, ***$p < 0.001$; #$p < 0.05$, ##$p < 0.01$, ###$p < 0.001$ (compared to to FBS low/DMSO)).

comparable in cells infected with SARS-CoV-2 or treated with spike protein only, displaying a marked increase after hypoxic priming. Interestingly, whereas TLR4 inhibition (TAK-242, 10 µM) did not alter enhanced *OAS1* and *IRF7* expression in response to hypoxic priming and SARS-CoV-2 infection, it completely abolished the expression of chemokine ISGs *CCL2* and *CXCL10* (Figure 7B), despite the fact that the infection rate was not affected (Supplementary Figure 9). Interfering with intracellular cholesterol dynamics using fatostatin (10 µM) selectively prevented the hypoxia-evoked increase of the ISGs, irrespective of the presence or absence of SARS-CoV-2, without affecting the virus infection rate (Figure 7B; Supplementary Figure 9). To validate the functional relevance of chemokine ISG expression changes in the context of SARS-CoV-2 infection of monocytic cells under conditions of reduced oxygen availability, we finally determined protein amounts of CCL2 and CXCL10 in the supernatants of THP-1 cells. In line with mRNA expression changes, hypoxia markedly enhanced secretion of CCL2 and CXCL10 upon infection with SARS-CoV-2 (Figure 7C). Hypoxic induction again was completely abolished when either TLR4 or SCAP-associated trafficking were inhibited.

Our data suggest that hypoxia increases expression of chemokine ISGs in monocytic THP-1 cells upon infection with SARS-CoV-2 by enhancing spike protein-mediated TLR4 signaling. Severe cases of COVID-19 are characterized by hypoxemia, implying that monocytes regularly encounter hypoxic conditions. Our findings therefore provide a concept of how hypoxia might prime monocytes for TLR4-dependent chemokine ISG production in response to SARS-CoV-2 infection, thus potentially contributing to systemic inflammation.

4 Discussion

In this study, we characterized a so far unknown connection between hypoxia-evoked disturbances in cholesterol metabolism

and altered IFN responses in monocytes. Cholesterol biosynthesis flux was reduced under hypoxia, resulting in a compensatory SREBP2 activation and consequently enhanced expression of cholesterol biosynthesis enzymes. Also, a broad range of ISGs was induced under hypoxia, but their hypoxic regulation was independent of SREBP2 activity. While a complex regulatory network affected various subgroups of ISGs, intracellular distribution of cholesterol appeared crucial for the hypoxic, TLR4/MyD88-mediated induction of chemokine ISGs. Hypoxia further enhanced chemokine ISG expression in monocytes upon infection with SARS-CoV-2, potentially contributing to systemic inflammatory responses in severe cases of COVID-19 (Figure 8).

Our observation that early cholesterol biosynthesis intermediates accumulated, while late intermediates were reduced under hypoxic conditions in THP-1 monocytes, corroborates previous findings of an altered sterol composition under hypoxia (51–53). Moreover, massive and rapid accumulation of lanosterol and 24,25-dihydrolanosterol agrees with previous findings that squalene epoxidase remains active under low oxygen tensions for an extended period of time, thus allowing cholesterol biosynthetic flux to reach lanosterol and 24,25-dihydrolanosterol (51, 54). In contrast to earlier reports claiming that SREBP2 is not activated under hypoxia (55–57), we found a strong feedback activation of SREBP2 despite marginal changes in total cholesterol levels. Supplementation of late cholesterol precursors sufficed to block SREBP2 activity, which suggests that local cholesterol availability (e.g., at the ER) rather than total cholesterol levels are critical in hypoxic monocytes. Differences in sub-cellular cholesterol dynamics or cellular cholesterol requirements might account for the pronounced cell type-specificity of SREBP2 activation in the context of hypoxia. Interestingly, the key enzyme of the cholesterol biosynthesis cascade HMGCR was previously shown to be a direct target of the hypoxia-inducible factor 1 (HIF-1) (58), which might contribute to the enhanced formation of early cholesterol intermediates as well.

Strikingly, expression of IFN response targets closely followed cholesterol biosynthesis changes in hypoxic monocytes, pointing to a potential interplay. Indeed, there is increasing evidence that cholesterol metabolism and IFN responses are tightly interwoven. On the one hand, IFNs and viral infections appear to reduce SREBP2 target expression (14, 15), while on the other hand, cholesterol intermediates were shown to affect ISG expression. Specifically, the early cholesterol intermediate lanosterol repressed IFN signaling in macrophages (59), whereas accumulation of the direct cholesterol precursor 7-dehydrocholesterol or reduced desmosterol levels enhanced ISG expression (13, 60). Furthermore, York et al. (12) provide evidence for an immunometabolic circuit where type I IFN shifts the balance

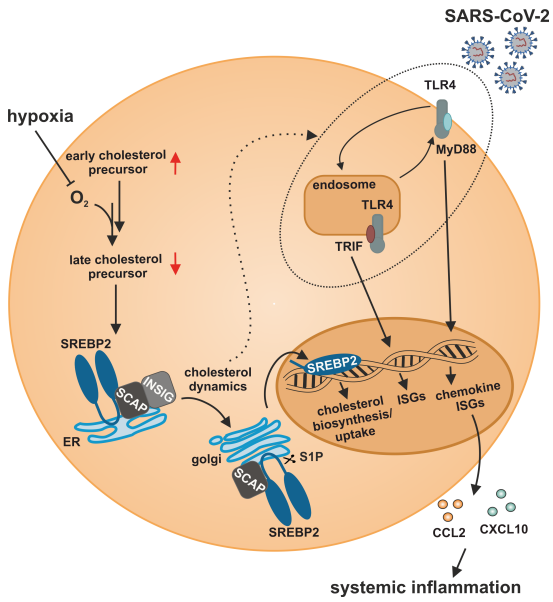

FIGURE 8
Model of the impact of hypoxia on IFN responses to SARS-CoV-2 infection in monocytes. Hypoxia alters cholesterol biosynthesis flux and subcellular cholesterol dynamics, consequently enhancing TLR4/MyD88-dependent chemokine ISG production in response to SARS-CoV-2 infection.

from cholesterol synthesis to uptake, without altering total cholesterol availability. A reduced flux through the cholesterol biosynthesis cascade in turn enhances IFN responses, putatively via lowered cholesterol levels at the ER (12). On a mechanistic side note, SREBP2 was further shown to directly bind to and activate the promotor of various ISGs (38). In contrast, hypoxia-induced ISG expression in monocytes occurred independently of SREBP2, as inhibition of the activating cleavage of SREBP2 by S1P did not attenuate hypoxic ISG induction. Surprisingly though, fatostatin, a commonly used SREBP2 inhibitor, efficiently reduced hypoxia-dependent ISG expression. Fatostatin prevents SREBP2 activation by inhibiting SCAP-coupled ER-to-Golgi transfer. SCAP-associated trafficking was further shown to enhance inflammatory and IFN signaling independent of SREBP2 activation (9, 61). Since cholesterol supplementation did not affect hypoxic *OAS1* and *IRF7* expression, a direct SCAP effect appeared unlikely. Considering SCAP-independent effects of fatostatin, such as a general interference with ER-to-Golgi transport or the inhibition of tubulin polymerization (62, 63), hypoxic ISG induction in monocytes might result from altered intracellular trafficking processes due to changes in subcellular cholesterol distribution instead. Indeed, cholesterol has been shown to influence intracellular trafficking by altering membrane properties or regulating motor proteins (64, 65). As a side note, differentiated, primary macrophages did not show the same phenotype as the monocytic THP-1 cells (data not shown), which might be due to differences in cell culture conditions, likely affecting cellular cholesterol availability and uptake. Yet, further studies are needed to elucidate the exact differences in hypoxic ISG induction between monocytes and macrophages, also with respect to the functional relevance in the context of inflammatory diseases.

Our data suggest that elevated ISG expression under hypoxia demands sensitization of TLR signaling linked to altered intracellular cholesterol dynamics. In fact, associations between cholesterol distribution and TLR trafficking are well-characterized (66, 67) and intracellular trafficking (e.g., between plasma membrane, endosome, or lysosome) has been shown to be critical for activation and termination of TLR signaling as well as recycling (68). Localization is of particular importance in the case of TLR4. TLR4 exclusively activates MyD88-dependent NF-κB signaling when it resides at the plasma membrane, whereas endosomal TLR4 additionally activates TRIF to elicit type I IFN signals (69). In line, accumulation of both TLR4 and cholesterol in endosomal compartments was previously shown to enhance NF-κB as well as IFN signaling upon LPS-treatment in NPC1-deficient cells (70).The observation that TLR4-dependent ISG induction prevailed in hypoxic THP-1 monocytes agrees with the previously described TLR4-dependent upregulation of IFN responses in microglia during ischemia/reperfusion (71). The strict dependency of the hypoxic chemokine ISG induction on MyD88 further corroborates a recent report showing that the direct interaction of cholesterol with MyD88 contributes to signaling amplification of the latter (72). Strikingly, hypoxic induction of chemokine ISGs in monocytes appeared particularly sensitive to changes in intracellular cholesterol trafficking as they showed a more pronounced increase in the hypoxic induction compared to the other ISGs when either extracellular cholesterol availability was reduced or the proper distribution of extracellularly supplied cholesterol was attenuated by inhibition of NPC1. Considering that NPC1 inhibition interferes with cholesterol distribution not only to the ER but also to mitochondria, it can be speculated that changes in mitochondrial integrity, due to altered sterol shuttling to the mitochondria, might contribute to hypoxic ISG induction as well. In line, it is well established that mitochondrial DNA in the cytosol elicits interferon responses (73). Nevertheless, this mechanism was proposed to rely on intact cGAS/STING signaling, which appeared to be not required for the hypoxic ISG induction in THP-1 cells.

While IFN responses are of specific relevance in the context of viral infections (74), SARS-CoV-2 infections were initially deemed to elicit only low levels of type I and III IFNs (41). Interestingly, while we observed a moderate induction of *OAS1* and *IRF7*, chemokine ISGs were markedly induced in response to SARS-CoV-2 infection in hypoxic monocytes. As inhibition of TLR4 activation or interference with cholesterol dynamics completely abolished the enhanced IFN response, TLR sensitization under hypoxia emerged as a potential mechanism. While cholesterol dynamics appeared to be crucial for the hypoxic elevation of all ISGs in the context of SARS-CoV-2 infection, TLR4 was specifically relevant for enhanced chemokine ISGs. Considering the complex regulation of IFN responses via various PRRs, the observation that MAVS also contribute to the hypoxic induction of some ISGs further supports the notion that the hypoxic ISG response integrates numerous receptor-dependent but also -independent signals. Monocytes and monocyte-derived macrophages were previously proposed to resist infection with SARS-CoV-2 due to only minimal expression of the main SARS-CoV-2 receptor ACE2 and its associated serine protease TMPRSS2 (42). Here, we observed infection of THP-1 monocytes with SARS-CoV-2, which corroborates recent findings that monocytes, despite the lack of intrinsic ACE2 expression, can be infected by SARS-CoV-2 (75). In line with previous observations that monocytes/macrophages show no productive infection with SARS-CoV-2 (76), we also did not detect active replication (subgenomic RNA4 encoding E gene). Still, increased production of ISGs and IFN-mediated inflammatory responses after SARS-CoV-2 infection of monocyte-derived cells were previously described (76, 77) and the relevance of monocytes/macrophages with respect to the clinical outcome of COVID-19 is widely accepted (78, 79). Our data suggest that hypoxia-enhanced chemokine ISG responses to SARS-CoV-2 are mediated via TLR4, which likely is activated via the spike protein, as recently suggested (50). Nevertheless, while the exact role of IFN signaling for the pathogenesis of COVID-19 is still controversially discussed and likely depends on the stage of the disease (80–82), our finding that hypoxia specifically enhances chemokine ISG expression in the context of SARS-CoV-2 infection suggests that monocytes within a hypoxemic environment might contribute to the progression from a local inflammatory disease to a systemic inflammatory response syndrome (83–85). Cholesterol homeostasis was not only identified to be important for the infection with SARS-CoV-2 (86), but activation of SREBP2 in blood mononuclear cells was put forward as an indicator of disease severity as it correlated with the development of a cytokine storm in severe cases of COVID-19 (85).

Taken together, we identified hypoxia-mediated changes in cholesterol homeostasis to induce interferon responses in monocytes. Our finding that hypoxic monocytes produce elevated chemokine ISG levels upon SARS-CoV-2 infection in a TLR4- and cholesterol-dependent manner might open new therapeutic opportunities to prevent systemic progression of severe COVID-19 cases.

Data availability statement

The datasets presented in this study can be found in online repositories. The names of the repository/repositories and accession number(s) can be found in the article/Supplementary Material.

Author contributions

RB, DF, TS and BB conceived the study and designed the experiments. RB and SM performed the experiments. VR, GC, SR, RR, MH and MP contributed to the acquisition of data. DL conducted the sterol measurements. RB, KZ and TS analyzed the data. FR, AW and MW supported the BSL3 experiments. RB and TS wrote the original draft. MW, TS and BB acquired funding. All authors contributed to the article and approved the submitted version.

Funding

This work was supported by the DFG (BR999/25-1 to BB; SFB 1039, B04 to BB; GRK 2336, TP06 to BB and TS; WI5086/1-1 to MW) and the Goethe Corona Fonds (to MW and TS). Parts of this work were supported by the Clusterproject ENABLE and the High-Performance Center TheraNova funded by the Hessian Ministry for Science and the Arts (MW), and the Federal Ministry of Education and Research (BMBF; grant 02WRS1621C (MW)).

Acknowledgments

The authors would like to thank Anja Kerksiek, Christiane Pallas, Bettina Wenzel, and Tanja Keppler for excellent technical assistance.

Conflict of interest

The authors declare that the research was conducted in the absence of any commercial or financial relationships that could be construed as a potential conflict of interest.

Publisher's note

Supplementary material

The Supplementary Material for this article can be found online at: https://www.frontiersin.org/articles/10.3389/fimmu.2023.1121864/full#supplementary-material

SUPPLEMENTARY TABLE 2
Hypoxia-induced gene expression changes and associated functions.

SUPPLEMENTARY TABLE 3
Putative hypoxia-induced ISGs identified by Interferome.

References

1. Nakazawa MS, Keith B, Simon MC. Oxygen availability and metabolic adaptations. *Nat Rev Cancer* (2016) 16:663–73. doi: 10.1038/nrc.2016.84

2. Fuhrmann DC, Brüne B. Mitochondrial composition and function under the control of hypoxia. *Redox Biol* (2017) 12:208–15. doi: 10.1016/j.redox.2017.02.012

3. Luo Z, Tian M, Yang G, Tan Q, Chen Y, Li G, et al. Hypoxia signaling in human health and diseases: implications and prospects for therapeutics. *Signal Transduct Target Ther* (2022) 7:218. doi: 10.1038/s41392-022-01080-1

4. Mathis D, Shoelson SE. Immunometabolism: an emerging frontier. *Nat Rev Immunol* (2011) 11:81. doi: 10.1038/nri2922

5. Hotamisligil GS, Shargill NS, Spiegelman BM. Adipose expression of tumor necrosis factor-α: direct role in obesity-linked insulin resistance. *Science* (1993) 259:87–91. doi: 10.1126/science.7678183

6. Moore KJ, Tabas I. Macrophages in the pathogenesis of atherosclerosis. *Cell* (2011) 145:341–55. doi: 10.1016/j.cell.2011.04.005

7. Li G, Zhao J, Li B, Zhang X, Ma J, Ma X, et al. The anti-inflammatory effects of statins on patients with rheumatoid arthritis: a systemic review and meta-analysis of 15 randomized controlled trials. *Autoimmun Rev* (2018) 17:215–25. doi: 10.1016/j.autrev.2017.10.013

8. Tabrizi R, Tamtaji OR, Mirhosseini N, Lankarani KB, Akbari M, Dadgostar E, et al. The effects of statin use on inflammatory markers among patients with metabolic syndrome and related disorders: a systematic review and meta-analysis of randomized controlled trials. *Pharmacol Res* (2019) 141:85–103. doi: 10.1016/j.phrs.2018.12.010

9. Guo C, Chi Z, Jiang D, Xu T, Yu W, Wang Z, et al. Cholesterol homeostatic regulator SCAP-SREBP2 integrates NLRP3 inflammasome activation and cholesterol biosynthetic signaling in macrophages. *Immunity* (2018) 49:842–856.e7. doi: 10.1016/j.immuni.2018.08.021

10. de la Roche M, Hamilton C, Mortensen R, Jeyaprakash AA, Ghosh S, Anand PK. Trafficking of cholesterol to the ER is required for NLRP3 inflammasome activation. *J Cell Biol* (2018) 217:3560–76. doi: 10.1083/jcb.201709057

11. Bekkering S, Arts RJW, Novakovic B, Kourtzelis I, van der Heijden CDCC, Li Y, et al. Metabolic induction of trained immunity through the mevalonate pathway. *Cell* (2018) 172:135–146.e9. doi: 10.1016/j.cell.2017.11.025

12. York AG, Williams KJ, Argus JP, Zhou QD, Brar G, Vergnes L, et al. Limiting cholesterol biosynthetic flux spontaneously engages type I IFN signaling. *Cell* (2015) 163:1716–29. doi: 10.1016/j.cell.2015.11.045

13. Xiao J, Li W, Zheng X, Qi L, Wang H, Zhang C, et al. Targeting 7-dehydrocholesterol reductase integrates cholesterol metabolism and IRF3 activation to eliminate infection. *Immunity* (2020) 52:109–122.e6. doi: 10.1016/j.immuni.2019.11.015

14. Blanc M, Hsieh WY, Robertson KA, Watterson S, Shui G, Lacaze P, et al. Host defense against viral infection involves interferon mediated down-regulation of sterol biosynthesis. *PloS Biol* (2011) 9:e1000598. doi: 10.1371/journal.pbio.1000598

15. Reboldi A, Dang EV, McDonald JG, Liang G, Russell DW, Cyster JG. 25-hydroxycholesterol suppresses interleukin-1–driven inflammation downstream of type I interferon. *Science* (2014) 345:679–84. doi: 10.1126/science.1254790

16. Mankan AK, Schmidt T, Chauhan D, Goldeck M, Höning K, Gaidt M, et al. Cytosolic RNA:DNA hybrids activate the cGAS –STING axis. *EMBO J* (2014) 33:2937–46. doi: 10.15252/embj.201488726

17. Widera M, Wilhelm A, Toptan T, Raffel JM, Kowarz E, Roesmann F, et al. Generation of a sleeping beauty transposon-based cellular system for rapid and sensitive screening for compounds and cellular factors limiting SARS-CoV-2 replication. *Front Microbiol* (2021) 12:701198. doi: 10.3389/fmicb.2021.701198

18. Toptan T, Hoehl S, Westhaus S, Bojkova D, Berger A, Rotter B, et al. Optimized qRT-PCR approach for the detection of intra- and extra-cellular SARS-CoV-2 RNAs. *IJMS* (2020) 21:4396. doi: 10.3390/ijms21124396

19. Widera M, Westhaus S, Rabenau HF, Hoehl S, Bojkova D, Cinatl J, et al. Evaluation of stability and inactivation methods of SARS-CoV-2 in context of laboratory settings. *Med Microbiol Immunol* (2021) 210:235–44. doi: 10.1007/s00430-021-00716-3

20. Bauer R, Meyer SP, Kloss KA, Guerrero Ruiz VM, Reuscher S, Zhou Y, et al. Functional RNA dynamics are progressively governed by RNA destabilization during the adaptation to chronic hypoxia. *Int J Mol Sci* (2022) 23:5824. doi: 10.3390/ijms23105824

21. Martin M. Cutadapt removes adapter sequences from high-throughput sequencing reads. *EMBnet J* (2011) 17:10. doi: 10.14806/ej.17.1.200

22. Dobin A, Davis CA, Schlesinger F, Drenkow J, Zaleski C, Jha S, et al. STAR: ultrafast universal RNA-seq aligner. *Bioinformatics* (2013) 29:15–21. doi: 10.1093/bioinformatics/bts635

23. Anders S, Pyl PT, Huber W. HTSeq–a Python framework to work with high-throughput sequencing data. *Bioinformatics* (2015) 31:166–9. doi: 10.1093/bioinformatics/btu638

24. Love MI, Huber W, Anders S. Moderated estimation of fold change and dispersion for RNA-seq data with DESeq2. *Genome Biol* (2014) 15:550. doi: 10.1186/s13059-014-0550-8

25. Gu Z, Eils R, Schlesner M. Complex heatmaps reveal patterns and correlations in multidimensional genomic data. *Bioinformatics* (2016) 32:2847–9. doi: 10.1093/bioinformatics/btw313

26. Huang DW, Sherman BT, Lempicki RA. Systematic and integrative analysis of large gene lists using DAVID bioinformatics resources. *Nat Protoc* (2009) 4:44–57. doi: 10.1038/nprot.2008.211

27. Sherman BT, Hao M, Qiu J, Jiao X, Baseler MW, Lane HC, et al. DAVID: a web server for functional enrichment analysis and functional annotation of gene lists (2021 update). *Nucleic Acids Res* (2022) 50:W216–21. doi: 10.1093/nar/gkac194

28. Rusinova I, Forster S, Yu S, Kannan A, Masse M, Cumming H, et al. INTERFEROME v2.0: an updated database of annotated interferon-regulated genes. *Nucleic Acids Res* (2012) 41:D1040–6. doi: 10.1093/nar/gks1215

29. Chen H, Boutros PC. VennDiagram: a package for the generation of highly-customizable Venn and Euler diagrams in r. *BMC Bioinf* (2011) 12:35. doi: 10.1186/1471-2105-12-35

30. Bankhead P, Loughrey MB, Fernández JA, Dombrowski Y, McArt DG, Dunne PD, et al. QuPath: open source software for digital pathology image analysis. *Sci Rep* (2017) 7:16878. doi: 10.1038/s41598-017-17204-5

31. Snodgrass RG, Benatzy Y, Schmid T, Namgaladze D, Mainka M, Schebb NH, et al. Efferocytosis potentiates the expression of arachidonate 15-lipoxygenase (ALOX15) in alternatively activated human macrophages through LXR activation. *Cell Death Differ* (2021) 28:1301–16. doi: 10.1038/s41418-020-00652-4

32. Mackay DS, Jones PJH, Myrie SB, Plat J, Lütjohann D. Methodological considerations for the harmonization of non-cholesterol sterol bio-analysis. *J Chromatogr B* (2014) 957:116–22. doi: 10.1016/j.jchromb.2014.02.052

33. Lütjohann D, Stellaard F, Kerksiek A, Lütsch J, Oertel BG. Serum 4β-hydroxycholesterol increases during fluconazole treatment. *Eur J Clin Pharmacol* (2021) 77:659–69. doi: 10.1007/s00228-020-03041-5

34. R Core Team. *R: a language and environment for statistical computing* (2021). Available at: https://www.R-project.org/.

35. Tall AR, Yvan-Charvet L. Cholesterol, inflammation and innate immunity. *Nat Rev Immunol* (2015) 15:104–16. doi: 10.1038/nri3793

36. Wang X, Briggs MR, Hua X, Yokoyama C, Goldstein JL, Brown MS. Nuclear protein that binds sterol regulatory element of low density lipoprotein receptor promoter. II. purification and characterization. *J Biol Chem* (1993) 268:14497–504. doi: 10.1016/S0021-9258(19)85266-3

37. Bilotta MT, Petillo S, Santoni A, Cippitelli M. Liver X receptors: regulators of cholesterol metabolism, inflammation, autoimmunity, and cancer. *Front Immunol* (2020) 11:584303. doi: 10.3389/fimmu.2020.584303

38. Kusnadi A, Park SH, Yuan R, Pannellini T, Giannopoulou E, Oliver D, et al. The cytokine TNF promotes transcription factor SREBP activity and binding to inflammatory genes to activate macrophages and limit tissue repair. *Immunity* (2019) 51:241–257.e9. doi: 10.1016/j.immuni.2019.06.005

39. Zhou P, Yang X-L, Wang X-G, Hu B, Zhang L, Zhang W, et al. A pneumonia outbreak associated with a new coronavirus of probable bat origin. *Nature* (2020) 579:270–3. doi: 10.1038/s41586-020-2012-7

40. Zhu N, Zhang D, Wang W, Li X, Yang B, Song J, et al. A novel coronavirus from patients with pneumonia in China, 2019. *N Engl J Med* (2020) 382:727–33. doi: 10.1056/NEJMoa2001017

41. Blanco-Melo D, Nilsson-Payant BE, Liu W-C, Uhl S, Hoagland D, Møller R, et al. Imbalanced host response to SARS-CoV-2 drives development of COVID-19. *Cell* (2020) 181:1036–1045.e9. doi: 10.1016/j.cell.2020.04.026

42. Zankharia U, Yadav A, Yi Y, Hahn BH, Collman RG. Highly restricted SARS-CoV-2 receptor expression and resistance to infection by primary human monocytes and monocyte-derived macrophages. *J Leukoc Bio* (2022) 112:569–76. doi: 10.1002/JLB.4COVA1121-579RR

43. Kim Y-M, Shin E-C. Type I and III interferon responses in SARS-CoV-2 infection. *Exp Mol Med* (2021) 53:750–60. doi: 10.1038/s12276-021-00592-0

44. Merad M, Martin JC. Pathological inflammation in patients with COVID-19: a key role for monocytes and macrophages. *Nat Rev Immunol* (2020) 20:355–62. doi: 10.1038/s41577-020-0331-4

45. Kawai T, Takahashi K, Sato S, Coban C, Kumar H, Kato H, et al. IPS-1, an adaptor triggering RIG-i- and Mda5-mediated type I interferon induction. *Nat Immunol* (2005) 6:981–8. doi: 10.1038/ni1243

46. Ablasser A, Goldeck M, Cavlar T, Deimling T, Witte G, Röhl I, et al. cGAS produces a 2'-5'-linked cyclic dinucleotide second messenger that activates STING. *Nature* (2013) 498:380–4. doi: 10.1038/nature12306

47. Fitzgerald KA, Kagan JC. Toll-like receptors and the control of immunity. *Cell* (2020) 180:1044–66. doi: 10.1016/j.cell.2020.02.041

48. Ullah MO, Sweet MJ, Mansell A, Kellie S, Kobe B. TRIF-dependent TLR signaling, its functions in host defense and inflammation, and its potential as a therapeutic target. *J Leukoc Biol* (2016) 100:27–45. doi: 10.1189/jlb.2RI1115-531R

49. Liu Z-M, Yang M-H, Yu K, Lian Z-X, Deng S-L. Toll-like receptor (TLRs) agonists and antagonists for COVID-19 treatments. *Front Pharmacol* (2022) 13:989664. doi: 10.3389/fphar.2022.989664

50. Zhao Y, Kuang M, Li J, Zhu L, Jia Z, Guo X, et al. SARS-CoV-2 spike protein interacts with and activates TLR4. *Cell Res* (2021) 31:818–20. doi: 10.1038/s41422-021-00495-9

51. Nguyen AD, McDonald JG, Bruick RK, DeBose-Boyd RA. Hypoxia stimulates degradation of 3-Hydroxy-3-methylglutaryl-coenzyme a reductase through accumulation of lanosterol and hypoxia-inducible factor-mediated induction of insigs. *J Biol Chem* (2007) 282:27436–46. doi: 10.1074/jbc.M704976200

52. Zhu J, Jiang X, Chehab FF. FoxO4 interacts with the sterol regulatory factor SREBP2 and the hypoxia inducible factor HIF2α at the CYP51 promoter. *J Lipid Res* (2014) 55:431–42. doi: 10.1194/jlr.M043521

53. Song B-L, Javitt NB, DeBose-Boyd RA. Insig-mediated degradation of HMG CoA reductase stimulated by lanosterol, an intermediate in the synthesis of cholesterol. *Cell Metab* (2005) 1:179–89. doi: 10.1016/j.cmet.2005.01.001

54. Kucharzewska P, Christianson HC, Belting M. Global profiling of metabolic adaptation to hypoxic stress in human glioblastoma cells. *PloS One* (2015) 10:e0116740. doi: 10.1371/journal.pone.0116740

55. Cao R, Zhao X, Li S, Zhou H, Chen W, Ren L, et al. Hypoxia induces dysregulation of lipid metabolism in HepG2 cells via activation of HIF-2a. *Cell Physiol Biochem* (2014) 34:1427–41. doi: 10.1159/000366348

56. Dolt KS, Karar J, Mishra MK, Salim J, Kumar R, Grover SK, et al. Transcriptional downregulation of sterol metabolism genes in murine liver exposed to acute hypobaric hypoxia. *Biochem Biophys Res Commun* (2007) 354:148–53. doi: 10.1016/j.bbrc.2006.12.159

57. Kondo A, Yamamoto S, Nakaki R, Shimamura T, Hamakubo T, Sakai J, et al. Extracellular acidic pH activates the sterol regulatory element-binding protein 2 to promote tumor progression. *Cell Rep* (2017) 18:2228–42. doi: 10.1016/j.celrep.2017.02.006

58. Pallottini V, Guantario B, Martini C, Totta P, Filippi I, Carraro F, et al. Regulation of HMG-CoA reductase expression by hypoxia. *J Cell Biochem* (2008) 104:701–9. doi: 10.1002/jcb.21757

59. Araldi E, Fernández-Fuertes M, Canfrán-Duque A, Tang W, Cline GW, Madrigal-Matute J, et al. Lanosterol modulates TLR4-mediated innate immune responses in macrophages. *Cell Rep* (2017) 19:2743–55. doi: 10.1016/j.celrep.2017.05.093

60. Zhang X, McDonald JG, Aryal B, Canfrán-Duque A, Goldberg EL, Araldi E, et al. Desmosterol suppresses macrophage inflammasome activation and protects against vascular inflammation and atherosclerosis. *Proc Natl Acad Sci USA* (2021) 118:e2107682118. doi: 10.1073/pnas.2107682118

61. Chen W, Li S, Yu H, Liu X, Huang L, Wang Q, et al. ER adaptor SCAP translocates and recruits IRF3 to perinuclear microsome induced by cytosolic microbial DNAs. *PloS Pathog* (2016) 12:e1005462. doi: 10.1371/journal.ppat.1005462

62. Gholkar AA, Cheung K, Williams KJ, Lo Y-C, Hamideh SA, Nnebe C, et al. Fatostatin inhibits cancer cell proliferation by affecting mitotic microtubule spindle assembly and cell division. *J Biol Chem* (2016) 291:17001–8. doi: 10.1074/jbc.C116.737346

63. Shao W, Machamer CE, Espenshade PJ. Fatostatin blocks ER exit of SCAP but inhibits cell growth in a SCAP-independent manner. *J Lipid Res* (2016) 57:1564–73. doi: 10.1194/jlr.M069583

64. Sarkar P, Kumar GA, Shrivastava S, Chattopadhyay A. Chronic cholesterol depletion increases f-actin levels and induces cytoskeletal reorganization via a dual mechanism. *J Lipid Res* (2022) 63:100206. doi: 10.1016/j.jlr.2022.100206

65. Lebrand C, Corti M, Goodson H, Cosson P, Cavalli V, Mayran N, et al. Late endosome motility depends on lipids via the small GTPase Rab7. *EMBO J* (2002) 21:1289–300. doi: 10.1093/emboj/21.6.1289

66. Azzam KM, Fessler MB. Crosstalk between reverse cholesterol transport and innate immunity. *Trends Endocrinol Metab* (2012) 23:169–78. doi: 10.1016/j.tem.2012.02.001

67. Sun Y, Ishibashi M, Seimon T, Lee M, Sharma SM, Fitzgerald KA, et al. Free cholesterol accumulation in macrophage membranes activates toll-like receptors and p38 mitogen-activated protein kinase and induces cathepsin K. *Circ Res* (2009) 104:455–65. doi: 10.1161/CIRCRESAHA.108.182568

68. McGettrick AF, O'Neill LA. Localisation and trafficking of toll-like receptors: an important mode of regulation. *Curr Opin Immunol* (2010) 22:20–7. doi: 10.1016/j.coi.2009.12.002

69. Ciesielska A, Matyjek M, Kwiatkowska K. TLR4 and CD14 trafficking and its influence on LPS-induced pro-inflammatory signaling. *Cell Mol Life Sci* (2021) 78:1233–61. doi: 10.1007/s00018-020-03656-y

70. Suzuki M, Sugimoto Y, Ohsaki Y, Ueno M, Kato S, Kitamura Y, et al. Endosomal accumulation of toll-like receptor 4 causes constitutive secretion of cytokines and activation of signal transducers and activators of transcription in niemann-pick disease type c (NPC) fibroblasts: a potential basis for glial cell activation in the NPC brain. *J Neurosci* (2007) 27:1879–91. doi: 10.1523/JNEUROSCI.5282-06.2007

71. McDonough A, Lee RV, Noor S, Lee C, Le T, Iorga M, et al. Ischemia/Reperfusion induces interferon-stimulated gene expression in microglia. *J Neurosci* (2017) 37:8292–308. doi: 10.1523/JNEUROSCI.0725-17.2017

72. Hayakawa S, Tamura A, Nikiforov N, Koike H, Kudo F, Cheng Y, et al. Activated cholesterol metabolism is integral for innate macrophage responses by amplifying Myd88 signaling. *JCI Insight* (2022) 7:e138539. doi: 10.1172/jci.insight.138539

73. Sprenger H-G, MacVicar T, Bahat A, Fiedler KU, Hermans S, Ehrentraut D, et al. Cellular pyrimidine imbalance triggers mitochondrial DNA–dependent innate immunity. *Nat Metab* (2021) 3:636–50. doi: 10.1038/s42255-021-00385-9

74. Katze MG, He Y, Gale M. Viruses and interferon: a fight for supremacy. *Nat Rev Immunol* (2002) 2:675–87. doi: 10.1038/nri888

75. Yao Y, Subedi K, Liu T, Khalasawi N, Pretto-Kernahan CD, Wotring JW, et al. Surface translocation of ACE2 and TMPRSS2 upon TLR4/7/8 activation is required for SARS-CoV-2 infection in circulating monocytes. *Cell Discov* (2022) 8:89. doi: 10.1038/s41421-022-00453-8

76. Zheng J, Wang Y, Li K, Meyerholz DK, Allamargot C, Perlman S. Severe acute respiratory syndrome coronavirus 2–induced immune activation and death of monocyte-derived human macrophages and dendritic cells. *J Infect Dis* (2021) 223:785–95. doi: 10.1093/infdis/jiaa753

77. Wilk AJ, Rustagi A, Zhao NQ, Roque J, Martínez-Colón GJ, McKechnie JL, et al. A single-cell atlas of the peripheral immune response in patients with severe COVID-19. *Nat Med* (2020) 26:1070–6. doi: 10.1038/s41591-020-0944-y

78. Junqueira C, Crespo Â, Ranjbar S, de Lacerda LB, Lewandrowski M, Ingber J, et al. FcγR-mediated SARS-CoV-2 infection of monocytes activates inflammation. *Nature* (2022) 606:576–84. doi: 10.1038/s41586-022-04702-4

79. Sefik E, Qu R, Junqueira C, Kaffe E, Mirza H, Zhao J, et al. Inflammasome activation in infected macrophages drives COVID-19 pathology. *Nature* (2022) 606:585–93. doi: 10.1038/s41586-022-04802-1

80. Soltani-Zangbar MS, Parhizkar F, Abdollahi M, Shomali N, Aghebati-Maleki L, Shahmohammadi Farid S, et al. Immune system-related soluble mediators and COVID-19: basic mechanisms and clinical perspectives. *Cell Commun Signal* (2022) 20:131. doi: 10.1186/s12964-022-00948-7

81. Eskandarian Boroujeni M, Sekrecka A, Antonczyk A, Hassani S, Sekrecki M, Nowicka H, et al. Dysregulated interferon response and immune hyperactivation in severe COVID-19: targeting STATs as a novel therapeutic strategy. *Front Immunol* (2022) 13:888897. doi: 10.3389/fimmu.2022.888897

82. Channappanavar R, Perlman S. Pathogenic human coronavirus infections: causes and consequences of cytokine storm and immunopathology. *Semin Immunopathol* (2017) 39:529–39. doi: 10.1007/s00281-017-0629-x

83. Grant RA, Morales-Nebreda L, Markov NS, Swaminathan S, Querrey M, Guzman ER, et al. Circuits between infected macrophages and T cells in SARS-CoV-2 pneumonia. *Nature* (2021) 590:635–41. doi: 10.1038/s41586-020-03148-w

84. Grieb P, Swiatkiewicz M, Prus K, Rejdak K. Hypoxia may be a determinative factor in COVID-19 progression. *Curr Res Pharmacol Drug Discov* (2021) 2:100030. doi: 10.1016/j.crphar.2021.100030

85. Lee W, Ahn JH, Park HH, Kim HN, Kim H, Yoo Y, et al. COVID-19-activated SREBP2 disturbs cholesterol biosynthesis and leads to cytokine storm. *Signal Transduct Target Ther* (2020) 5:186. doi: 10.1038/s41392-020-00292-7

86. Wang R, Simoneau CR, Kulsuptrakul J, Bouhaddou M, Travisano KA, Hayashi JM, et al. Genetic screens identify host factors for SARS-CoV-2 and common cold coronaviruses. *Cell* (2021) 184:106–119.e14. doi: 10.1016/j.cell.2020.12.004

International Journal of
Molecular Sciences

MDPI

Article

Functional RNA Dynamics Are Progressively Governed by RNA Destabilization during the Adaptation to Chronic Hypoxia

Rebekka Bauer [1], Sofie Patrizia Meyer [1], Karolina Anna Kloss [2], Vanesa Maria Guerrero Ruiz [1], Samira Reuscher [2], You Zhou [2], Dominik Christian Fuhrmann [1,3], Kathi Zarnack [2,*], Tobias Schmid [1,3,*,†] and Bernhard Brüne [1,3,4,5,†]

1 Faculty of Medicine, Institute of Biochemistry I, Goethe-University Frankfurt, 60590 Frankfurt, Germany; bauer@biochem.uni-frankfurt.de (R.B.); s.meyer@biochem.uni-frankfurt.de (S.P.M.); guerreroruiz@biochem.uni-frankfurt.de (V.M.G.R.); fuhrmann@biochem.uni-frankfurt.de (D.C.F.); b.bruene@biochem.uni-frankfurt.de (B.B.)
2 Faculty of Biological Sciences, Buchmann Institute for Molecular Life Sciences (BMLS), Goethe-University Frankfurt, 60438 Frankfurt, Germany; karo.kloss@googlemail.com (K.A.K.); samira.reuscher@gmail.com (S.R.); you.zhou@bmls.de (Y.Z.)
3 German Cancer Consortium (DKTK), Partner Site Frankfurt, 60590 Frankfurt, Germany
4 Frankfurt Cancer Institute, Goethe-University Frankfurt, 60596 Frankfurt, Germany
5 Fraunhofer Institute for Translational Medicine and Pharmacology, 60596 Frankfurt, Germany
* Correspondence: kathi.zarnack@bmls.de (K.Z.); t.schmid@biochem.uni-frankfurt.de (T.S.)
† These authors contributed equally to this work.

Abstract: Previous studies towards reduced oxygen availability have mostly focused on changes in total mRNA expression, neglecting underlying transcriptional and post-transcriptional events. Therefore, we generated a comprehensive overview of hypoxia-induced changes in total mRNA expression, global de novo transcription, and mRNA stability in monocytic THP-1 cells. Since hypoxic episodes often persist for prolonged periods, we further compared the adaptation to acute and chronic hypoxia. While total mRNA changes correlated well with enhanced transcription during short-term hypoxia, mRNA destabilization gained importance under chronic conditions. Reduced mRNA stability not only added to a compensatory attenuation of immune responses, but also, most notably, to the reduction in nuclear-encoded mRNAs associated with various mitochondrial functions. These changes may prevent the futile production of new mitochondria under conditions where mitochondria cannot exert their full metabolic function and are indeed actively removed by mitophagy. The post-transcriptional mode of regulation might further allow for the rapid recovery of mitochondrial capacities upon reoxygenation. Our results provide a comprehensive resource of functional mRNA expression dynamics and underlying transcriptional and post-transcriptional regulatory principles during the adaptation to hypoxia. Furthermore, we uncover that RNA stability regulation controls mitochondrial functions in the context of hypoxia.

Keywords: hypoxia; monocytes; de novo transcription; RNA stability; SLAM-seq; GRAND-SLAM

Citation: Bauer, R.; Meyer, S.P.; Kloss, K.A.; Guerrero Ruiz, V.M.; Reuscher, S.; Zhou, Y.; Fuhrmann, D.C.; Zarnack, K.; Schmid, T.; Brüne, B. Functional RNA Dynamics Are Progressively Governed by RNA Destabilization during the Adaptation to Chronic Hypoxia. *Int. J. Mol. Sci.* **2022**, *23*, 5824. https://doi.org/10.3390/ijms23105824

Academic Editors: Elena Rybnikova and Ludmila D. Lukyanova

Received: 6 April 2022
Accepted: 20 May 2022
Published: 22 May 2022

1. Introduction

Hypoxia is a common environmental factor both in physiological and pathophysiological contexts. Specifically, while high altitudes as well as certain cellular niches, such as the bone marrow, are inherently characterized by low oxygen tensions, hypoxic conditions pathologically occur, e.g., upon vascular thrombosis, within rapidly growing tumors, as well as in diseases associated with severe inflammatory conditions [1,2]. Since ambient oxygen availability is critical for numerous cellular processes, such as energy production by mitochondrial oxidative phosphorylation, it is not surprising that adaptive processes to hypoxia have been in the limelight of research for many decades [3]. Specifically, hypoxia induces a rapid increase in glucose transporters and glycolytic enzymes to ensure sufficient energy supply and, furthermore, even represses mitochondrial function [4,5]. Under

prolonged hypoxic conditions this metabolic rewiring appears to be further stabilized by autophagy-dependent removal of the mitochondria [6–8].

Nevertheless, despite the fact that disease conditions commonly reflect conditions of chronic hypoxia, efforts to molecularly characterize hypoxia responses have so far largely focused on acute hypoxic conditions, identifying the oxygen-sensitive transcription factors hypoxia-inducible factor (HIF) 1 and 2 as key regulators of adaptive processes [9–11]. Interestingly though, during extended hypoxia, both HIFs are downregulated again [12,13], which in combination with a new steady state expression of classical hypoxia response genes, was recently put forward as an indicator for chronic hypoxia [14,15]. Importantly, this definition of chronic hypoxia encompasses a cellular response state rather than an exact duration of hypoxic conditions, and was detected in THP-1 monocytes as well as in various multiple myeloma after 72 h of hypoxia [14,15]. Notably, in line with the decreasing relevance of HIF-mediated adaptations during prolonged hypoxia, post-transcriptional regulatory mechanisms, including mRNA stability regulation, translational changes, and alternative splicing, have been shown to contribute to hypoxic responses as well [12,16–19].

2. Results

As the contribution of different regulatory layers on gene expression changes throughout the course of hypoxia remains largely elusive, we aimed at characterizing altered mRNA dynamics during acute and chronic oxygen deprivation. To this end, we exposed THP-1 monocytes to acute (AH, 8 h, 1% oxygen) and chronic hypoxia (CH, 72 h, 1% oxygen) [14] and employed SLAM-seq (thiol(SH)-linked alkylation for the metabolic sequencing of RNA) [20]. Specifically, we added 4-thiouridine (4sU; 300 µM) during the last hour of the respective incubations to label newly synthesized mRNA and determined differential gene expression (DGE) changes and differentially de novo synthesized (DDNS) mRNAs by RNA sequencing based on changes in total read counts and reads harboring T-to-C transitions due to 4sU incorporation, respectively.

2.1. Hypoxia Induces Dynamic Changes in mRNA Expression

Initially, we focused on global gene expression changes in THP-1 monocytes from acute to extended hypoxic exposures (Figure 1A). Overall, more pronounced DGE changes compared to normoxia (N) (Benjamini–Hochberg-corrected *p*-value (padj) < 0.05) occurred under CH than under AH (DGE(CH/N): 1824; DGE(AH/N): 370) (Figure 1B). The observation that a large proportion of the additional genes regulated under CH significantly changed between CH and AH, supports the notion that a major part of the adaptive processes to hypoxia is induced under extended hypoxic incubations only. To obtain further insights into the expression dynamics under hypoxia, we used *k*-means clustering analysis of all DGE targets significantly regulated between AH, CH, and/or N, identifying five clusters of targets following different expression patterns in the course of hypoxia (Figure 1C (*left panels*); Figure S1): A small group of DGE targets (8% of all DGE; cluster 1) rapidly increased already under AH, remaining stable or decreasing under CH (Figure 1C (*annotation columns 1–3*)). Two larger groups of genes steadily increased (cluster 2) or decreased (cluster 5) in expression across the course of hypoxia, representing 19% and 21% of all DGE changes, respectively. In line with the above described observation that CH induced more substantial DGE changes, the two largest clusters were characterized by a predominant or exclusive up- (cluster 3; 25%) or downregulation (cluster 4; 26%) under CH. Notably, while the mean absolute read counts of genes appeared to be similar across all clusters, targets in cluster 4 (predominantly downregulated under CH) appeared to be expressed at higher basal (N) levels (Figure S1; Table S1).

To assess potential functional implications of the altered mRNA expression profiles in the course of hypoxia, gene set enrichment analyses (GSEA) for specific well-defined biological states or processes (hallmarks) were carried out for all mRNA expression changes occurring under AH and CH relative to N. Despite the marked difference in DGE changes between AH and CH, the same functional implications were enriched in both conditions

(Table S2), i.e., hypoxia and cholesterol homeostasis emerged among the top enriched upregulated hallmarks, while Myc targets, E2F targets, and DNA repair were among the top enriched downregulated hallmarks (Figures 1D and S2).

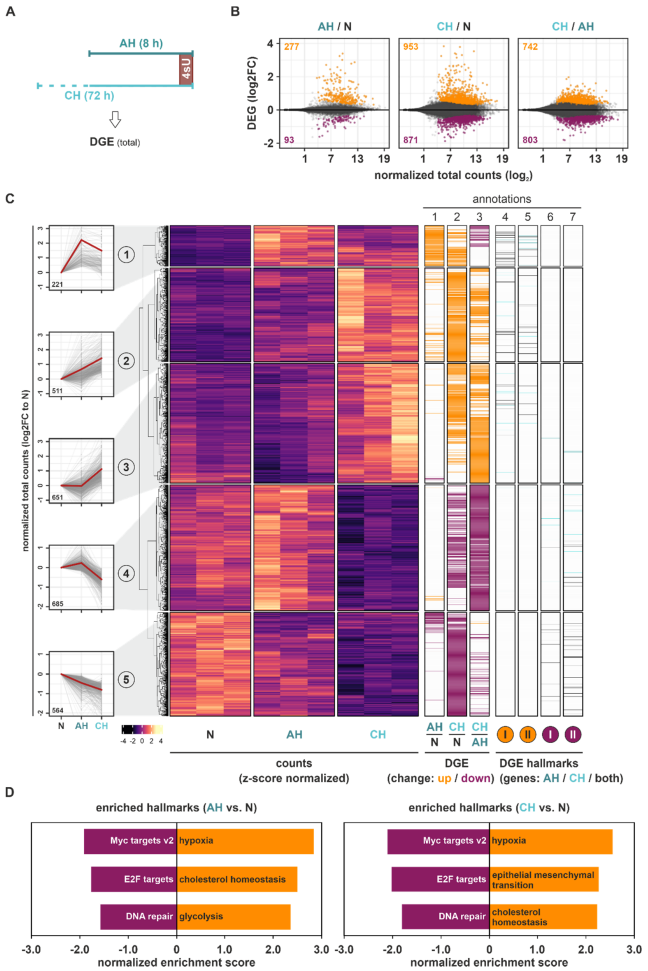

Figure 1. Differential gene expression (DGE) changes under hypoxia. (**A**) THP-1 cells were incubated under hypoxia (1% oxygen) for 8 h (acute hypoxia, AH) or 72 h (chronic hypoxia, CH), or under normoxia, supplemented with 300 µM 4-thiouridine (4sU) for the last hour. DGE changes were determined based on changes in total read counts. (**B**) MA plots representing DGE changes (log2FC) between AH and N (*left*), CH and N (*middle*), or CH and AH (*right*). Significant DGE targets (padj < 0.05) are indicated in orange (up) or purple (down). (**C**) Heatmap representing *z*-score-normalized counts of all DGE targets significantly altered in at least one of the comparisons. Five groups representing different DGE dynamics were identified by *k*-means clustering analysis (*left panels*). Annotation columns 1–3 depict DGE changes (up: orange; down: purple) for the comparison

of AH and N, CH and N, and CH and AH. Annotation columns 4–7 depict targets contributing to the GSEA-enriched hallmarks either upregulated (I: hypoxia; II: cholesterol homeostasis (*orange*)) or downregulated (I: Myc targets v2; II: E2F targets (*purple*)) in DGE of either AH vs. N, CH vs. N, or both. (**D**) Top three enriched up- or downregulated hallmarks identified by GSEA of total mRNA expression under AH or CH relative to N.

In line with this, many of the DGE targets constituting the enriched hallmarks hypoxia and cholesterol homeostasis were upregulated, while Myc targets and E2F targets were downregulated in both AH and CH. A few DGE candidates associated with these functional hallmarks appeared to be altered exclusively under CH, mostly in clusters 3 and 4 (Figure 1C (*annotation columns 4–7*)).

Taken together, total mRNA expression changes during the course of hypoxia not only bore signs of enhanced classical hypoxia responses, but also were enriched for upregulated cholesterol metabolism and reduced Myc and E2F target expression. This suggests altered metabolic processes as well as reduced proliferation and cell cycle progression. The finding that chronic conditions generally induced more pronounced DGE changes than AH, and that the proportion of downregulated targets substantially increased under CH, implies that the regulatory principles underlying dynamic mRNA expression changes differ considerably between short- and long-term hypoxia.

2.2. Hypoxia Enhances Transcriptional Responses

In order to obtain further insights into the regulatory mechanisms governing the observed changes in total RNA dynamics, we next analyzed newly transcribed mRNAs (DDNS) by assessing T-to-C conversions resulting from chemical modification of incorporated 4sU in newly synthesized mRNAs (Figures 2A and S3A). The vast majority of AH- or CH-induced DDNS changes (padj < 0.1) reflected the enhanced transcription of targets, i.e., 94% and 76% of DDNS targets were upregulated under AH and CH, respectively (Figure 2B). Further comparison of the DDNS changes between CH and AH revealed only a few additional changes, pointing to the attenuation of hypoxia-induced transcription under chronic conditions. Alike to the DGE changes, *k*-means clustering of all DDNS targets regulated between AH, CH, and/or N identified five groups of targets representing different DDNS dynamics in the course of hypoxia (Figure 2C (*left panels*); Figure S4 (*upper panels*)). Three similarly-sized clusters, representing 66% of significant DDNS changes, corresponded to targets with enhanced transcription during hypoxia, either steadily increasing across the course of hypoxia (cluster 1) or alternatively increasing under AH, and thereafter remaining stable (cluster 2) or decreasing again (cluster 3). Clusters 4 (24%) and 5 (10%) depicted DDNS that were transcriptionally downregulated either exclusively under CH (cluster 4) or cumulatively throughout the hypoxic exposure (cluster 5) (Figure 2C (*annotation columns 1–3*); Table S3). Notably, transcriptional changes (Figure 2C (*annotation columns 1–3*)) in the identified DDNS targets appeared to closely resemble their changes in DGE level (Figure 2C (*annotation columns 4–6*)). Moreover, the increase in normalized T-to-C read counts under basal (N) conditions observed from DDNS clusters 1 to 4, which decreased again in cluster 5, closely followed the corresponding changes in total mRNA expression (Figure S4).

In line with the concurrent changes in DDNS and DGE, GSEA of the DDNS changes also identified hypoxia and cholesterol homeostasis as the top enriched upregulated hallmarks under AH and CH (Figures 2D and S5; Table S4). Due to the low number of downregulated DDNS targets, no enriched downregulated hallmarks were identified in DDNS under AH, yet E2F and Myc targets were again enriched under CH.

Thus, the analysis of changes in de novo mRNA synthesis suggested marked transcriptional adaptations under AH with only minor additional changes under CH. The enhanced transcription of hypoxia- and cholesterol metabolism-associated targets corroborated the changes in DGE level, while downregulated DDNS correlated with the DGE changes under CH related to cell cycle-associated hallmarks.

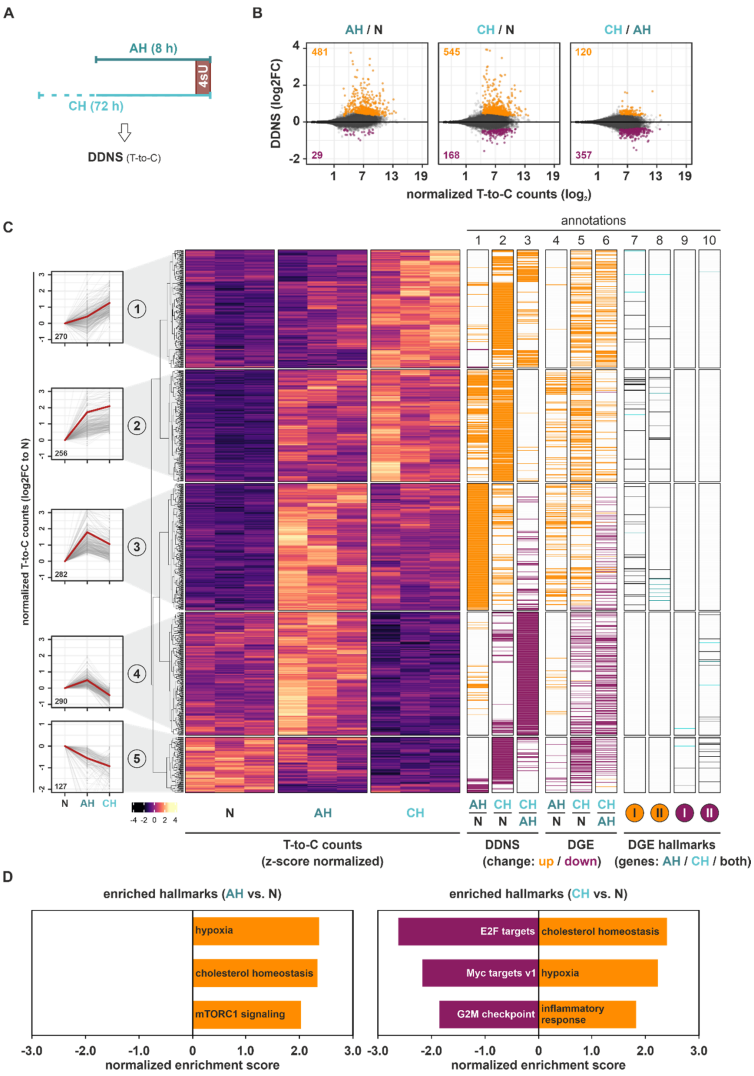

Figure 2. Differential de novo synthesis (DDNS) changes under hypoxia. (**A**) THP-1 cells were incubated under hypoxia (1% oxygen) for 8 h (acute hypoxia, AH) or 72 h (chronic hypoxia, CH), or under normoxia, supplemented with 300 µM 4-thiouridine (4sU) for the last hour. DDNS changes were determined based on 4sU alkylation-dependent changes in T-to-C conversions. (**B**) MA plots representing DDNS changes (log2FC) between AH and N (*left*), CH and N (*middle*), or CH and AH (*right*). Significant DDNS targets (padj < 0.1) are indicated in orange (up) or purple (down). (**C**) Heatmap reflecting *z*-score-normalized T-to-C read counts of all DDNS targets significantly altered

in at least one of the comparisons. Five groups representing different DDNS dynamics were identified by *k*-means clustering analysis (*left panels*). Annotation columns 1–3 contain DDNS changes (up: orange; down: purple) for the comparison of AH and N, CH and N, and CH and AH. Annotation columns 4–6 encompass DGE changes (up: orange; down: purple) for the comparison of AH and N, CH and N, and CH and AH. Annotation columns 7–10 reflect targets from the GSEA-enriched hallmarks either upregulated (I: hypoxia; II: cholesterol homeostasis) or downregulated (I: Myc targets v2; II: E2F targets) in DGE of either AH, CH, or both (Figure 1D). (**D**) Top three enriched up- or downregulated hallmarks identified by GSEA of T-to-C count changes under AH or CH relative to N.

2.3. Hypoxia Reduces RNA Stability

As transcriptional changes (DDNS) appeared to explain only parts of the total gene expression changes (DGE) under hypoxia, and since post-transcriptional modes of regulation, including mRNA stability regulation, are known to commonly contribute to gene expression changes in response to extended stimulations [21,22], we next determined differentially stability regulated (DSR) mRNAs under hypoxic conditions. Therefore, we labeled THP-1 cells for 8 h with 4sU, i.e., four pulses of 30 µM 4sU every 2 h during the last 8 h of the experiment to ensure sufficient labeling (Figure 3A). Indeed, 4 × 30 µM 4sU administered over a time course of 8 h strongly increased T-to-C conversion rates compared to a single dose of 300 µM, while it did not affect the viability of THP-1 cells (Figure S3B,C). mRNA half-lives were determined based on T-to-C conversions using the GRAND-SLAM pipeline [23]. Interestingly, not only were global mRNA half-lives significantly reduced under AH (median half-life = 3.30 h) and CH (3.16 h) as compared to N (3.71 h) (Figure S6A), but the vast majority (99%) of DSR changes in response to both AH and CH compared to N (padj < 0.1) corresponded to reduced mRNA stability, with only a few stabilized targets (Figure 3B). The stratification of all DSR targets comparing AH, CH, and/or N by *k*-means clustering again identified five groups representing different half-life dynamics across the course of hypoxia (Figure 3C (*left panels*); Figure S7 (*upper panels*)). Only 2% of DSR targets displayed enhanced half-lives in response to hypoxia, which appeared to transiently increase under AH only (cluster 1). All other groups were characterized by reduced mRNA half-lives already under AH. Specifically, cluster 2 represented targets with a steady reduction in target half-life from AH to CH. Despite their separation by clustering analysis, clusters 3 and 4, representing 65% of all DSR targets, showed markedly reduced mRNA half-lives under AH, which remained low under CH. Cluster 5 contained DSR targets with a strong, yet transient reduction in half-lives during the course of hypoxia (Figure 3C (*annotation columns 1–3*); Table S5). In contrast to the distribution in DDNS, DSR changes (Figure 3C (*annotation columns 1–3*)) poorly correlated with changes in DGE level (Figure 3C (*annotation columns 4–6*)).

Notably, the few targets showing an increase in half-lives under hypoxia (cluster 1) shared rather short basal (N) half-lives (median half-life = 1.41 h), whereas the targets in cluster 5 (transient decrease in half-lives) had the longest basal (N) half-lives (16.89 h), and clusters 2–4 ranked at 7.49 h, 12.31 h, and 11.15 h, respectively (Figure S7).

In line with the observation that downregulated DSR targets vastly outnumbered upregulated ones, the GSEA of mRNA half-lives identified predominantly downregulated hallmarks (Figures 3D and S8; Table S6). Specifically, Myc targets, oxidative phosphorylation, and fatty acid metabolism emerged as the top enriched downregulated hallmarks under both AH and CH, and only TNFα signaling via NFκB and downregulated Kras signaling appeared to be enriched in upregulated DSR under CH.

In summary, our data on the differential stability regulation of mRNAs in the course of hypoxia indicated that most DSR targets are destabilized under hypoxia and that the major regulated groups show only slight changes between acute and chronic conditions. Enriched hallmarks within the downregulated DSR targets pointed to altered Myc activation and adaptation of metabolic processes (oxidative phosphorylation, fatty acid metabolism) under both AH and CH.

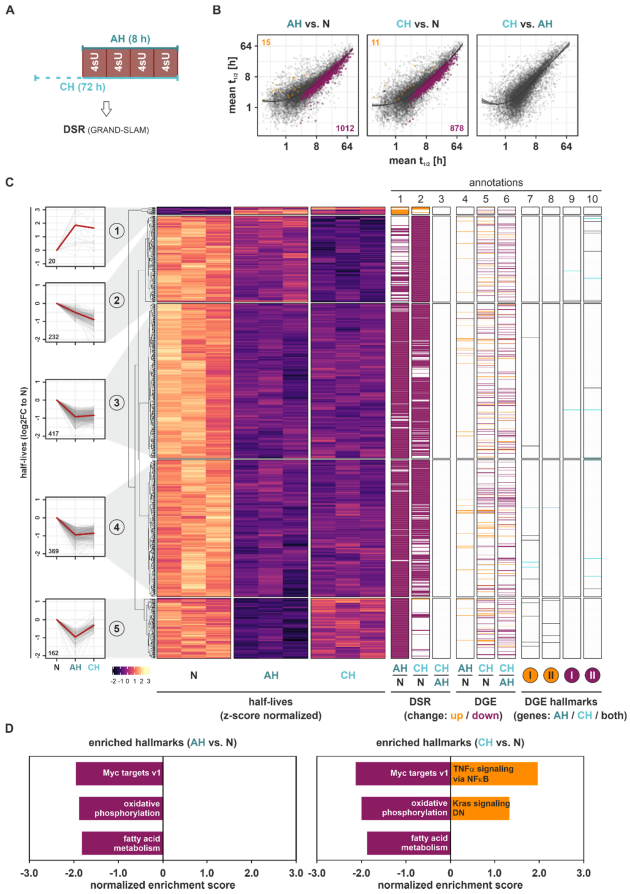

Figure 3. Differential stability regulation (DSR) changes under hypoxia. (**A**) THP-1 cells were incubated under hypoxia (1% oxygen) for 8 h (acute hypoxia, AH) or 72 h (chronic hypoxia, CH), or under normoxia, supplemented with 4 ×30 µM 4-thiouridine (4sU) during the last 8 h. DSR changes were determined based on 4sU alkylation-dependent changes in T-to-C conversions using GRAND-SLAM. (**B**) Scatter plots comparing mean mRNA half-lives at AH vs. N (*left*), CH vs. N (*middle*), and CH vs. AH (*right*) highlighting significantly increased (orange) or decreased (purple) half-lives between the conditions (padj < 0.1, local linear regression + 95% confidence intervals). (**C**) Heatmap reflecting *z*-score-normalized half-lives of all DSR targets significantly altered in at least one of the comparisons. Five groups representing different DSR dynamics were identified by *k*-means clustering analysis (*left panels*). Annotation columns 1–3 contain DSR changes (up: orange; down: purple) for the comparison of AH and N, CH and N, and CH and AH. Annotation columns 4–6 encompass DGE changes (up: orange; down: purple) for the comparison of AH and N, CH and N, and CH and AH. Annotation columns 7–10 reflect targets contributing to the GSEA-enriched hallmarks either upregulated (I: hypoxia; II: cholesterol homeostasis) or downregulated (I: Myc targets v2; II: E2F targets) in DGE of either AH, CH, or both (Figure 1D). (**D**) Top three enriched up- or downregulated hallmarks identified by GSEA of mRNA half-life changes under AH or CH relative to N.

2.4. Functional DDNS and DSR Determine Specific Changes in DGE Dynamics in Hypoxia

Having established differential regulatory patterns for transcriptional and stability regulation under hypoxia and the divergent correlation with the prime enriched DGE hallmarks, we next assessed which of the identified DDNS and DSR changes might influence total gene expression (DGE). First, we focused on DGE targets upregulated in the course of hypoxia (DGE clusters 1–3) and determined how DGE targets within these clusters behaved on DDNS and DSR levels (Figure 4A; Table S7). Herein, DDNS changes closely resembled the DGE changes, whereas DSR changes appeared to rather counteract the DGE changes, i.e., upregulated mRNAs at DDNS and DGE level were destabilized at the DSR level at the same time. Furthermore, DDNS overlapped better with DGE targets induced already under AH (clusters 1 and 2), suggesting the early induction of transcriptional responses. To assess which adaptive cellular processes induced under hypoxia might be regulated at a transcriptional or a post-transcriptional level, we determined enriched functional annotations in upregulated DGE targets concomitantly upregulated in DDNS (functional DDNS) or in upregulated DGE targets downregulated in DSR (compensatory DSR). In line with the observation that DGE changes representing the enriched hallmarks hypoxia and cholesterol homeostasis (Table S2) were also found in the upregulated DDNS clusters 1–3 (Figure 2C (*annotation columns 7–8*)), functional DDNS were enriched for cholesterol metabolism and hypoxia response (Figure 4B (*middle panel*); Table S8) as identified for all DGE (Figure 1D) and DDNS changes (Figure 2D). Instead, upregulated DGE (clusters 1–3) showed an enrichment of rather general annotations referring to altered membrane composition and communication with the microenvironment (extracellular, immune response) (Figure 4B (*left panel*); Table S8). Interestingly, functional annotations enriched within the compensatory DSR indeed appeared to counteract the DGE-associated functions' extracellular and immune response (Figure 4B (*right panel*); Table S8). Collectively, these observations suggested that adaptive processes induced by hypoxia are facilitated by transcriptional programs, while mRNA stability changes rather appear to counteract enhanced functional programs.

We next asked how downregulated DGE targets (DGE clusters 4 and 5) changed at the DDNS and DSR levels (Figure 5A; Table S7). Generally, downregulated DGE targets overlapped to a much smaller extent with both DDNS and DSR changes. Furthermore, downregulation of DGE targets and concomitant DDNS changes mostly occurred under chronic conditions. In contrast, DSR changes corresponding to downregulated DGE targets were observed similarly under AH and CH. As most DDNS and DSR changes corresponded to downregulated DGE in clusters 4 and 5, only targets decreasing exclusively on DDNS (functional DDNS) or DSR level (functional DSR) in parallel to downregulated DGE were used for the subsequent functional enrichment analyses to allow for an unambiguous assignment to either transcriptional or post-transcriptional regulatory processes. Functional DDNS were enriched in the nucleus, RNA metabolism, and cell cycle annotations (Figure 5B (*middle panel*); Table S8), which corroborated that DGE targets constituting the enriched downregulated DGE hallmarks associated with the cell cycle and transcription (Table S2) were also found in the downregulated DDNS clusters 1–3 (Figure 2C (*annotation columns 9–10*)). Thus, transcriptional changes appeared to correlate well with global gene expression changes. In contrast, the hallmarks enriched in global DGE changes were only poorly reflected on DSR levels (Figure 3C (*annotation columns 7–10*)). Interestingly though, functional DSR targets showed a massive enrichment in mitochondrial functions, and to a lesser extent in translation and oxidative metabolism (Figure 5B (*right panel*); Table S8), corroborating the functional annotation with the highest enrichment in all downregulated DGE targets within clusters 4 and 5 (Figure 5B (*left panel*); Table S8). STRING analysis further supported the tight connection of mitochondria and metabolic changes within the hypoxia-downregulated functional DSR targets (Figure S9; Table S9).

Taken together, general adaptations during the course of hypoxia appear to be determined largely at a transcriptional level. Yet, our data further suggest that post-transcriptional regulatory principles, i.e., mRNA destabilization, also might play an important role. The later may act, e.g., by limiting the extent of hypoxia-induced immune responses, but also

by implementing a reduction in nuclear-encoded, mitochondria-associated mRNAs (see below), thereby contributing to the establishing of specific adaptive processes to (extended) hypoxic conditions.

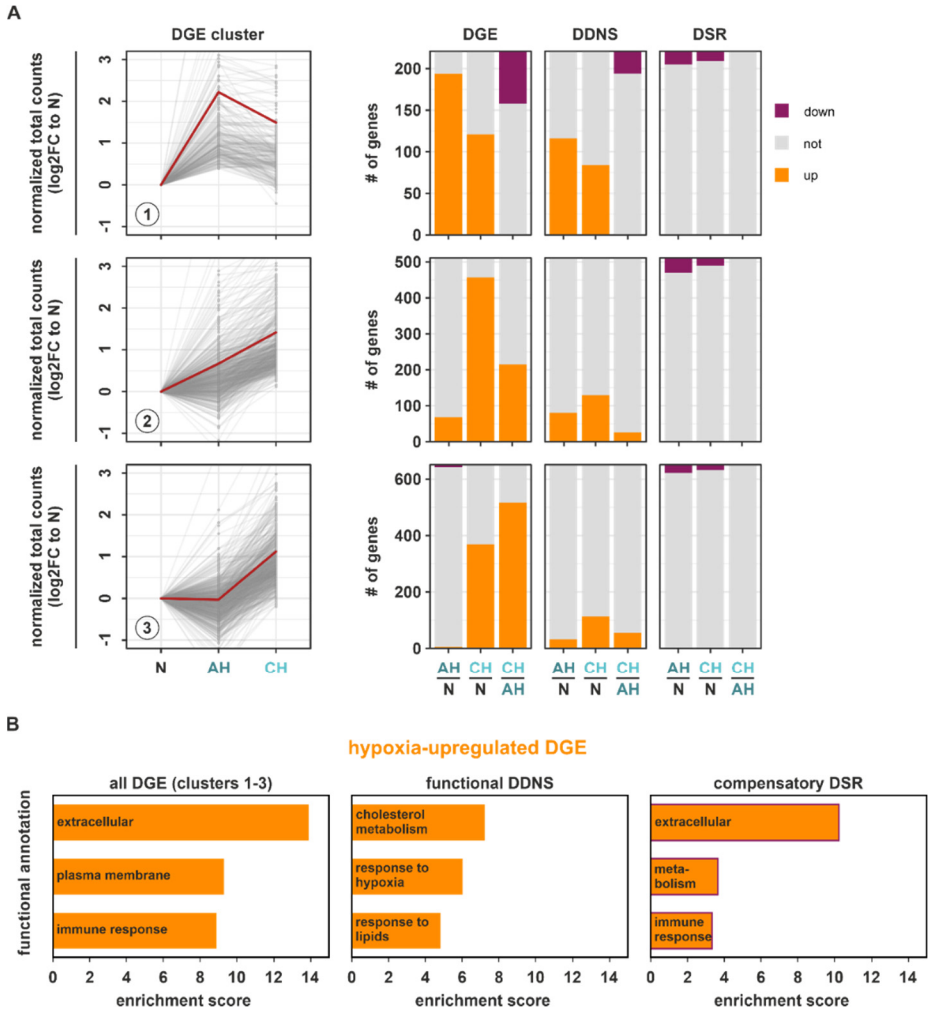

Figure 4. Impact of DDNS and DSR on upregulated DGE targets during hypoxia. (**A**) Changes in the upregulated DGE target clusters (1–3) on the level of DGE, DDNS, and DSR comparing AH and N, CH and N, and CH and AH are depicted as stacked bar graphs. (**B**) Top enriched functional annotations in all upregulated DGE within clusters 1–3 (*left panel*), in functional DDNS, i.e., genes which are upregulated on DGE and DDNS level (*middle panel*), and in compensatory DSR, i.e., genes which are upregulated on DGE and downregulated on DSR level (*right panel*) as determined by DAVID.

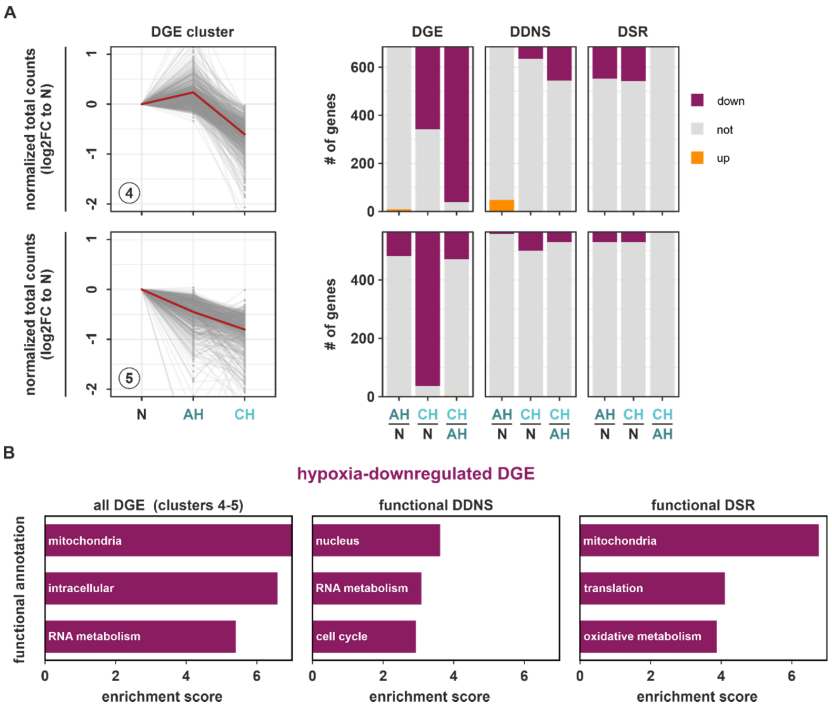

Figure 5. Impact of DSR and DDNS on downregulated DGE targets during hypoxia. (**A**) Changes in the downregulated DGE target clusters (4–5) on the level of DGE, DDNS, and DSR comparing AH and N, CH and N, and CH and AH are depicted as stacked bar graphs. (**B**) Top enriched functional annotations in all downregulated DGE within clusters 4–5 (*left panel*), in functional DDNS, i.e., genes which are downregulated on DGE and DDNS level and unaltered in DSR (*middle panel*), and in functional DSR, i.e., genes which downregulated on DGE and on DSR level and unaltered in DDNS (*right panel*) as determined by DAVID.

2.5. Nuclear-Encoded Mitochondrial mRNAs Are Destabilized in the Course of Hypoxia

A marked reduction in mitochondria in chronic hypoxia in THP-1 cells was previously shown to be mediated by the autophagic removal of mitochondria, i.e., mitophagy. Moreover, the expression of numerous mitochondrial proteins involved in mitochondrial membranes and respiratory chain complexes was also strongly reduced, though not exclusively associated to autophagy [14]. In line with this, we observed reduced mitochondrial mass and oxygen consumption rates, representing mitochondrial function, in THP-1 cells under CH (Figure S10). We therefore asked if mRNAs encoding mitochondrial proteins are indeed destabilized during hypoxia. This may prevent the futile production of novel mitochondria under conditions where excess mitochondrial activity would not only be limited due to reduced oxygen availability, but instead might be deleterious to cells due to the uncontrolled production of reactive oxygen species [24].

In total, 59 functional DSR targets within 10 GO terms comprised the enriched functional annotation mitochondria, termed functional mito-DSR targets (Figure 6A). Interestingly, the median half-life of these functional mito-DSR targets was reduced from 16.02 h under normoxia to 8.31 h under both AH and CH (Figure 6B).

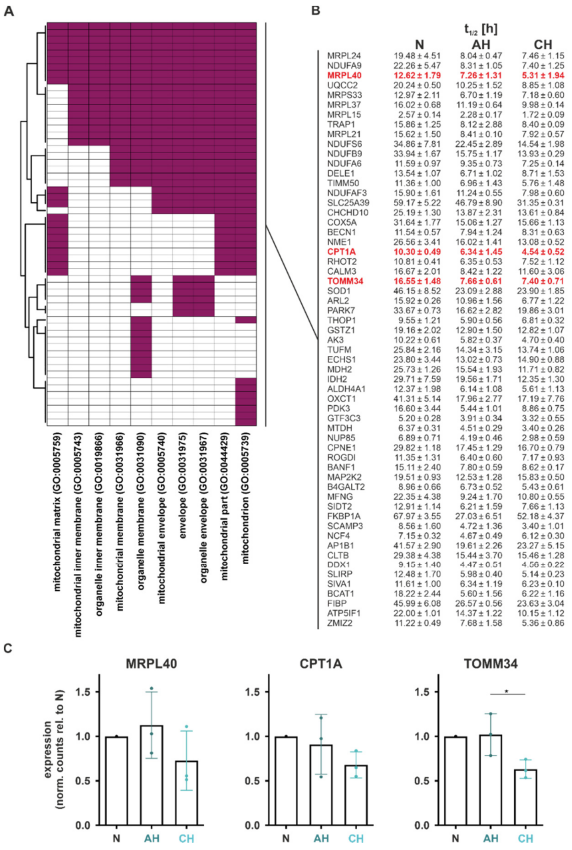

Figure 6. Validation of functional DSR during hypoxia associated with mitochondria. (**A**) GO terms corresponding to mitochondrial functions (Figure 5) and the contributing hypoxia-regulated functional DSR. (**B**) Half-lives of hypoxia-regulated functional DSR under N, AH, or CH as determined by GRAND-SLAM. (**C**) DGE changes in selected functional DSR. Residuals were tested for normality using Shapiro–Wilk test, and one-way ANOVA with Tukey's multiple comparison test was performed (* $p < 0.05$).

In order to validate the half-life changes in mitochondrial targets, we selected the mRNAs encoding MRPL40 (mitochondrial ribosomal protein L40), CPT1A (carnitine palmitoyltransferase 1A), and TOMM34 (translocase of outer mitochondrial membrane 34) for further analyses, based on their association with different mitochondrial functions. While reduced half-lives were already observed under AH for all candidates ($t_{1/2}$ (AH relative to N): *MRLP40*: 58%; *CPT1A*: 62%; *TOMM34*: 46%), functional consequences, i.e., the decrease in total mRNA levels, were appreciable only under CH (Figure 6C).

Considering that these half-lives were determined using a wash-in strategy, i.e., estimating half-lives based on the contribution of mRNA synthesis and decay (GRAND-SLAM), we further aimed to validate the half-lives in an orthogonal wash-out experiment. In this setting, we followed the decay of mRNAs, i.e., the remaining T-to-C conversions for up to 6 h after removal of 4sU and the addition of excess uridine (Figure 7A (*left*)). Notably,

half-lives determined using the wash-out approach appeared to be substantially longer than those predicted by GRAND-SLAM (Figure 7B). Moreover, while the so-determined half-lives of *MRPL40* and *CPT1A* reflected a destabilization under AH and CH, the half-life reduction in *TOMM34* was only observed under AH (Figure 7B (*right panel*)).

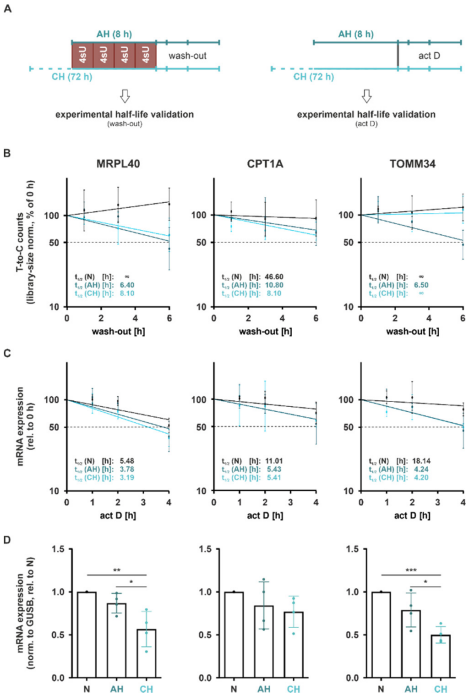

Figure 7. Validation of altered functional mRNA stability under hypoxia. (**A**) THP-1 cells were incubated under hypoxia (1% oxygen) for 8 h (acute hypoxia, AH) or 72 h (chronic hypoxia, CH), or under normoxia. For experimental validation of half-life changes, cells were supplemented with 4 ×30 µM 4-thiouridine (4sU) during the last 8 h, followed by a wash-out with excess uridine of up to 6 h and RNA sequencing (*left*). Alternatively, transcription was blocked by the addition of actinomycin D (2.5 µg/mL; act D) at the end of the incubations, and mRNA expression was followed for up to 4 h by RT-qPCR analyses (*right*). (**B**) mRNA stability of selected functional DSR was determined by wash-out analyses. Library-size corrected T-to-C counts were normalized to 0 h wash-out. (**C**) mRNA stability of selected functional DSR was further analyzed by following mRNA levels after transcriptional blockade. mRNA expression was assessed by RT-qPCR. Half-lives ($t_{1/2}$) were determined by linear regression (**B**,**C**). (**D**) Total mRNA expression of selected functional DSR after AH or CH as compared to N was assessed by RT-qPCR. Residuals were tested for normality using Shapiro–Wilk test, and one-way ANOVA with Tukey's multiple comparison test was performed ($n \geq 3$; * $p < 0.05$, ** $p < 0.01$, *** $p < 0.001$).

To obtain independent experimental evidence on the half-lives, we next blocked de novo mRNA synthesis by adding the transcription inhibitor actinomycin D (2.5 µg/mL; act D) at the end of incubations under N, AH, or CH and followed mRNA levels of the selected candidates for up to 4 h (Figure 7A (*right*)). As seen before, half-lives were already substantially reduced under AH, and remained low or slightly increased again under CH

(Figure 7C). This resulted in a marked downregulation in total mRNA expression of all candidates under CH and to a minor degree already under AH (Figure 7D). Interestingly, half-lives determined using this approach resembled the GRAND-SLAM-calculated half-lives much closer than the wash-out data.

In summary, we provide evidence that nuclear-encoded mRNAs of mitochondrial proteins are indeed downregulated under chronic hypoxia by a reduction in their mRNA stability. These changes appear to be initiated already under acute hypoxia, suggesting that post-transcriptional programs support or stabilize reduced mitochondrial activities, thereby facilitating the metabolic readjustment to prolonged low oxygen availabilities [24].

3. Discussion

Our study provides a comprehensive picture of total mRNA expression changes (DGE), with contributing transcriptional (DDNS) and mRNA stability (DSR) changes in the course of hypoxia. Interestingly, more pronounced changes in gene expression occurred under chronic as compared to acute hypoxia. Adaptations to acute hypoxia were almost exclusively reflected by enhanced mRNA expression, resulting from induced transcription, whereas total mRNA dynamics during prolonged hypoxic incubations were characterized by reduced expression of numerous targets. While transcriptional changes also contributed to the observed reduction in DGE, certain adaptive traits, most notably mitochondrial functions, instead appeared to be determined mostly by reduced mRNA stability, which was initiated already during acute hypoxic conditions.

Gene expression changes in response to oxygen deprivation have been characterized extensively [25–29], and only recently has a comparative analysis of mRNA synthesis and decay under hypoxia been carried out [19]. Nevertheless, a comprehensive analysis of mRNA expression determining transcriptional and post-transcriptional changes during the course of hypoxia was lacking. Our approach combined the analysis of differential gene expression (DGE) changes with contributions of differential de novo synthesis (DDNS) and stability regulated (DSR) targets during both short- and long-term hypoxia. Our observation that hypoxia induces marked transcriptional changes corroborates the notion that hypoxia-inducible transcription factors are of major importance to coordinate hypoxic responses [30]. The enrichment of similar functions in all DGE and DDNS changes during both acute and chronic hypoxia further underscores that major phenotypic adaptations to hypoxia are determined transcriptionally. In line with this, the transcription factors HIF-1 and 2 have been shown to be essential for an appropriate adaptation to hypoxia [11]. Tiana and colleagues recently showed that the majority of hypoxia-induced changes at mRNA level resulted from altered transcription during short-term hypoxia in HUVEC cells using a similar approach [19]. In contrast, total DSR changes are dominated by reduced target stabilities under both acute and chronic conditions. While global DSR changes appeared to only marginally affect total gene expression programs (i.e., Myc targets), altered metabolic requirements associated with lower oxygen availability (i.e., reduction in oxidative phosphorylation and fatty acid metabolism) were enriched in downregulated DSR. Focusing on functional DSR only, i.e., downregulated DSR that correlated with downregulated DGE, not only supported this observation, but extended it to an mRNA stability-dependent reduction in mitochondria and associated metabolic functions on a broader scale. In addition, these observations add a post-transcriptional component to the previously reported autophagy-mediated reduction in mitochondria and reduced expression of various mitochondrial proteins under prolonged hypoxia [6–8,14], which again was supported by our findings of reduced mitochondrial mass and oxygen consumption rate under chronic hypoxia. Functionally, reduced mRNA stability might serve to prevent the futile production of new mitochondrial proteins and mitochondria under conditions where these are actively degraded. On the other hand, the fact that regulation occurs on a post-transcriptional level should allow for a rapid production of mitochondrial proteins once hypoxic conditions are overcome, thereby allowing for an efficient post-hypoxic recovery of mitochondrial energy production. This might be of great relevance in the context of pathophysiological

conditions associated with ischemia-reperfusion, to ensure a rapid normalization of the energetic deficits. Since enhanced activities of the respiratory chain are known to elevate levels of reactive oxygen species (ROS), a rapid recovery of mitochondrial functions during reoxygenation might also prove to be detrimental if protective systems against oxidative stress are not upregulated equally as fast [31]. Thus, it will be interesting to see in future studies how fast mRNA stability-evoked repression of mitochondrial functions is alleviated upon reoxygenation and how this impacts mitochondrial energy and ROS production.

As a side note, functional DSR were further enriched in translation-associated mRNAs, suggesting that reduced mRNA stabilities contribute to reduced translation under hypoxia. Interestingly, while the processes of RNA stability and translational regulation have been shown to be tightly connected [32], coupled or parallel regulatory mechanisms were suggested [19]. In contrast, our data suggest that translational processes are subject to mRNA stability regulation under hypoxic conditions.

We further identified a small group of compensatory DSR, i.e., targets which, while being upregulated on total mRNA level, had reduced mRNA half-lives. The observation that immune responses experience a compensatory mRNA stability reduction under hypoxic conditions corroborates earlier reports that LPS-induced pro-inflammatory mRNAs are destabilized under hypoxia [33]. Importantly, inflammatory conditions commonly bear hypoxic characteristics due to the reduced oxygen availability in the local niches as a result of the infiltration and activation of immune cells [1,2]. Thus, it can be speculated that the importance of compensatory destabilization of immune response-related targets might be even greater during inflammation, where it could contribute to the resolution of inflammation.

Interestingly, the median global mRNA half-life in THP-1 cells under normoxia (3.71 h) appeared to be substantially shorter than in HUVEC cells (8.7 h) [19]. A similar discrepancy was observed in different murine cells, i.e., while the median global mRNA half-life ranged between 5 h [34] and 9 h [35] in NIH3T3 cells, it was only 3.9 h in mESCs [20]. Thus, not surprisingly, similarly to the cell type-specific transcriptional profiles, mRNA stabilities appear to vary between different cellular contexts as well. Despite the overarching differences, the reduced global mRNA half-lives in response to hypoxia observed in our study corroborate the marked reduction found in HUVECs [19]. Furthermore, we observed substantial differences in the half-lives of the different DSR clusters, where mRNAs that showed increased stability under hypoxia shared an extremely short median half-life (2.3 h). In contrast, clusters containing mRNAs with reduced stability had median half-lives of up to 12.3 h (cluster 5). Notably, the total mRNA expression levels appeared to follow a similar distribution, i.e., the cluster with the shortest median half-life had the lowest median expression (cluster 1) and the cluster with the longest half-life had the highest median expression (cluster 5). Strikingly, the functional, mitochondrial DSR targets had an even higher median half-life under normoxia (16.02 h), which was reduced by almost 50% under acute and chronic hypoxia.

Our finding that the experimental validation of selected half-lives by actinomycin D treatment correlated better with the bioinformatically determined half-lives than those determined by 4sU wash-out is in line with previous observations [23]. Yet, others have shown similarly good correlations for the wash-out approach [20]. Considering the great variability in cell-type-, stimulus-, and even mRNA sub-group-specific half-lives, the selection of an experimental approach to determine global and selected mRNA half-lives as well as the bioinformatics tools needs to be made carefully as recently shown in a comparative analysis of various experimental and bioinformatical approaches [36].

In conclusion, while major gene expression changes during the course of hypoxia result from the enhanced transcription of numerous mRNAs, we provide evidence that the reduction in half-lives of specific groups of mRNAs adds to functional traits such as the downregulation of mitochondrial function. Considering the importance of metabolic rewiring during hypoxia and the detrimental effects of reactive oxygen species during hypoxia, but also during reoxygenation, these findings appear of major importance since they might open new opportunities for intervention.

4. Materials and Methods

4.1. Chemicals

All chemicals were purchased from Thermo Fisher Scientific GmbH (Dreieich, Germany), if not indicated otherwise. Primers were ordered from Biomers (Ulm, Germany).

4.2. Cell Culture

THP-1 cells were maintained in RPMI 1640 containing 10% FCS (Capricorn Scientific GmbH, Ebsdorfergrund, Deutschland), 100 U/mL penicillin, and 100 µg/mL streptomycin in an incubator with 5% CO_2 (normoxia = N). For hypoxic incubation, cells were transferred into a hypoxia workstation (SCI-tive, Baker Ruskinn, Bridgend, South Wales, USA) with 5% CO_2 adjusted to 1% O_2 with N_2 for either 8 h (acute hypoxia = AH) or 72 h (chronic hypoxia = CH). For all experiments performed under hypoxic conditions, freshly prepared hypoxic media and PBS (Sigma-Aldrich Chemie GmbH, Taufkirchen, Germany) were used, and cells were kept under hypoxic conditions until lysis.

4.3. Viability Assay

THP-1 cells were labeled with increasing concentrations of 4-thiouridine (4sU, Biosynth Carbosynth, Staad, Switzerland) for 8 h under normoxic conditions. Every 2 h, fresh 4sU was added without exchange of the medium. After 8 h, medium was removed, and the cells were incubated for further 16 h in 4sU-free medium prior to determining viability using the CellTiter-Glo® assay (Promega GmbH, Walldorf, Germany) as described in the manufacturer's instructions. The IC10 value was determined using nonlinear regression in GraphPad Prism 8.

4.4. SLAM-seq

For estimation of transcriptome-wide changes in de novo synthesis and stability of mRNA, thiol-linked alkylation for the metabolic sequencing of RNA (SLAM-seq) was used as previously described [20] with minor modifications.

Briefly, THP-1 cells were seeded in medium at a density of 3.5×10^5/mL and incubated under normoxic or hypoxic conditions. For estimating de novo synthesis, cells were labeled during the last hour of normoxic or hypoxic incubations with 300 µM 4sU. To analyze RNA stability, cells were labeled with 4 pulses of 30 µM 4sU every 2 h during the last 8 h of the incubations without exchanging the medium in between. For wash-out analyses, cells were washed twice in PBS after 8 h labeling (4×30 µM 4sU), resuspended in medium containing 3 mM uridine (Sigma-Aldrich Chemie GmbH), and incubated for additional 1, 3, or 6 h under normoxic or hypoxic conditions. At the respective endpoints, cells were lysed in RLT buffer and RNA was isolated using the RNeasy Plus Mini Kit (Qiagen, Hilden, Germany) according to the manufacturer's instructions with the modification that dithiothreitol (DTT; Carl Roth GmbH & Co. KG, Karlsruhe, Deutschland) was added in all washing steps (0.1 mM) and to the final eluate (1 mM). Five µg extracted total RNA were alkylated using 10 mM iodoacetamide (in 50 mM sodium phosphate buffer, pH 8, 50% DMSO). After 15 min incubation at 50 °C, the reaction was quenched by addition of 20 mM DTT, followed by subsequent ethanol precipitation. RNA integrity was analyzed with an Agilent 2100 Bioanalyzer using the RNA 6000 Nano Kit (Agilent Technologies Germany GmbH & Co. KG, Waldbronn, Germany). 3′UTR libraries were generated from 500 ng alkylated RNA using the QuantSeq 3′ mRNA-Seq Library Prep Kit FWD for Illumina with the UMI Second Strand Synthesis Module for QuantSeq (Lexogen, Vienna, Austria). Library sequencing (single-read; 75 or 150 cycles) was performed on a NextSeq 500 sequencer using a High Output Kit v2 (Illumina, San Diego, CA, USA).

4.5. Read Processing, Mapping and Counting

Illumina BaseSpace was used for Bcl2fastq conversion and demultiplexing of pooled libraries. Quality of fastq files was examined using FastQC [37]. Initially, all fastq files were trimmed to 75 nt followed by quality-, adapter- and polyA-trimming with Cutadapt [38].

Subsequently, the unique molecular identifier (UMI) and linker sequences were removed from the reads, and reads were aligned to the human genome (GRCh38) with Ensembl gene annotation (release 80) using STAR (version 2.7.6a) [39] with the following parameters: –alignEndsType EndToEnd –outSAMattributes MD NH –outFilterMultimapNmax 1 –clip5pNbases 12. The resulting bam files were converted to sam files using SAMtools [40], and mutations in the alignments relative to the reference genome were extracted using the Perl script parseAlignment.pl from of the CLIP Tool Kit (CTK, v1.1.3) [41]. The resulting list specified all found mutations, their locations in the genome, as well as the names of the reads in which they were found. The list was filtered for T-to-C mutations using basic Bash commands and kept in bed file format as described in [42]. Based on the filtered list of T-to-C mutations, de-duplicated reads were separated into two bam files holding reads with and without T-to-C mutation, respectively, using SAMtools and basic Bash commands. Separate bam files were generated for total and T-to-C reads, and transcript counts were determined using htseq-count with default parameters [43] and Ensembl gene annotation (release 80).

4.6. Differential Gene Expression Analysis of Total (DGE) and T-to-C (DDNS) Data Set

Differential gene expression analysis was performed with DESeq2 in R [44]. Log_2-transformed fold changes in genes were shrunken using the estimator "ashr". Benjamini–Hochberg correction was used to determine adjusted *p*-values (padj). Data were visualized using the R packages ggplot2 [45] and ComplexHeatmap [42]. For generation of heatmaps, read counts of significantly changed genes were corrected for library size using DESeq2 size factors and subjected to a row-wise *z*-score normalization.

4.7. Determination of mRNA Half-Lives Using GRAND-SLAM

RNA half-lives were estimated based on "globally refined analysis of newly transcribed RNA and decay rates using SLAM-seq" (GRAND-SLAM [23]). Briefly, GRAND-SLAM extrapolates the new-to-total ratio (NTR) and the corresponding posterior distribution based on SLAM-seq data, which allows RNA half-lives to be estimated. Bam files of the 8 h 4sU-labeled samples (for N, AH, and CH) and, in addition, unlabeled control bam files were used for running GRAND-SLAM using the default parameters. The mode of the posterior distribution for the NTR π (output from GRAND-SLAM) was used to calculate half-lives λ using the formula $\lambda = \frac{-8 \log(2)}{\log(1-\pi)}$. Transcripts with >0 read counts in all samples and half-lives >0 h and <100 h were included in further analyses. Significant global mRNA half-life changes between N, AH, and CH were determined using a Kruskal–Wallis test with subsequent Dunn's test. Significant single transcript half-life changes between N, AH, and CH were determined using a one-way ANOVA followed by pairwise *t*-tests with Benjamini–Hochberg multiple testing correction. Data were visualized using the R packages ggplot2 [45] and ComplexHeatmap [42]. For generation of heatmaps, half-lives of significantly changed DSR targets were subjected to a row-wise *z*-score normalization.

4.8. Gene Set Enrichment Analysis (GSEA)

GSEA was performed using GSEA v4.2.1 [46,47]. Library-size normalized counts (basemean > 0, for all conditions), T-to-C counts (T-to-C basemean >0, for all conditions), or half-lives (half-lives >0 h and <100 h, for all conditions) were used as input and the hallmark gene set "h.all.v7.5.1.symbols.gmt" was as reference gene set. The hallmark genes sets represent specific well-defined biological states or processes. The permutation type was set to "gene_set" and 1000 permutations were performed.

4.9. Functional Annotation Clustering

Functional annotation clustering was carried out using the Database for Annotation, Visualization and Integrated Discovery (DAVID) against the gene sets "GOTERM_BP_ALL", "GOTERM_CC_ALL", and "REACTOME_PATHWAY" [48,49]. A list of all detected transcripts (basemean > 0, for all conditions) served as background data set.

4.10. Transcription Inhibition Using Actinomycin D

THP-1 cells were seeded at a density of 3.5×10^5 cells/mL and incubated under normoxic, acute, or chronic hypoxic conditions, before de novo transcription was blocked by the addition of 2.5 µM actinomycin D (act D; Sigma-Aldrich Chemie GmbH). RNA was isolated using TRIzol (Thermo Fisher Scientific) according to the manufacturer's instructions, either before (=0 h timepoint) or 1, 2, and 4 h after the administration of act D. RNA concentration was determined by a Nanodrop ND-1000 spectrophotometer (Peqlab Biotechnologie GmbH, Erlangen, Germany). RNA was reverse transcribed using the Maxima First Strand cDNA synthesis kit (Thermo Fisher Scientific) and qPCR analyses were carried out using the PowerUp SYBR Green Master Mix on QuantStudio 3 and 5 PCR Real-Time Systems (all Thermo Fisher Scientific) using primers against MRPL40 (fwd: GAC CAA GAA GCA AAG GAG CGC T; rev: CCT CTC AGT CTC CTC AAA GGT G), CPT1A (fwd: TCG TCA CCT CTT CTG CCT TT; rev: ACA CAC CAT AGC CGT CAT CA), TOMM34 (fwd: CGG CAA TGA GAG TTT CCG C; rev: TCT GAA GAA CCT TGC GCC TG), and GUSB (fwd: CAT TCC TAT GCC ATC GTG TGG G; rev: GGG GGT GAG TGT GTT GTT GAT).

4.11. Experimental Validation of mRNA Half-Lives

RNA half-lives were estimated from act D experiments or from SLAM-seq wash-out data by normalizing C_t values or library-size normalized T-to-C counts, respectively, to the 0 h control time points. Linear regression in GraphPad Prism 8 was used to determine RNA half-lives.

4.12. Statistics

Statistical analyses were carried out using GraphPad Prism v8.2.1 (GraphPad Software, San Diego, CA, USA) or R v4.0.5 [50].

Supplementary Materials: The following supporting information can be downloaded at: https://www.mdpi.com/article/10.3390/ijms23105824/s1.

Author Contributions: Conceptualization, R.B., D.C.F., T.S. and B.B.; data curation, R.B., K.Z. and T.S.; formal analysis, R.B., K.A.K., S.R., Y.Z., K.Z. and T.S.; funding acquisition, K.Z., T.S. and B.B.; investigation, R.B., S.P.M., V.M.G.R. and D.C.F.; methodology, R.B.; visualization, R.B., K.A.K., S.R., K.Z. and T.S.; writing—original draft, R.B., K.Z. and T.S.; writing—review and editing, R.B., K.Z., T.S. and B.B. All authors have read and agreed to the published version of the manuscript.

Funding: This work was supported by the DFG (BR999/25-1 to B.B.; SFB 1039, B04 to B.B.; GRK 2336, TP06 to B.B. and T.S.; SCHM2663/7-1 to T.S.; TRR 267, A1 to K.Z.). APC were funded by the Open Access Publication Fund of Goethe-University.

Data Availability Statement: The sequencing data presented in this study are available in GEO accession number GSE199947.

Acknowledgments: The authors would like to thank Dara da Silva Weirich for the initial analyses.

Conflicts of Interest: The authors declare no conflict of interest. The funders had no role in the design of the study; in the collection, analyses, or interpretation of data; in the writing of the manuscript, or in the decision to publish the results.

References

1. Egners, A.; Erdem, M.; Cramer, T. The Response of Macrophages and Neutrophils to Hypoxia in the Context of Cancer and Other Inflammatory Diseases. *Mediat. Inflamm.* **2016**, *2016*, 2053646. [CrossRef] [PubMed]
2. Imtiyaz, H.Z.; Simon, M.C. Hypoxia-Inducible Factors as Essential Regulators of Inflammation. *Curr. Top. Microbiol. Immunol.* **2010**, *345*, 105–120. [CrossRef] [PubMed]
3. Fandrey, J.; Schödel, J.; Eckardt, K.-U.; Katschinski, D.M.; Wenger, R.H. Now a Nobel Gas: Oxygen. *Pflug. Arch.* **2019**, *471*, 1343–1358. [CrossRef]
4. Kim, J.-W.; Tchernyshyov, I.; Semenza, G.L.; Dang, C.V. HIF-1-mediated expression of pyruvate dehydrogenase kinase: A metabolic switch required for cellular adaptation to hypoxia. *Cell Metab.* **2006**, *3*, 177–185. [CrossRef] [PubMed]

5. Belisario, D.C.; Kopecka, J.; Pasino, M.; Akman, M.; De Smaele, E.; Donadelli, M.; Riganti, C. Hypoxia Dictates Metabolic Rewiring of Tumors: Implications for Chemoresistance. *Cells* **2020**, *9*, 2598. [CrossRef]
6. Zhang, H.; Bosch-Marce, M.; Shimoda, L.A.; Tan, Y.S.; Baek, J.H.; Wesley, J.B.; Gonzalez, F.J.; Semenza, G.L. Mitochondrial autophagy is an HIF-1-dependent adaptive metabolic response to hypoxia. *J. Biol. Chem.* **2008**, *283*, 10892–10903. [CrossRef]
7. Bellot, G.; Garcia-Medina, R.; Gounon, P.; Chiche, J.; Roux, D.; Pouysségur, J.; Mazure, N.M. Hypoxia-induced autophagy is mediated through hypoxia-inducible factor induction of BNIP3 and BNIP3L via their BH3 domains. *Mol. Cell. Biol.* **2009**, *29*, 2570–2581. [CrossRef]
8. Liu, L.; Feng, D.; Chen, G.; Chen, M.; Zheng, Q.; Song, P.; Ma, Q.; Zhu, C.; Wang, R.; Qi, W.; et al. Mitochondrial outer-membrane protein FUNDC1 mediates hypoxia-induced mitophagy in mammalian cells. *Nat. Cell Biol.* **2012**, *14*, 177–185. [CrossRef]
9. Ivan, M.; Kaelin, W.G. The EGLN-HIF O 2 -Sensing System: Multiple Inputs and Feedbacks. *Mol. Cell* **2017**, *66*, 772–779. [CrossRef]
10. Pugh, C.W.; Ratcliffe, P.J. New Horizons in Hypoxia Signaling Pathways. *Exp. Cell Res.* **2017**, *356*, 116–121. [CrossRef]
11. Semenza, G.L. Hypoxia-Inducible Factors in Physiology and Medicine. *Cell* **2012**, *148*, 399–408. [CrossRef] [PubMed]
12. Fuhrmann, D.C.; Tausendschön, M.; Wittig, I.; Steger, M.; Ding, M.G.; Schmid, T.; Dehne, N.; Brüne, B. Inactivation of Tristetraprolin in Chronic Hypoxia Provokes the Expression of Cathepsin B. *Mol. Cell. Biol.* **2015**, *35*, 619–630. [CrossRef] [PubMed]
13. Lin, Q.; Cong, X.; Yun, Z. Differential Hypoxic Regulation of Hypoxia-Inducible Factors 1α and 2α. *Mol. Cancer Res.* **2011**, *9*, 757–765. [CrossRef] [PubMed]
14. Fuhrmann, D.C.; Wittig, I.; Heide, H.; Dehne, N.; Brüne, B. Chronic Hypoxia Alters Mitochondrial Composition in Human Macrophages. *Biochim. Biophys. Acta BBA Proteins Proteom.* **2013**, *1834*, 2750–2760. [CrossRef] [PubMed]
15. Clees, A.S.; Stolp, V.; Häupl, B.; Fuhrmann, D.C.; Wempe, F.; Seibert, M.; Weber, S.; Banning, A.; Tikkanen, R.; Williams, R.; et al. Identification of the Cysteine Protease Legumain as a Potential Chronic Hypoxia-Specific Multiple Myeloma Target Gene. *Cells* **2022**, *11*, 292. [CrossRef] [PubMed]
16. Gorospe, M.; Tominaga, K.; Wu, X.; Fähling, M.; Ivan, M. Post-Transcriptional Control of the Hypoxic Response by RNA-Binding Proteins and MicroRNAs. *Front. Mol. Neurosci.* **2011**, *4*, 7. [CrossRef]
17. Natua, S.; Ashok, C.; Shukla, S. Hypoxia-Induced Alternative Splicing in Human Diseases: The Pledge, the Turn, and the Prestige. *Cell. Mol. Life Sci.* **2021**, *78*, 2729–2747. [CrossRef]
18. Spriggs, K.A.; Bushell, M.; Willis, A.E. Translational Regulation of Gene Expression during Conditions of Cell Stress. *Mol. Cell* **2010**, *40*, 228–237. [CrossRef]
19. Tiana, M.; Acosta-Iborra, B.; Hernández, R.; Galiana, C.; Fernández-Moreno, M.Á.; Jimenez, B.; del Peso, L. Metabolic Labeling of RNA Uncovers the Contribution of Transcription and Decay Rates on Hypoxia-Induced Changes in RNA Levels. *RNA* **2020**, *26*, 1006–1022. [CrossRef]
20. Herzog, V.A.; Reichholf, B.; Neumann, T.; Rescheneder, P.; Bhat, P.; Burkard, T.R.; Wlotzka, W.; von Haeseler, A.; Zuber, J.; Ameres, S.L. Thiol-Linked Alkylation of RNA to Assess Expression Dynamics. *Nat. Methods* **2017**, *14*, 1198–1204. [CrossRef]
21. Rappl, P.; Brüne, B.; Schmid, T. Role of Tristetraprolin in the Resolution of Inflammation. *Biology* **2021**, *10*, 66. [CrossRef] [PubMed]
22. Uchida, Y.; Chiba, T.; Kurimoto, R.; Asahara, H. Post-Transcriptional Regulation of Inflammation by RNA-Binding Proteins via Cis-Elements of mRNAs. *J. Biochem.* **2019**, *166*, 375–382. [CrossRef] [PubMed]
23. Jürges, C.; Dölken, L.; Erhard, F. Dissecting Newly Transcribed and Old RNA Using GRAND-SLAM. *Bioinformatics* **2018**, *34*, i218–i226. [CrossRef] [PubMed]
24. Fuhrmann, D.C.; Brüne, B. Mitochondrial Composition and Function under the Control of Hypoxia. *Redox Biol.* **2017**, *12*, 208–215. [CrossRef]
25. Chakraborty, A.A.; Laukka, T.; Myllykoski, M.; Ringel, A.E.; Booker, M.A.; Tolstorukov, M.Y.; Meng, Y.J.; Meier, S.R.; Jennings, R.B.; Creech, A.L.; et al. Histone Demethylase KDM6A Directly Senses Oxygen to Control Chromatin and Cell Fate. *Science* **2019**, *363*, 1217–1222. [CrossRef]
26. Hu, C.-J.; Wang, L.-Y.; Chodosh, L.A.; Keith, B.; Simon, M.C. Differential Roles of Hypoxia-Inducible Factor 1α (HIF-1α) and HIF-2α in Hypoxic Gene Regulation. *Mol. Cell. Biol.* **2003**, *23*, 9361–9374. [CrossRef]
27. Smythies, J.A.; Sun, M.; Masson, N.; Salama, R.; Simpson, P.D.; Murray, E.; Neumann, V.; Cockman, M.E.; Choudhry, H.; Ratcliffe, P.J.; et al. Inherent DNA-Binding Specificities of the HIF-1α and HIF-2α Transcription Factors in Chromatin. *EMBO Rep.* **2019**, *20*. [CrossRef]
28. Weigand, J.E.; Boeckel, J.-N.; Gellert, P.; Dimmeler, S. Hypoxia-Induced Alternative Splicing in Endothelial Cells. *PLoS ONE* **2012**, *7*, e42697. [CrossRef]
29. Xia, X.; Kung, A.L. Preferential Binding of HIF-1 to Transcriptionally Active Loci Determines Cell-Type Specific Response to Hypoxia. *Genome Biol.* **2009**, *10*, R113. [CrossRef]
30. Susen, R.M.; Bauer, R.; Olesch, C.; Fuhrmann, D.C.; Fink, A.F.; Dehne, N.; Jain, A.; Ebersberger, I.; Schmid, T.; Brüne, B. Macrophage HIF-2α Regulates Tumor-suppressive Spint1 in the Tumor Microenvironment. *Mol. Carcinog.* **2019**, *58*, 2127–2138. [CrossRef]
31. Kasparova, D.; Neckar, J.; Dabrowska, L.; Novotny, J.; Mraz, J.; Kolar, F.; Zurmanova, J. Cardioprotective and Nonprotective Regimens of Chronic Hypoxia Diversely Affect the Myocardial Antioxidant Systems. *Physiol. Genom.* **2015**, *47*, 612–620. [CrossRef] [PubMed]

32. Garneau, N.L.; Wilusz, J.; Wilusz, C.J. The Highways and Byways of mRNA Decay. *Nat. Rev. Mol. Cell Biol.* **2007**, *8*, 113–126. [CrossRef] [PubMed]
33. Werno, C.; Schmid, T.; Schnitzer, S.E.; Peters, K.; Milke, L.; Brüne, B. A Combination of Hypoxia and Lipopolysaccharide Activates Tristetraprolin to Destabilize Proinflammatory mRNAs Such as Tumor Necrosis Factor-α. *Am. J. Pathol.* **2010**, *177*, 1104–1112. [CrossRef] [PubMed]
34. Dölken, L.; Ruzsics, Z.; Rädle, B.; Friedel, C.C.; Zimmer, R.; Mages, J.; Hoffmann, R.; Dickinson, P.; Forster, T.; Ghazal, P.; et al. High-Resolution Gene Expression Profiling for Simultaneous Kinetic Parameter Analysis of RNA Synthesis and Decay. *RNA* **2008**, *14*, 1959–1972. [CrossRef] [PubMed]
35. Schwanhäusser, B.; Busse, D.; Li, N.; Dittmar, G.; Schuchhardt, J.; Wolf, J.; Chen, W.; Selbach, M. Global Quantification of Mammalian Gene Expression Control. *Nature* **2011**, *473*, 337–342. [CrossRef] [PubMed]
36. Boileau, E.; Altmüller, J.; Naarmann-de Vries, I.S.; Dieterich, C. A Comparison of Metabolic Labeling and Statistical Methods to Infer Genome-Wide Dynamics of RNA Turnover. *Brief. Bioinform.* **2021**, *22*, bbab219. [CrossRef] [PubMed]
37. Andrews, S. FastQC: A Quality Control Tool for High Throughput Sequence Data. 2010. Available online: https://www.bioinformatics.babraham.ac.uk/projects/fastqc/ (accessed on 6 June 2021).
38. Martin, M. Cutadapt Removes Adapter Sequences from High-Throughput Sequencing Reads. *EMBnet J.* **2011**, *17*, 10. [CrossRef]
39. Dobin, A.; Davis, C.A.; Schlesinger, F.; Drenkow, J.; Zaleski, C.; Jha, S.; Batut, P.; Chaisson, M.; Gingeras, T.R. STAR: Ultrafast Universal RNA-Seq Aligner. *Bioinformatics* **2013**, *29*, 15–21. [CrossRef]
40. Li, H.; Handsaker, B.; Wysoker, A.; Fennell, T.; Ruan, J.; Homer, N.; Marth, G.; Abecasis, G.; Durbin, R.; 1000 Genome Project Data Processing Subgroup. The Sequence Alignment/Map format and SAMtools. *Bioinformatics* **2009**, *25*, 2078–2079. [CrossRef]
41. Shah, A.; Qian, Y.; Weyn-Vanhentenryck, S.M.; Zhang, C. CLIP Tool Kit (CTK): A flexible and robust pipeline to analyze CLIP sequencing data. *Bioinformatics* **2017**, *33*, 566–567. [CrossRef]
42. Gu, Z.; Eils, R.; Schlesner, M. Complex Heatmaps Reveal Patterns and Correlations in Multidimensional Genomic Data. *Bioinformatics* **2016**, *32*, 2847–2849. [CrossRef] [PubMed]
43. Anders, S.; Pyl, P.T.; Huber, W. HTSeq–a Python Framework to Work with High-Throughput Sequencing Data. *Bioinformatics* **2015**, *31*, 166–169. [CrossRef] [PubMed]
44. Love, M.I.; Huber, W.; Anders, S. Moderated Estimation of Fold Change and Dispersion for RNA-Seq Data with DESeq2. *Genome Biol.* **2014**, *15*, 550. [CrossRef] [PubMed]
45. Wickham, H. *Ggplot2: Elegant Graphics for Data Analysis; Use R!* 2nd ed.; Springer International Publishing: Cham, Switzerland, 2016; ISBN 978-3-319-24277-4.
46. Mootha, V.K.; Lindgren, C.M.; Eriksson, K.-F.; Subramanian, A.; Sihag, S.; Lehar, J.; Puigserver, P.; Carlsson, E.; Ridderstråle, M.; Laurila, E.; et al. PGC-1α-Responsive Genes Involved in Oxidative Phosphorylation Are Coordinately Downregulated in Human Diabetes. *Nat. Genet.* **2003**, *34*, 267–273. [CrossRef] [PubMed]
47. Subramanian, A.; Tamayo, P.; Mootha, V.K.; Mukherjee, S.; Ebert, B.L.; Gillette, M.A.; Paulovich, A.; Pomeroy, S.L.; Golub, T.R.; Lander, E.S.; et al. Gene Set Enrichment Analysis: A Knowledge-Based Approach for Interpreting Genome-Wide Expression Profiles. *Proc. Natl. Acad. Sci. USA* **2005**, *102*, 15545–15550. [CrossRef] [PubMed]
48. Huang, D.W.; Sherman, B.T.; Lempicki, R.A. Bioinformatics Enrichment Tools: Paths toward the Comprehensive Functional Analysis of Large Gene Lists. *Nucleic Acids Res.* **2009**, *37*, 1–13. [CrossRef] [PubMed]
49. Huang, D.W.; Sherman, B.T.; Lempicki, R.A. Systematic and Integrative Analysis of Large Gene Lists Using DAVID Bioinformatics Resources. *Nat. Protoc.* **2009**, *4*, 44–57. [CrossRef]
50. R Core Team R. *A Language and Environment for Statistical Computing*; R Foundation for Statistical Computing: Vienna, Austria, 2021.

7. References

1. Nakazawa MS, Keith B, Simon MC. Oxygen availability and metabolic adaptations. *Nat Rev Cancer*. 2016;16(10):663-673. doi:10.1038/nrc.2016.84

2. Semenza GL. Hypoxia-Inducible Factors in Physiology and Medicine. *Cell*. 2012;148(3):399-408. doi:10.1016/j.cell.2012.01.021

3. Fuhrmann DC, Brüne B. Mitochondrial composition and function under the control of hypoxia. *Redox Biol*. 2017;12:208-215. doi:10.1016/j.redox.2017.02.012

4. Munir R, Lisec J, Swinnen JV, Zaidi N. Lipid metabolism in cancer cells under metabolic stress. *Br J Cancer*. 2019;120(12):1090-1098. doi:10.1038/s41416-019-0451-4

5. Nguyen AD, McDonald JG, Bruick RK, DeBose-Boyd RA. Hypoxia Stimulates Degradation of 3-Hydroxy-3-methylglutaryl-coenzyme A Reductase through Accumulation of Lanosterol and Hypoxia-Inducible Factor-mediated Induction of Insigs. *J Biol Chem*. 2007;282(37):27436-27446. doi:10.1074/jbc.M704976200

6. Zhu J, Jiang X, Chehab FF. FoxO4 interacts with the sterol regulatory factor SREBP2 and the hypoxia inducible factor HIF2α at the CYP51 promoter. *J Lipid Res*. 2014;55(3):431-442. doi:10.1194/jlr.M043521

7. Bhandari V, Hoey C, Liu LY, et al. Molecular landmarks of tumor hypoxia across cancer types. *Nat Genet*. 2019;51(2):308-318. doi:10.1038/s41588-018-0318-2

8. Vaupel P. Hypoxia and Aggressive Tumor Phenotype: Implications for Therapy and Prognosis. *The Oncologist*. 2008;13(S3):21-26. doi:10.1634/theoncologist.13-S3-21

9. Campbell EL, Bruyninckx WJ, Kelly CJ, et al. Transmigrating neutrophils shape the mucosal microenvironment through localized oxygen depletion to influence resolution of inflammation. *Immunity*. 2014;40(1):66-77. doi:10.1016/j.immuni.2013.11.020

10. Campbell EL, Colgan SP. Neutrophils and inflammatory metabolism in antimicrobial functions of the mucosa. *J Leukoc Biol*. 2015;98(4):517-522. doi:10.1189/jlb.3MR1114-556R

11. Cummins EP, Berra E, Comerford KM, et al. Prolyl hydroxylase-1 negatively regulates IkappaB kinase-beta, giving insight into hypoxia-induced NFkappaB activity. *Proc Natl Acad Sci U S A*. 2006;103(48):18154-18159. doi:10.1073/pnas.0602235103

12. Murdoch C, Giannoudis A, Lewis CE. Mechanisms regulating the recruitment of macrophages into hypoxic areas of tumors and other ischemic tissues. *Blood*. 2004;104(8):2224-2234. doi:10.1182/blood-2004-03-1109

13. Casazza A, Laoui D, Wenes M, et al. Impeding Macrophage Entry into Hypoxic Tumor Areas by Sema3A/Nrp1 Signaling Blockade Inhibits Angiogenesis and Restores Antitumor Immunity. *Cancer Cell*. 2013;24(6):695-709. doi:10.1016/j.ccr.2013.11.007

14. Chiu DKC, Xu IMJ, Lai RKH, et al. Hypoxia induces myeloid-derived suppressor cell recruitment to hepatocellular carcinoma through chemokine (C-C motif) ligand 26: Chiu et al. *Hepatology*. 2016;64(3):797-813. doi:10.1002/hep.28655

15. Kinne RW, Stuhlmüller B, Burmester GR. Cells of the synovium in rheumatoid arthritis. Macrophages. *Arthritis Res Ther*. 2007;9(6):224. doi:10.1186/ar2333

16. Fandrey J, Schödel J, Eckardt KU, Katschinski DM, Wenger RH. Now a Nobel gas: oxygen. *Pflüg Arch - Eur J Physiol*. 2019;471(11-12):1343-1358. doi:10.1007/s00424-019-02334-8

17. Clees AS, Stolp V, Häupl B, et al. Identification of the Cysteine Protease Legumain as a Potential Chronic Hypoxia-Specific Multiple Myeloma Target Gene. *Cells*. 2022;11(2):292. doi:10.3390/cells11020292

18. Fuhrmann DC, Wittig I, Heide H, Dehne N, Brüne B. Chronic hypoxia alters mitochondrial composition in human macrophages. *Biochim Biophys Acta BBA - Proteins Proteomics*. 2013;1834(12):2750-2760. doi:10.1016/j.bbapap.2013.09.023

19. Fortenbery GW, Sarathy B, Carraway KR, Mansfield KD. Hypoxic stabilization of mRNA is HIF-independent but requires mtROS. *Cell Mol Biol Lett*. 2018;23:48. doi:10.1186/s11658-018-0112-2

20. Fuhrmann DC, Tausendschön M, Wittig I, et al. Inactivation of Tristetraprolin in Chronic Hypoxia Provokes the Expression of Cathepsin B. *Mol Cell Biol*. 2015;35(3):619-630. doi:10.1128/MCB.01034-14

21. Herzog VA, Reichholf B, Neumann T, et al. Thiol-linked alkylation of RNA to assess expression dynamics. *Nat Methods*. 2017;14(12):1198-1204. doi:10.1038/nmeth.4435

22. Jürges C, Dölken L, Erhard F. Dissecting newly transcribed and old RNA using GRAND-SLAM. *Bioinformatics*. 2018;34(13):i218-i226. doi:10.1093/bioinformatics/bty256

23. Tiana M, Acosta-Iborra B, Hernández R, et al. Metabolic labeling of RNA uncovers the contribution of transcription and decay rates on hypoxia-induced changes in RNA levels. *RNA*. 2020;26(8):1006-1022. doi:10.1261/rna.072611.119

24. Taylor CT, Doherty G, Fallon PG, Cummins EP. Hypoxia-dependent regulation of inflammatory pathways in immune cells. *J Clin Invest*. 2016;126(10):3716-3724. doi:10.1172/JCI84433

25. Anderson P. Post-transcriptional regulons coordinate the initiation and resolution of inflammation. *Nat Rev Immunol*. 2010;10(1):24-35. doi:10.1038/nri2685

26. Roy B, Jacobson A. The intimate relationships of mRNA decay and translation. *Trends Genet*. 2013;29(12):691-699. doi:10.1016/j.tig.2013.09.002

27. Yamasaki S, Anderson P. Reprogramming mRNA translation during stress. *Curr Opin Cell Biol*. 2008;20(2):222-226. doi:10.1016/j.ceb.2008.01.013

28. Mathis D, Shoelson SE. Immunometabolism: an emerging frontier. *Nat Rev Immunol*. 2011;11(2):81. doi:10.1038/nri2922

29. Rusinova I, Forster S, Yu S, et al. INTERFEROME v2.0: an updated database of annotated interferon-regulated genes. *Nucleic Acids Res*. 2012;41(D1):D1040-D1046. doi:10.1093/nar/gks1215

30. Schoggins JW, Rice CM. Interferon-stimulated genes and their antiviral effector functions. *Curr Opin Virol*. 2011;1(6):519-525. doi:10.1016/j.coviro.2011.10.008

31. Xiao J, Li W, Zheng X, et al. Targeting 7-Dehydrocholesterol Reductase Integrates Cholesterol Metabolism and IRF3 Activation to Eliminate Infection. *Immunity*. 2020;52(1):109-122.e6. doi:10.1016/j.immuni.2019.11.015

32. York AG, Williams KJ, Argus JP, et al. Limiting Cholesterol Biosynthetic Flux Spontaneously Engages Type I IFN Signaling. *Cell*. 2015;163(7):1716-1729. doi:10.1016/j.cell.2015.11.045

33. Blanc M, Hsieh WY, Robertson KA, et al. Host Defense against Viral Infection Involves Interferon Mediated Down-Regulation of Sterol Biosynthesis. Virgin SW, ed. *PLoS Biol*. 2011;9(3):e1000598. doi:10.1371/journal.pbio.1000598

34. Reboldi A, Dang EV, McDonald JG, Liang G, Russell DW, Cyster JG. 25-Hydroxycholesterol suppresses interleukin-1–driven inflammation downstream of type I interferon. *Science*. 2014;345(6197):679-684. doi:10.1126/science.1254790

35. Zhang X, McDonald JG, Aryal B, et al. Desmosterol suppresses macrophage inflammasome activation and protects against vascular inflammation and atherosclerosis. *Proc Natl Acad Sci*. 2021;118(47):e2107682118. doi:10.1073/pnas.2107682118

36. Kusnadi A, Park SH, Yuan R, et al. The Cytokine TNF Promotes Transcription Factor SREBP Activity and Binding to Inflammatory Genes to Activate Macrophages and Limit Tissue Repair. *Immunity*. 2019;51(2):241-257.e9. doi:10.1016/j.immuni.2019.06.005

37. Gholkar AA, Cheung K, Williams KJ, et al. Fatostatin Inhibits Cancer Cell Proliferation by Affecting Mitotic Microtubule Spindle Assembly and Cell Division. *J Biol Chem*. 2016;291(33):17001-17008. doi:10.1074/jbc.C116.737346

38. Shao W, Machamer CE, Espenshade PJ. Fatostatin blocks ER exit of SCAP but inhibits cell growth in a SCAP-independent manner. *J Lipid Res*. 2016;57(8):1564-1573. doi:10.1194/jlr.M069583

39. Kawai T, Takahashi K, Sato S, et al. IPS-1, an adaptor triggering RIG-I- and Mda5-mediated type I interferon induction. *Nat Immunol*. 2005;6(10):981-988. doi:10.1038/ni1243

40. Ablasser A, Goldeck M, Cavlar T, et al. cGAS produces a 2'-5'-linked cyclic dinucleotide second messenger that activates STING. *Nature*. 2013;498(7454):380-384. doi:10.1038/nature12306

41. Ciesielska A, Matyjek M, Kwiatkowska K. TLR4 and CD14 trafficking and its influence on LPS-induced pro-inflammatory signaling. *Cell Mol Life Sci*. 2021;78(4):1233-1261. doi:10.1007/s00018-020-03656-y

42. Sarkar P, Kumar GA, Shrivastava S, Chattopadhyay A. Chronic cholesterol depletion increases F-actin levels and induces cytoskeletal reorganization via a dual mechanism. *J Lipid Res*. 2022;63(5):100206. doi:10.1016/j.jlr.2022.100206

43. Lebrand C, Corti M, Goodson H, et al. Late endosome motility depends on lipids via the small GTPase Rab7. *EMBO J*. 2002;21(6):1289-1300. doi:10.1093/emboj/21.6.1289

44. Zankharia U, Yadav A, Yi Y, Hahn BH, Collman RG. Highly restricted SARS-CoV-2 receptor expression and resistance to infection by primary human monocytes and monocyte-derived macrophages. *J Leukoc Biol*. 2022;112(3):569-576. doi:10.1002/JLB.4COVA1121-579RR

45. Zheng J, Wang Y, Li K, Meyerholz DK, Allamargot C, Perlman S. Severe Acute Respiratory Syndrome Coronavirus 2–Induced Immune Activation and Death of Monocyte-Derived Human Macrophages and Dendritic Cells. *J Infect Dis*. 2021;223(5):785-795. doi:10.1093/infdis/jiaa753

46. Cillo AR, Somasundaram A, Shan F, et al. People critically ill with COVID-19 exhibit peripheral immune profiles predictive of mortality and reflective of SARS-CoV-2 lung viral burden. *Cell Rep Med*. 2021;2(12):100476. doi:10.1016/j.xcrm.2021.100476

47. Zhang F, Mears JR, Shakib L, et al. IFN-γ and TNF-α drive a CXCL10+ CCL2+ macrophage phenotype expanded in severe COVID-19 lungs and inflammatory diseases with tissue inflammation. *Genome Med*. 2021;13(1):64. doi:10.1186/s13073-021-00881-3

48. Grant RA, Morales-Nebreda L, Markov NS, et al. Circuits between infected macrophages and T cells in SARS-CoV-2 pneumonia. *Nature*. 2021;590(7847):635-641. doi:10.1038/s41586-020-03148-w

49. Grieb P, Swiatkiewicz M, Prus K, Rejdak K. Hypoxia may be a determinative factor in COVID-19 progression. *Curr Res Pharmacol Drug Discov*. 2021;2:100030. doi:10.1016/j.crphar.2021.100030

50. Lee W, Ahn JH, Park HH, et al. COVID-19-activated SREBP2 disturbs cholesterol biosynthesis and leads to cytokine storm. *Signal Transduct Target Ther*. 2020;5(1):186. doi:10.1038/s41392-020-00292-7

51. Zhao Y, Kuang M, Li J, et al. SARS-CoV-2 spike protein interacts with and activates TLR4. *Cell Res*. 2021;31(7):818-820. doi:10.1038/s41422-021-00495-9

52. Salvi V, Nguyen HO, Sozio F, et al. SARS-CoV-2-associated ssRNAs activate inflammation and immunity via TLR7/8. *JCI Insight*. 2021;6(18):e150542. doi:10.1172/jci.insight.150542

53. Peng T, Du SY, Son M, Diamond B. HIF-1α is a negative regulator of interferon regulatory factors: Implications for interferon production by hypoxic monocytes. *Proc Natl Acad Sci*. 2021;118(26):e2106017118. doi:10.1073/pnas.2106017118

54. Ha JS, Choi HR, Kim IS, Kim EA, Cho SW, Yang SJ. Hypoxia-Induced S100A8 Expression Activates Microglial Inflammation and Promotes Neuronal Apoptosis. *Int J Mol Sci*. 2021;22(3):1205. doi:10.3390/ijms22031205

8. Danksagung

An dieser Stelle möchte ich allen Menschen danken, die durch ihre fachliche oder persönliche Unterstützung zum Gelingen dieser Arbeit beigetragen haben.

Mein herzlicher Dank gilt **Prof. Dr. Bernhard Brüne** für die Möglichkeit, meine Dissertation in seinem Institut anzufertigen. Insbesondere danke ich für hilfreiche fachliche Diskussionen und kritisches Feedback sowie das Vertrauen mir und meiner Arbeit gegenüber, das mir ermöglichte, meine eigenen Ideen umzusetzen.

Ein besonderer Dank gilt **PD Dr. Tobias Schmid** für eine hervorragende Betreuung und eine ansteckende Begeisterung für die Forschung. Danke für zahllose Stunden intensivster fachlicher Diskussionen, die mich in meinem wissenschaftlichen Denken nachhaltig geprägt haben und das Projekt erst zu dem gemacht haben, was es letztendlich ist.

Außerdem möchte ich **Dr. Dominik Fuhrmann** für die umfassende Einarbeitung und die große Hilfsbereitschaft und Unterstützung im Labor-Alltag danken.

Mein großer Dank gilt außerdem **PD Dr. Marek Widera, Dr. Alexander Wilhelm, Fabian Roesmann** und **dem gesamten Team des Instituts für Medizinische Virologie.** Trotz einiger Verzögerungen bei der Beschaffung des Sauerstoff-regulierbaren Inkubators für das BSL3-Labor konnte ich dank der Unterstützung und Geduld aller schließlich meine Experimente durchführen.

Ein großes Dankeschön geht an **das gesamte Team des Instituts für Biochemie I** für die gute Arbeitsatmosphäre und die ausgezeichnete Zusammenarbeit. Insbesondere möchte ich **Dr. Rosa Susen, Dr. Anica Scholz, Dr. Elisabeth Strack und Dr. Peter Rappl** danken, die mir während der ersten Jahre immer mit Rat und Tat zur Seite standen. Genauso möchte ich mich bei **Sofie Meyer, Vanesa Maria Guerrero Ruiz, Silvia Rösser, Dr. Rebecca Raue und Dr. Giulia Cardamone** bedanken, die nicht nur hilfreiches Feedback zum Projekt in der Endphase gaben, sondern auch Freunde geworden sind.

Mein besonderer Dank gilt **meiner Familie, meinen Freunden** und **meinem Partner Sebastian**, die mir den nötigen Rückhalt in schwierigen Phasen und einen Gegenpol zum Labor-Alltag gegeben haben.

Schriftliche Erklärung

Ich erkläre ehrenwörtlich, dass ich die dem Fachbereich Medizin der Johann Wolfgang Goethe-Universität Frankfurt am Main zur Prüfung eingereichte Thesis mit dem Titel

Changes in RNA dynamics in the course of hypoxia in myeloid cells

im Zentrum der Biochemie, Institut für Biochemie I (Pathobiochemie) unter Betreuung und Anleitung von Prof. Dr. Bernhard Brüne mit Unterstützung durch PD Dr. Tobias Schmid ohne sonstige Hilfe selbst durchgeführt und bei der Abfassung der Arbeit keine anderen als die in der Thesis angeführten Hilfsmittel benutzt habe. Darüber hinaus versichere ich, nicht die Hilfe einer kommerziellen Promotionsvermittlung in Anspruch genommen zu haben.

Ich habe bisher an keiner in- oder ausländischen Universität ein Gesuch um Zulassung zur Promotion oder zu einem PhD-Verfahren eingereicht. Die vorliegende Arbeit wurde bisher nicht als Thesis oder Dissertation eingereicht.

Die Grundsätze der Johann Wolfgang Goethe-Universität Frankfurt am Main zur Sicherung guter wissenschaftlicher Praxis in ihrer gültigen Form liegen mir vor und wurden bei der wissenschaftlichen Arbeit eingehalten.

Vorliegende Ergebnisse der Arbeit wurden (oder werden) in folgenden Publikationsorganen veröffentlicht:

Bauer R, Meyer SP, Raue R, Palmer MA, Guerrero Ruiz VM, Cardamone G, Rösser S, Heffels M, Roesmann F, Wilhelm A, Lütjohann D, Zarnack K, Fuhrmann DC, Widera M, Schmid T, Brüne B. Hypoxia-altered cholesterol homeostasis enhances the expression of interferon-stimulated genes upon SARS-CoV-2 infections in monocytes. *Front Immunol.* 2023;14:1121864. doi: 10.3389/fimmu.2023.1121864

Bauer R, Meyer SP, Kloss KA, Guerrero Ruiz VM, Reuscher S, Zhou Y, Fuhrmann DC, Zarnack K, Schmid T, Brüne B. Functional RNA Dynamics Are Progressively Governed by RNA Destabilization during the Adaptation to Chronic Hypoxia. *Int J Mol Sci*. 2022;23(10):5824. doi: 10.3390/ijms23105824

_____ _____

(Ort, Datum) (Unterschrift)